Synthesis of sugar-derived esters and carbamate compounds

by

Caleb Josiah Tatebe

Submitted in Partial Fulfillment of the Requirements

for the Degree of

Masters of Science

in the

Chemistry

Program

YOUNGSTOWN STATE UNIVERSITY

August 2014

Synthesis of sugar-derived esters and carbamate compounds

Caleb J Tatebe

I hereby release this thesis to the public. I understand that this thesis will be made available from the OhioLINK ETD Center and the Maag Library Circulation Desk for public access. I also authorize the University or other individuals to make copies of this thesis as needed for scholarly research.

Signature:

_____

Caleb Josiah Tatebe, Student Date

Approvals:

_____

Dr. Peter Norris, Thesis Advisor Date

_____

Dr. John Jackson, Committee Member Date

_____

Dr. Nina Stourman, Committee Member Date

_____

Dr. Salvatore A. Sanders, Associate Dean of Graduate Studies Date

Abstract

This thesis deals with the synthesis of sugar-derived esters and carbamate compounds. The attempted decomposition of diazo ester sugars is also a topic of this thesis. The synthesis of sugar-derived esters began with commercially available sugars and experimentation led to the synthesis of two compounds that have not been previously reported. Successful synthesis of these esters was confirmed by ^{1}H and ^{13}C NMR, as well as COSY and XRD. Carbamate compounds were synthesized by a bis-Curtius rearrangement and those results were also confirmed by ^{1}H and ^{13}C NMR.

Acknowledgements

First and foremost I would like to thank Dr. Peter Norris, my advisor, for giving me the opportunity to be a member of his research group. The advice and guidance he has provided is definitely second-to-none at Youngstown State University and has helped shape my career and character for the future. He has given me great insight into what to expect as I pursue my own career as a chemist and educator. Thank you for all the help in both undergraduate, as well as graduate study.

I would also like to thank the members of my committee, Dr. John Jackson and Dr. Nina Stourman. I am grateful for the aid that Drs. Jackson and Stourman have provided throughout my time at YSU in coursework and in helping refine my thesis. My first teaching experiences were well directed by Dr. Jackson and under his guidance, I was able to sharpen my teaching skills over the past two years. Dr. Stourman has showed me how to improve my professionalism as a chemist and the importance of community involvement in academia. A special thank you is needed for Dr. Matthias Zeller, who has helped in collecting and processing x-ray crystallography data that I bring him, (even when it is hydrated-DCC). All of these individuals have helped inspire me to pursue chemistry at a much deeper and detailed level.

I don't think I would have made the switch to chemistry without my first research experience under Dr. Timothy Wagner. He showed me how much chemistry touched the entire world and the first real research experience I gained in my undergraduate career was one of the driving factors behind my decision to make a career out of chemistry. That being said, the assistance of Ashley Barker (née Wolf) gave me an invaluable

exposure to new ideas about chemistry and positioned me in the direction to get my first hands-on experience with sophisticated instrumentation.

I can say with confidence that the members of the Norris Group have been a grand support system over the years. For lab mates both past and present, graduate and undergraduate, I am extremely thankful for your support.

I would also like to extend my gratitude to Tim Styranec for providing a foundation for proper chemical hygiene and safety within the laboratory. This will prove to be a useful base for my future endeavors.

My wife, Vanessa Tatebe, has supported me in every day of this journey. I am certain that I wouldn't have made it this far without her support. I look forward to spending the rest of our lives together. I would be remiss if I did not thank my parents for encouraging me during my years at YSU. My siblings have been a support system of their own and I couldn't imagine growing up without them.

Thank you to all my family and friends!

Table of Contents

List of Figures

Introduction

Bifunctional Molecules

A growing topic of interest in both chemistry and biology is the application and design of bifunctional molecules. These types of molecules can have multiple interactions with proteins, or other compounds, that would traditionally be impossible to address with a single small molecule. Binding to two different compounds simultaneously has attracted research from many disciplines of science. Bifunctional molecules can be classified by what types of monomers can be linked. When they can dimerize identical proteins, the pieces are identical (homobifunctional); if the pieces are different, they can bond with different proteins (heterobifunctional).[1] Regardless of their classification, bifunctional molecules have been studied extensively for their biochemical properties.[2][3] Heterobifunctional drugs may have been a distant dream in the past, but with advances in chemistry and drug technology there are molecules being synthesized with two different active components. The simple idea behind bifunctional molecules is shown in Figure 1.

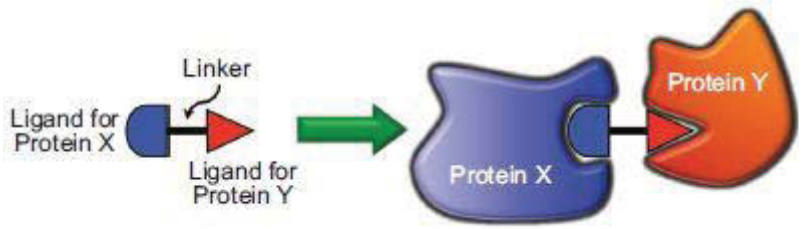

Figure 1: Cartoon depiction of heterobifunctional molecule.

There exists a variety of applications for bifunctional compounds. They have been used as building blocks in studies with hopes of drug discovery and, as with other small molecules, it is sensible to create a diverse library of bifunctional building blocks.[4] Biochemical applications of bifunctional compounds can lead to protein binding or cellular activity that is usually unattainable.[5][6] Bifunctional compounds have been used to build bifunctional catalysts, too. A bifunctional compound can even replace the copper (I) catalyst in click chemistry and still yield the expected click product.[7] Some bifunctional molecules have the potential to be used in medicinal applications.

Prodrugs

While they are not the most common of all pharmaceuticals, prodrugs are still a vital and important part of the biochemical and pharmacological world. At times, they may be referred to as molecules that are "drug-like" or "predrugs." Drug delivery is a major component of drug discovery and research; without any capability to enter the bloodstream, any drug would be useless. When complications in research arise, creative

solutions are needed to find viable methods and prodrugs are an example of these resolutions. Some problems may be as trivial as an unpleasant taste or as severe as a lack of site specificity.[8] In many situations, there have been clever ways to circumvent these issues by using functional groups that alleviate the aforementioned problems.

Although they provide a useful solution, prodrugs were not very common until the 21st century and new ideas, journal articles, and patents involving prodrugs have caused a large surge in the development of these types of drugs. Prodrugs are found annually on the list of best-selling pharmaceutical drugs; two of the largest grossing drugs Plavix and Tamiflu are both categorized as prodrugs. Tamiflu, as any prodrug, is not active until metabolized by the body; once Tamiflu enters the liver, it is converted into its activated form.[9] The drug Plavix requires binding to a specific protein to activate the prodrug, as well. The chemical structures of Plavix and Tamiflu are shown in Figures 2 and 3, respectively.

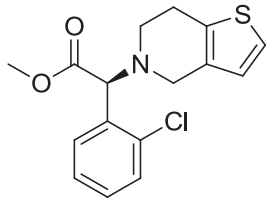

Figure 2: Chemical structure of clopidogrel, commonly known as Plavix.

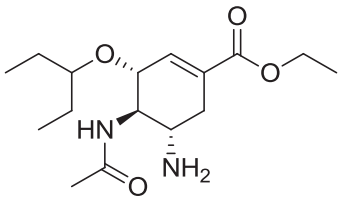

Figure 3: Chemical structure of oseltamivir, commonly known as Tamiflu.

Organic Azides

The use of azides has expanded at a high rate in recent years; their versatility has made them compounds of interest for many applications in synthetic research. An organic azide is classified as any carbon-containing molecule that possesses an N_3 group. As a result of the way charge can build up on an azide, certain azides (like sodium azide or heavy metal azides) are explosive and should be handled with great care. The structure of azide ion is shown in Figure 4.

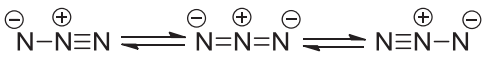

Figure 4: General azide ion, showing resonance structures.

One application of azides is that they can be used as a source of nitrogen in the synthesis of nitrogen-containing compounds. A very common azide source is sodium azide (NaN_3). Alkyl azides can be synthesized by a nucleophilic substitution reaction (S_N2-like), where the azide group replaces a leaving group on a compound. One example of this type of azide application is shown in Equation 1, where a glucosyl bromide is reacted with sodium azide to give inversion at the anomeric carbon, forming a glucosyl azide.[10]

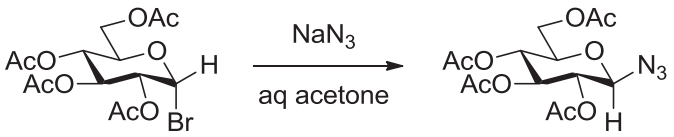

Equation 1: S_N2 inversion during azide formation.

Once they have been isolated and purified, organic azides can be used in further reactions. The versatile azide group can be used in substitution, elimination, addition, or other types of reactions. Its unique properties allow the azide group to have an effect on the reaction pathway and outcome. Azides can additionally be formed by a diazo transfer, where an N_2 group is inserted. [11][14]

Rearrangement Reactions

While there are many different types of predictable organic reactions, the results of rearrangement reactions can be some of the most difficult to anticipate. Rearrangement reactions can be tricky to execute, because they tend to work with specific solvents and specific starting materials. There are quite a few different rearrangement reactions that bear the name of the chemist whom first observed that change. Even though many variations of rearrangement reactions exist, it is necessary to find the conditions that work best for a particular synthetic route.

One of the earliest reported rearrangement reactions is known as the Curtius rearrangement or the Curtius reaction. In this reaction, an acyl azide is converted to an isocyanate, which is a highly-reactive compound. The reactive isocyanate is

subsequently trapped by some nucleophile.[12] The suggested mechanism for the conversion of acyl azide to isocyanate is depicted in Figure 5.

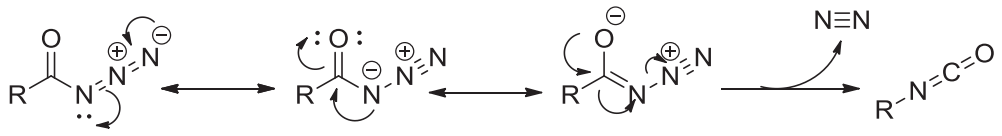

Figure 5: Reaction scheme of the Curtius reaction.

Through this rearrangement, carbamates can be synthesized, following the isocyanate formation. This modification of the Curtius rearrangement gives a stable product and a practical method to prepare carbamate linkages. An example of this reaction scheme involves *tert*-butyl alcohol being added to the isocyanate.[13] A carbamate formation is shown in Figure 6.

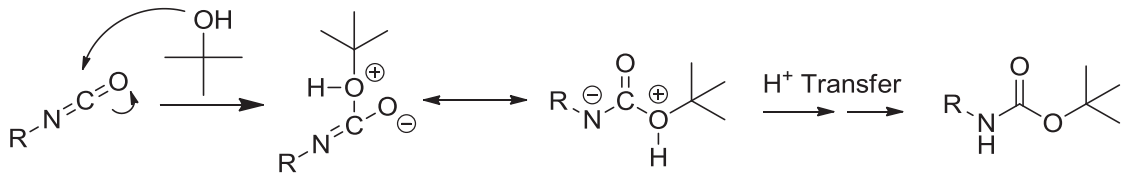

Figure 6: The conversion of isocyanate to carbamate.

Diazocarbonyl Compounds

The diazo functional group is composed of a pair of nitrogen atoms which are double bonded to each other, as well as one of the nitrogen atoms being also bonded to carbon. The general diazo notation is $R_2C{=}N_2$ (Figure 7).[14] Diazo compounds feature a nitrogen atom with a positive charge, while a negative charge is distributed between the other nitrogen and carbon. Compounds such as α-diazoketones and α-diazoesters distribute the negative charge through the carbonyl, which allows them to be more stable than a simple diazo compound. Following the synthesis of a diazo compound, decomposition can take place in the presence of a metal catalyst. This decomposition generates a carbene, which can be subjected to insertion reactions.[14]

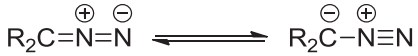

Figure 7: Charge distribution in a generic diazo compound.

The synthesis of diazo compounds can be carried out under acidic or basic conditions. α-Diazocarbonyl compounds have been synthesized by a diazo transfer using tosyl azide and base. An example of this simple transformation is depicted in Equation 2.[15]

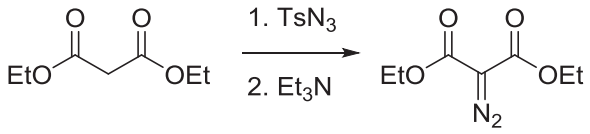

Equation 2: Simple diazo transfer.

In certain situations, a simple diazo transfer may not be feasible. One reason for complications is that some modification might be necessary before a diazo transfer could take place. An example of making modifications to synthesize diazocarbonyl compounds is converting an ester to a β-ketoester before performing a diazo transfer (Scheme 1).[16]

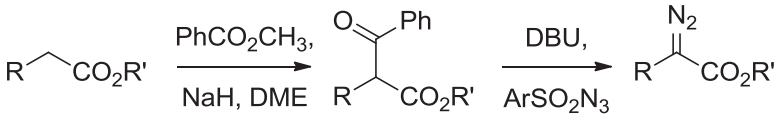

Scheme 1: Modified diazo transfer.

This type of reaction has been a common modification in the past several decades. A variation of this practice has been used to put a diazo group on a carbohydrate platform. By using a protected sugar and esterification of the remaining hydroxyl group allows for subsequent diazo transfer to take place.[17] When a sugar has more than one free hydroxyl group present, as with xylose, additional modifications need to be made to the carbohydrate platform in order to perform a diazo transfer.[18] To show the utility of this variation, two different reactions are presented in Scheme 2 and Scheme 3.

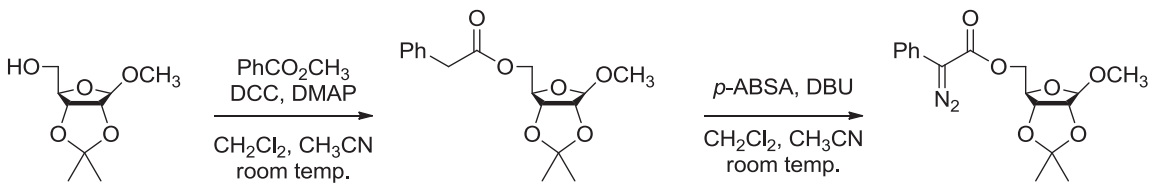

Scheme 2: Modification of ribose to perform diazo transfer.

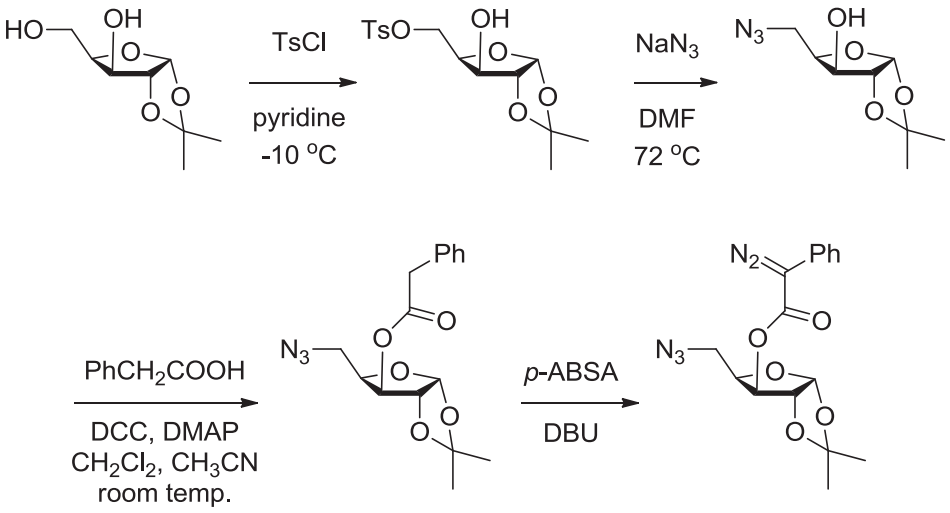

Scheme 3: Modification of xylose derivative to perform diazo transfer.

Diazocarbonyl compounds can be decomposed in the presence of a transition metal catalyst to synthesize macrocycles. A carbene is formed following the loss of N_2. The carbene is stabilized by the transition metal and acts as an electrophile which can react with a variety of different functional groups. Some of these functional groups can be C-H, N-H, O-H, double bonds, or carbonyl groups.[14] These decomposition reactions can lead to products that might not be anticipated. As shown in Equation 3, the decomposition of a diazocarbonyl compound leads to three different compounds.[19]

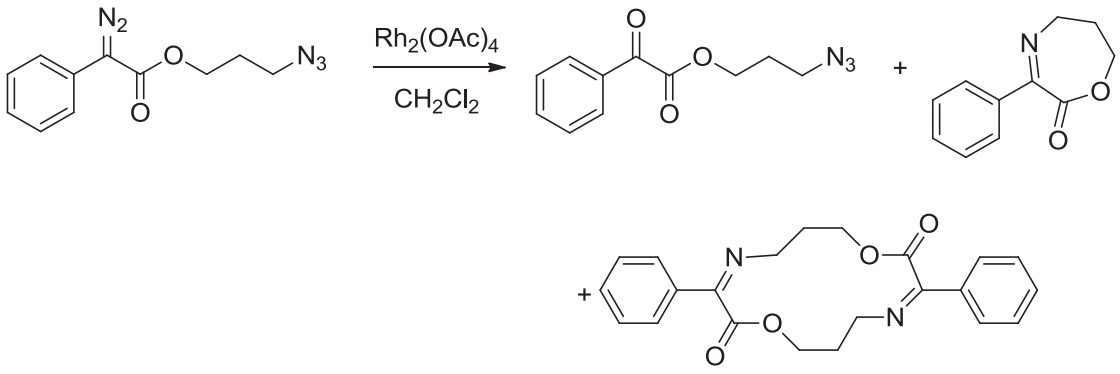

Equation 3: Decomposition of diazocarbonyl compound

The utility of diazocarbonyl decompositions has been noted as a component in the synthesis of prodrugs. A carbene insertion reaction is a key intermediate in the synthesis of novel 2,8-diazaspiro[4.5]decanes; this step of the synthesis is seen in Equation 4.[20]

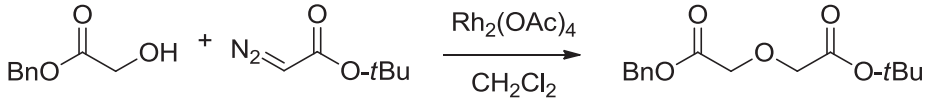

Equation 4: Carbene insertion

There has been research on the decomposition of diazo ester sugars which yields symmetrical ethers.[17] Using a rhodium (II) catalyst these reactions have produced dimeric ethers, as seen in Equation 5 and Equation 6.

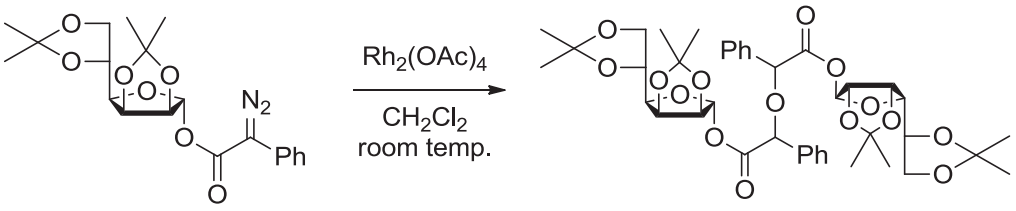

Equation 5: Diazo ester sugar decomposition from ribose

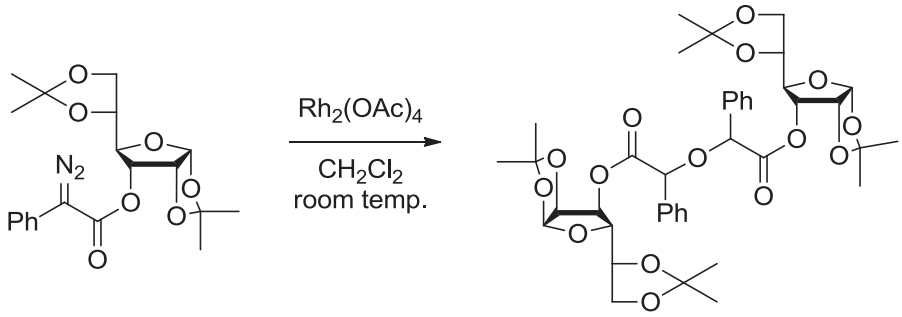

Equation 6: Diazo ester sugar decomposition from allose

Statement of Problem

This research set out to synthesize divalent compounds of potential biological interest. This was accomplished via the linkage of bioactive compounds, such as cholesterol and different sugars, through different functional groups.

Results and Discussion

Sugar-Derived Esters

Synthesis of (3a*R*,5*R*,6*S*,6a*R*)-5-((*R*)-2,2-dimethyl-1,3-dioxolan-4-yl)-2,2-dimethyl tetrahydrofuro[2,3-d][1,3]dioxol-6-yl 2-phenylacetate (2) from di-acetone glucose (1)

(3a*R*,5*R*,6*S*,6a*R*)-5-((*R*)-2,2-dimethyl-1,3-dioxolan-4-yl)-2,2-dimethyltetra hydrofuro[2,3-d][1,3]dioxol-6-yl 2-phenylacetate (**2**) was synthesized from 1,2;5,6-di-*O*-isopropylidene-α-D-glucofuranose (DAG) (**1**) as depicted in Equation 7. DAG and 4-dimethylaminopyridine (DMAP) were dissolved in acetonitrile. After a homogenous solution was obtained, *N,N'*-dicyclohexylcarbodiimide (DCC) was added dropwise to couple DAG with phenyl acetic acid (PAA). The reaction was allowed to stir until formation of **2** was determined by Thin Layer Chromatography (TLC) (via 5% H_2SO_4 staining). Following reaction completion the by-product was filtered off and the filtrate was concentrated under reduced pressure. The crude product was crystallized from hot ethanol; purified **2** was recovered as a colorless crystal in 71% yield.

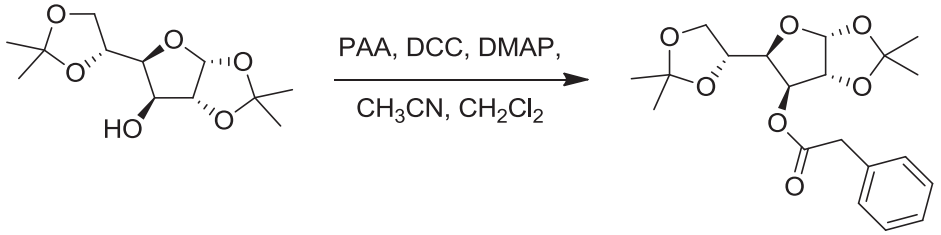

1 **2**

Equation 7

Evidence for the structure **2** was seen in ^{1}H NMR, which showed that both of the isopropylidene protecting groups were still present giving signals in the range from 1.26 to 1.51 ppm. The signal of benzyl –CH_2, which is in α position to carbonyl, is present at 3.67 ppm; this signal with a chemical shift is a result of being in α position to carbonyl, as well as α to the phenyl group. The chemical shift from 3.94 to 4.02 ppm integrates as two protons, which identifies this signal as H-6 and H-6'. With the assistance of correlation spectroscopy (COSY), the multiplet from 4.07 to 4.11 ppm was determined to be the 1H signal for H-5. The signal for H-4 was seen as a 1H doublet of doublets with a J_1 = 3.01 Hz and J_2 = 8.03 Hz. The downward shift is the result of neighboring oxygen. H-2 was found as a 1H doublet at 4.43 ppm with J = 3.5 Hz. H-3 was determined as a 1H doublet at 5.28 ppm with J = 3.0 Hz. The coupling constant of H-3 is identical to the J_1 of H-4, which suggests it is a direct neighbor. H-1 was found to be a 1H doublet at 5.82 ppm with J = 3.5 Hz, which signifies its neighboring proton at H-2. Phenyl protons appear as a 5H multiplet from 7.27 to 7.35 ppm.

The synthesis of ester **2** afforded colorless crystals that were good quality for X-ray diffraction (XRD). Single crystal XRD was successful in providing additional confirmation that phenylacetic acid and di-acetone glucose were coupled to synthesis ester **2**; this structure is seen in Figure 8.

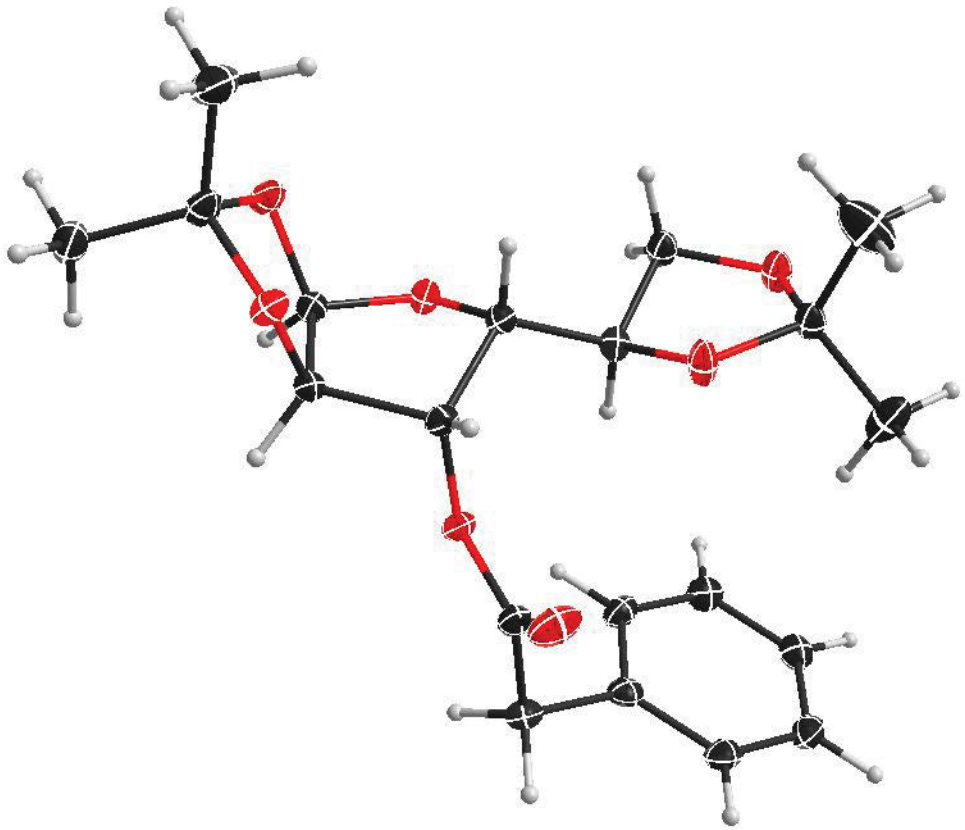

Figure 8: XRD structure of ester **2** at 50% probability

Synthesis of (3a*R*,5*R*,6*S*,6a*R*)-5-((*R*)-2,2-dimethyl-1,3-dioxolan-4-yl)-2,2-dimethyl tetrahydrofuro[2,3-d][1,3]dioxol-6-yl 2-diazo-2-phenylacetate (3) from (2)

In order to synthesize **3**, a diazo transfer was required; this method is shown in Equation 8. Pure **2** was dissolved in minimal amount of acetonitrile and 1,8-diazabicyclo [5.4.0]undec-7-ene (DBU) was the base used, which was added drop-wise to the reaction mixture. The nitrogen source, 4-nitrobenzenesulfonyl azide (*p*-ABSA), was dissolved in methylene chloride and added slowly. Once TLC showed the presence of **3**, the reaction

mixture was washed with diluted H_2SO_4 and the organic layers were rinsed with de-ionized water. After drying over $MgSO_4$, crude **3** was obtained by concentration under reduced pressure. The crude diazo compound was isolated by flash column chromatography (6:1 hexanes : ethyl acetate). Pure **3** was collected as an orange syrup in 33.5% yield. Diazo **3** was stored at -18 ºC until further use.

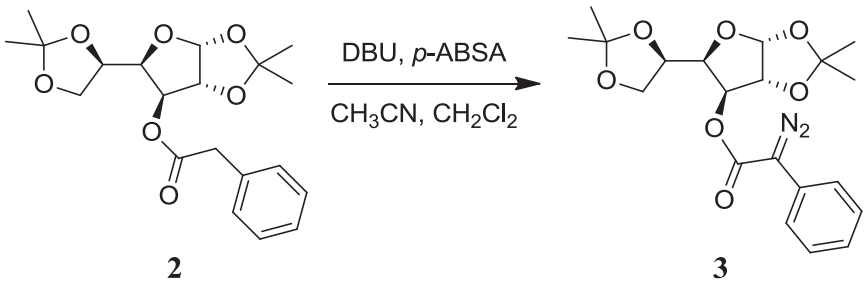

2 **3**

Equation 8

^{1}H NMR showed a chemical shift for the isopropylidene groups to the range of 1.32 to 1.56 ppm. The benzyl –CH_2 group from the ester was no longer present, which suggested that the diazo transfer was successful. This was confirmed by IR signal stretching at 2306.25 and 2093.70 cm^{-1}, which is typical of a diazo group. The two protons of C-6 are inequivalent and are both 1H doublet of doublets; H-6 was seen at 4.03 ppm with J_1 = 4.8 Hz and J_2 = 8.6 Hz, while H-6' was seen at 4.11 ppm with J_1 = 6.1 Hz and J_2 = 8.6 Hz. The matching J_2 coupling constants are what would be expected of geminally-coupled protons. COSY was needed to show that H-5 was the 1H multiplet in the 4.17 to 4.22 ppm range. The chemical shift of H-4 was also identified with the aid of COSY; this signal was seen at 4.27 ppm as a doublet of doublets with J_1 = 3.1 Hz and

J_2 = 8.1 Hz. H-2 was seen as a 1H doublet at 4.68 ppm with J = 3.8 Hz. The chemical shift for H-3 was seen at 5.39 ppm as a 1H doublet with J = 3.1 Hz, which matches J_1 of H-4. The H-1 signal was seen at 5.92 ppm as a 1H doublet with J = 3.6 Hz. The phenyl protons were seen as a 5H multiplet in the range 7.20 to 7.49 ppm. All of the protons exhibited a slight shift downfield following the diazo transfer.

Attempted decomposition of 3

Efforts to decompose **3** by a rhodium(II) catalyzed intramolecular reaction were unsuccessful. Decomposition conditions were modeled after the work of Malich[18] and Sacui.[17] As shown in Equation 9, rhodium(II) acetate was suspended in methylene chloride and **3**, diluted in methylene chloride, was added slowly. Reaction progress was monitored by TLC (2:1 hexanes : ethyl acetate) and the reaction mixture was filtered over celite. The crude reaction mixture was concentrated under reduced pressure and ^{1}H NMR was used for analysis.

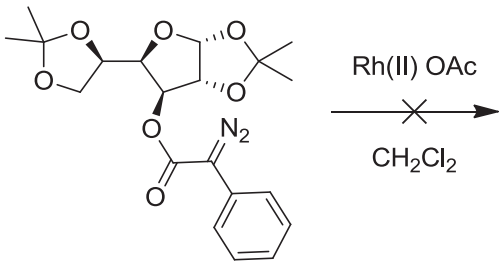

3

Equation 9

After multiple decomposition attempts, ^{1}H NMR spectra showed a mixture of compounds that was very complicated. While efforts to ensure an inert atmosphere were taken, the use of a glove box could have eliminated issues with oxygen entering the atmosphere and altering the reaction outcome. Further complications may have risen from the use of solvent that may have absorbed water, which introduced oxygen to the system. Tracking reaction progress via TLC showed that multiple compounds were present in the reaction mixture.

Synthesis of (3a*R*,5*R*,6*S*,6a*R*)-5-((*R*)-2,2-dimethyl-1,3-dioxolan-4-yl)-2,2-dimethyl tetrahydrofuro[2,3-d][1,3]dioxol-6-yl propionate (4) from DAG (1)

(3a*R*,5*R*,6*S*,6a*R*)-5-((*R*)-2,2-dimethyl-1,3-dioxolan-4-yl)-2,2-dimethyltetrahydro-furo[2,3-d][1,3]dioxol-6-yl propionate (**4**) was synthesized from **1** and propanoic acid. The process for this is seen in Equation 10. DAG, DMAP, and propanoic acid were dissolved in acetonitrile and once a homogenous solution was achieved, DCC was slowly added to the reaction mixture. The reaction mixture was allowed to stir overnight until change was noted by TLC. Unlike the synthesis of other sugar-derived esters (**2**), solid ester **4** was not the product of synthesis. After synthesis and isolating by concentrating under reduced pressure, a white slurry was formed; attempts to crystallize this compound were not successful. Following reaction completion, crude **4** was isolated by flash column chromatography (6:1 hexanes : ethyl acetate) as a colorless oil in 46% yield. Attempts to isolate a crystalline solid were unsuccessful.

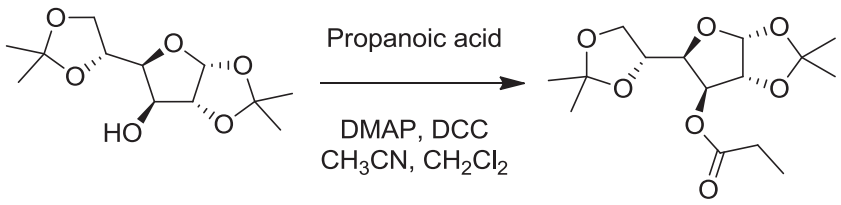

1 **4**

Equation 10

Following purification, **4** was characterized by ^{1}H NMR. The methyl group that is in β position to carbonyl is seen as a 3H triplet at 1.16 ppm with J = 7.7 Hz. The isopropylidene protecting groups appear as 3H singlets in the 1.30 to 1.52 ppm range. In α position to carbonyl –CH_2 group as a 2H doublet of quartets with J_1 = 3.5 Hz and J_2 = 7.6 Hz was identified; this chemical shift was seen at 2.37 ppm. The two protons of C-6 are inequivalent and are seen as two 1H doublet of doublets; H-6 was seen at 4.01 ppm with J_1 = 5.1 Hz and J_2 = 8.6 Hz, while H-6' was seen at 4.08 ppm with J_1 = 5.8 Hz and J_2 = 8.6 Hz. H-2 was seen as a 1H doublet with J = 3.5 Hz. The chemical shift for H-3 was identified at 5.28 ppm with J = 1.5 Hz as a 1H doublet. H-1 was determined to be a 1H doublet with J = 3.5 Hz at 5.88 ppm. H-4 and H-5 were seen as a 2H multiplet at 4.22 ppm. Efforts to perform a diazo transfer with ester **4** were unsuccessful.

Synthesis of (3a*R*,3b*S*,6*S*,6a*S*,7a*R*)-2,2-dimethyl-5-oxohexahydrofuro[2',3':4,5]furo [2,3-d][1,3]dioxol-6-yl 2-phenylacetate (6) from D-glucurono-6,3-lactone acetonide (GLA) (5)

(3a*R*,3b*S*,6*S*,6a*S*,7a*R*)-2,2-dimethyl-5-oxohexahydrofuro[2',3':4,5]furo[2,3-d][1,3] dioxol-6-yl 2-phenylacetate (**6**) from GLA. The synthesis of **6** was similar to the preparation of **2** and is shown in Equation 11. GLA, PAA, and DMAP were dissolved in methylene chloride. DCC was added slowly and the reaction mixture was allowed to stir until there was notable change by TLC. Once it was determined that GLA was consumed, the reaction mixture was quenched with 5% H_2SO_4 and rinsed with de-ionized water. The organic layers were dried over $MgSO_4$ and concentrated under reduced pressure, resulting in a white powder. Crude **6** was crystallized from hot ethanol to give colorless crystals in 87% yield.

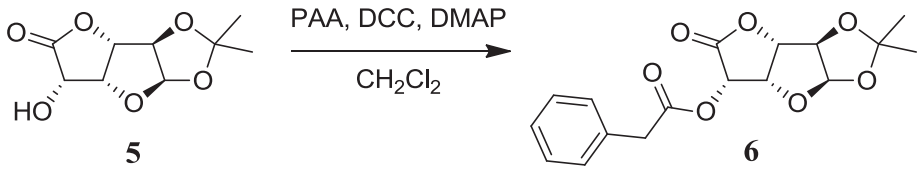

5 **6**

Equation 11

^{1}H NMR and COSY were used to characterize **6**. The isopropylidene protecting group remained intact and was seen as two 3H singlets at 1.34 and 1.50 ppm. The $-CH_2$ that is in α position to both carbonyl and phenyl appears as a 2H doublet with J = 6.5 Hz at 3.81 ppm. The chemical shifts for the phenyl protons are seen as a 5H multiplet in the

range of 7.28 to 7.36 ppm. With the aid of COSY, H-2 was determined as a 1H doublet at 4.83 ppm with $J = 3.8$ Hz. H-3 was seen as a 1H doublet at 4.86 ppm with $J = 3.0$ Hz. The chemical shift for H-4 was identified at 5.05 ppm as a 1H doublet of doublets with $J_1 = 3.4$ Hz and $J_2 = 4.4$ Hz. The proton from C-5 was seen as a 1H doublet at 5.51 ppm with $J = 4.5$ Hz. H-1 was determined to be a 1H doublet at 6.01 ppm with $J = 3.8$ Hz.

Purified **6** produced single crystals that were useful for XRD, which proved the ester coupling was successful; the structure is shown in Figure 9.

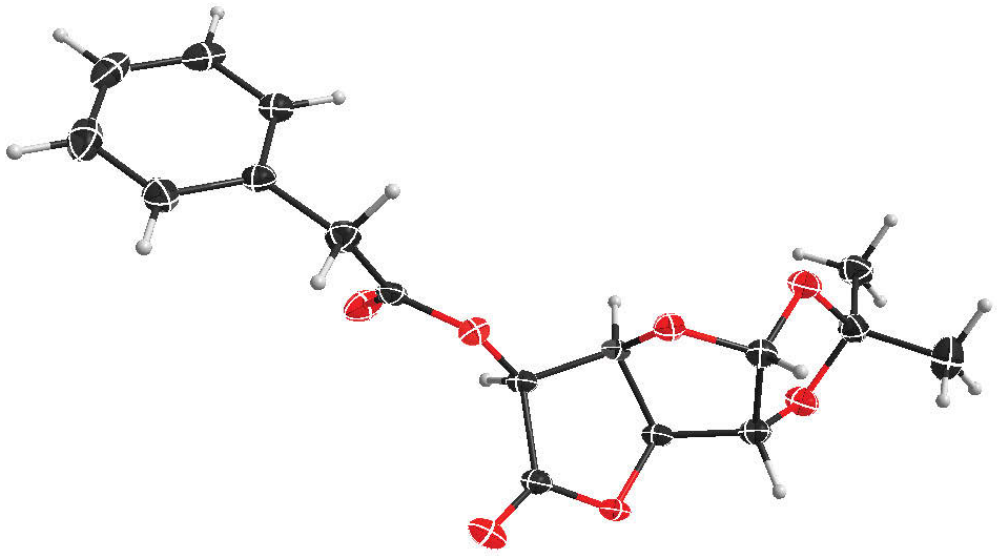

Figure 9: XRD structure of ester **6** at 50% probability

Synthesis of (3a*R*,5*R*,6*S*,6a*R*)-5-((*R*)-2,2-dimethyl-1,3-dioxolan-4-yl)-2,2-dimethyl tetrahydrofuro[2,3-d][1,3]dioxol-6-yl phenylmethanesulfonate (7) from GLA

The preparation of **7** from GLA, as a second type of diazo precursor, did not require the introduction of phenyl acetic acid, so different measures were taken; the reaction is shown in Equation 12. Phenylmethane sulfonyl chloride (PMS) and GLA were dissolved in methylene chloride and allowed to stir to a homogenous mixture. Pyridine was introduced to the reaction mixture and allowed to stir; reaction progress was determined by TLC stained with diluted H_2SO_4. The reaction mixture was quenched with dilute sulfuric acid and rinsed with de-ionized water. The organic extracts were dried over anhydrous $MgSO_4$ and concentrated under reduced pressure. Crude **7** was crystallized from hot ethanol and afforded a colorless crystalline solid in 81% yield.

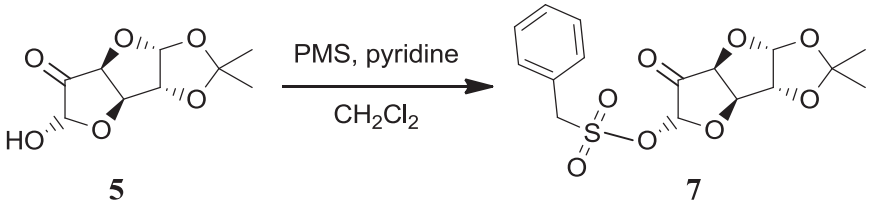

Equation 12

Pure **7** was characterized by COSY and ^{1}H NMR. The isopropylidene groups from GLA were seen as 3H singlets at 1.35 and 1.51 ppm. The only 2H signal seen at 4.64 ppm is a doublet that belongs to the $–CH_2$ group that is in α position to both sulfonyl and phenyl. The doublet has J = 7.0 Hz. H-2 and H-3 were seen as 1H singlets at 4.81

ppm; these peaks were determined by two-dimensional analysis. The chemical shift for H-4 was seen as a 1H multiplet in the range 4.85 to 4.87 ppm. H-5 was seen as a 1H doublet with J = 4.3 Hz at 5.19 ppm. H-1 was seen at 6.03 ppm as a 1H doublet with J = 3.5 Hz. The phenyl protons were seen as a 5H multiplet in the range 7.39 to 7.49 ppm. Following crystallization from hot ethanol, pure **7** was obtained as single crystals that were used for XRD analysis. The XRD data of **7** is seen in Figure 10.

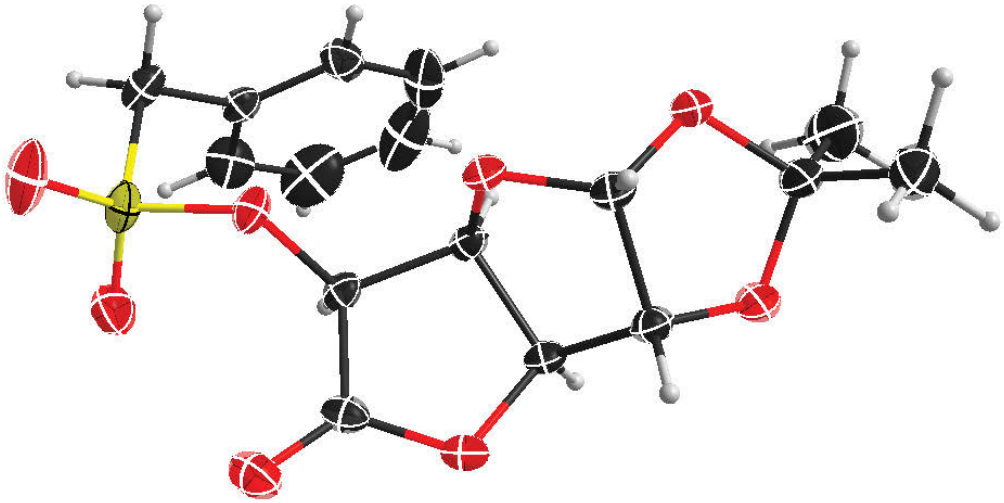

Figure 10: XRD structure of ester **7** at 50% probability

While there were successes in synthesizing sugar-derived esters, the results from the attempted decomposition of diazo ester **3** were not promising, so the focus of research shifted to synthesizing carbamate compounds. Ideally, esters **4**, **6**, and **7** could be converted to diazo esters and further decomposed to attain new compounds.

Carbamate Synthesis

Synthesis of isophthaloyl diazide (9) from isophthaloyl dichloride (8)

The synthesis of **9** was adapted from the work of Davis[21] and shown in Equation 13. Isophthaloyl dichloride was dissolved in acetone and sodium azide suspended in water was added very slowly. This mixture was allowed to stir at 0 ºC for one hour. Crude product was extracted with diethyl ether and the organic extracts were washed with water, saturated sodium carbonate, and saturated sodium chloride. The resulting organic solution was dried over magnesium sulfate and concentrated under reduced pressure. This afforded pure **9** as a colorless crystalline solid in 66% yield.

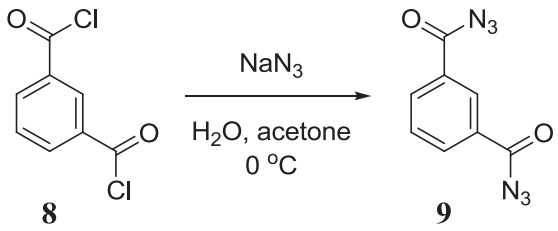

8 **9**

Equation 13

^{1}H NMR and IR were the primary tools to identify the presence of **9**. IR showed that ionic sodium azide was successfully converted to covalently bound azide giving a signal at 2141.27 cm^{-1}. The phenyl protons integrated to a ratio of 1:2:1, which is typical of a *meta*-disubstituted benzene ring. The first 1H chemical shift appears as a triplet at 7.73 ppm with J = 8.0 Hz. This signal corresponds to the phenyl proton which is in

between both substituents. Since **9** is symmetrical, a 2H doublet of doublets was seen at 8.42 ppm with J_1 = 1.9 Hz, J_2 = 8.0 Hz. A 1H triplet was seen at 8.84 ppm with J = 2.2 Hz, which is typical of ortho-coupling in benzene substituents. This proton corresponds with the hydrogen which is located at C-2 of the benzene ring. The synthesis of **9** resulted in copious amounts of colorless crystalline solid that was analyzed by XRD. This data is shown in Figure 11.

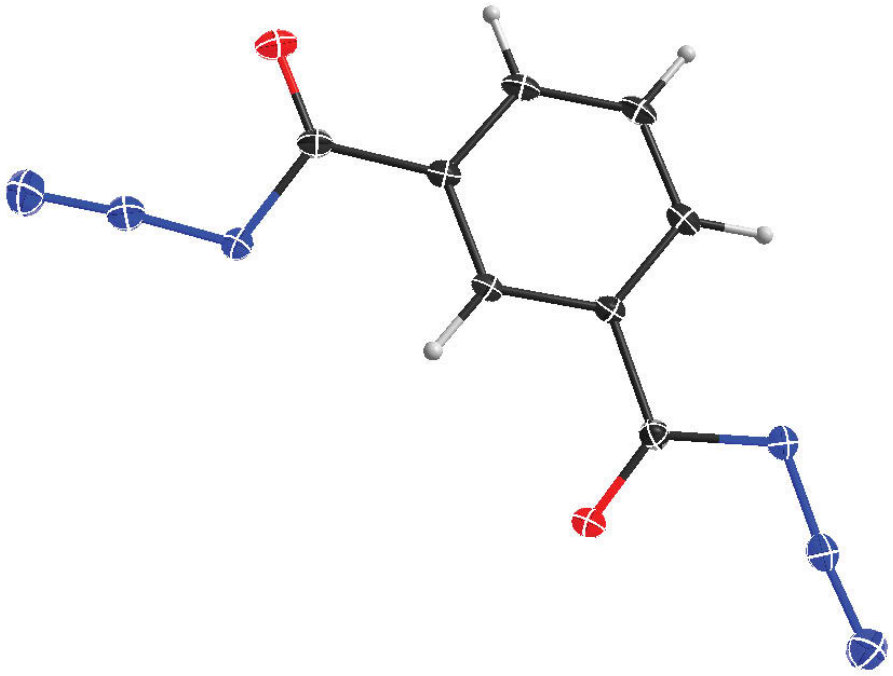

Figure 11: XRD structure of diazide **9** at 50% probability

Synthesis of terephthaloyl diazide (11) from terephthaloyl dichloride (10)

The synthesis of **11** is similar to the preparation of **9** and shown in Equation 14. Terephthaloyl dichloride was dissolved in acetone and sodium azide was suspended in

water added to the mixture over one hour. The product was extracted with diethyl ether and washed with water, sodium carbonate, and sodium chloride. The solution of crude **9** was dried over anhydrous $MgSO_4$ and concentrated under reduced pressure.

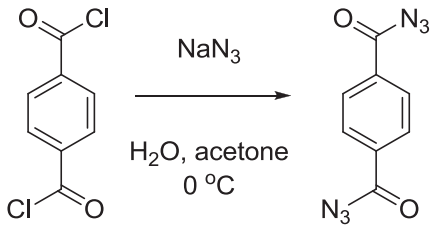

10 **11**

Equation 14

Analysis of ^1H NMR showed that only one type of proton was present. A 4H singlet was seen at 8.25 ppm. IR was vital in confirming the transformation of acyl chloride to acyl azide was successful. IR data exhibited a stretching peak at 2137.60 cm^{-1} , which correlates with covalent azide.

Attempted bis-Curtius synthesis of bis(5-(2,2-dimethyl-1,3-dioxolan-4-yl)-2,2-dimethyltetrahydrofuro[2,3-d][1,3]dioxol-6-yl) 1,3-phenylenedicarbamate (12) from 9

The synthesis of bis(5-(2,2-dimethyl-1,3-dioxolan-4-yl)-2,2-dimethyltetrahydrofuro[2,3-d][1,3]dioxol-6-yl) 1,3-phenylenedicarbamate (**12**) from (**9**) is shown in Equation 15. DAG and **9** were dissolved in toluene and allowed to reflux. Following

reflux, the reaction mixture was concentrated under reduced pressure to yield a yellow syrup.

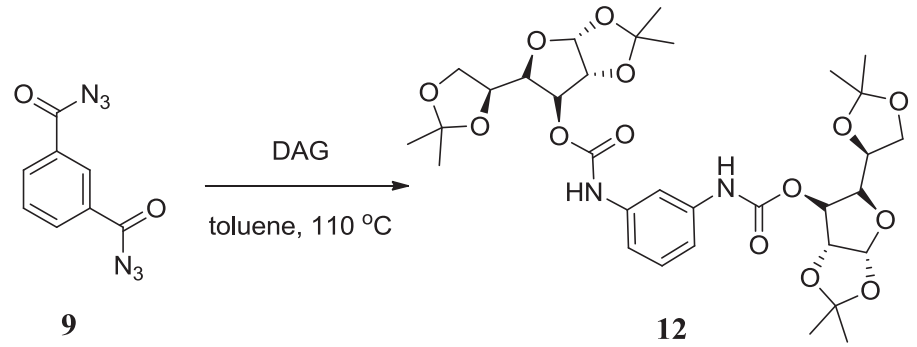

9 **12**

Equation 15

While ^{1}H NMR showed the isopropylidene groups from DAG were still intact, the rest of the spectrum was inconclusive. The phenyl proton region had a complex mixture and the carbohydrate protons also showed signs of molecule decomposition. This was evidence that the carbamate synthesis was unsuccessful.

Synthesis of (8*S*,9*S*,10*R*,13*R*,14*S*,17*R*)-10,13-dimethyl-17-((*R*)-6-methylheptan-2-yl)-2,3,4,7,8,9,10,11,12,13,14,15,16,17-tetradecahydro-1H-cyclopenta[a]phenanthren-3-yl ((8*R*,9*R*,10*S*,13*S*,14*R*,17*S*)-10,13-dimethyl-17-((*S*)-6-methylheptan-2-yl)-2,3,4,7,8,9,10,11,12,13,14,15,16,17-tetradecahydro-1H-cyclopenta[a]phenanthren-3-yl) 1,3-phenylenedicarbamate (13) from 6

(8*S*,9*S*,10*R*,13*R*,14*S*,17*R*)-10,13-dimethyl-17-((*R*)-6-methylheptan-2-yl)-2,3,4,7,8,9,10,11,12,13,14,15,16,17-tetradecahydro-1H-cyclopenta[a]phenanthren-3-yl ((8*R*,9*R*,

10*S*,13*S*,14*R*,17*S*)-10,13-dimethyl-17-((*S*)-6-methylheptan-2-yl)-2,3,4,7,8,9,10,11,12,13, 14,15,16,17-tetra decahydro- 1H-cyclopenta[a]phenanthren-3-yl) 1,3-phenylene dicarbamate (**13**) was synthesized from **9** as shown in Equation 16. After being dissolved in toluene, cholesterol and **9** were refluxed overnight. Once the disappearance of diazide **9** was seen by IR, the reaction mixture was concentrated under reduced pressure.

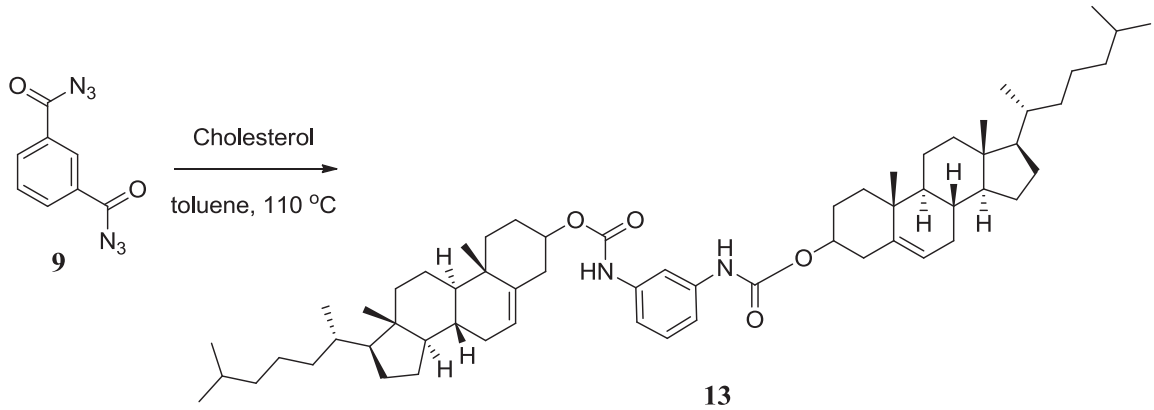

Equation 16

While the complex structure from cholesterol makes characterization difficult, there was evidence from ^{1}H NMR that proved the presence of **13**. The chemical shift of interest is a proton on the carbon where the hydroxyl group would be on cholesterol. Converting the –OH group to –OC(O)NH would cause a shift downfield of that proton signal. In the ^{1}H NMR spectra of cholesterol, the proton from the carbon bonded to the hydroxyl was a 1H multiplet in the range 3.49 to 3.57 ppm. Following reflux and concentration to **13**, it was seen that the carbon now bonded to the carbamate group was seen with a 2H multiplet with a chemical shift in the range 4.55 to 4.63 ppm.

Synthesis of (8*S*,9*S*,10*R*,13*R*,14*S*,17*R*)-10,13-dimethyl-17-((*R*)-6-methylheptan-2-yl)-2,3,4,7,8,9,10,11,12,13,14,15,16,17-tetradecahydro-1H-cyclopenta[a]phenanthren-3-yl ((8*R*,9*R*,10*S*,13*S*,14*R*,17*S*)-10,13-dimethyl-17-((*S*)-6-methylheptan-2-yl)-2,3,4,7,8,9,10,11,12,13,14,15,16,17-tetradecahydro-1H-cyclopenta[a]phenanthren-3-yl) 1,4-phenylenedicarbamate (14) from 11

Similar to the synthesis of **14**, cholesterol and **11** were dissolved in toluene and refluxed overnight, as shown in Equation 17. After reflux, the reaction was concentrated under reduced pressure.

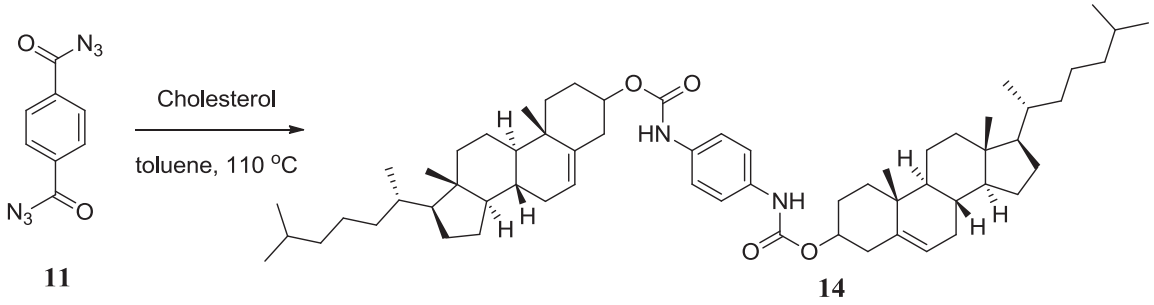

11 **14**

Equation 17

From examination of ^{1}H NMR, it was determined that the carbon containing the hydroxyl group had a shift downfield similar as with the synthesis of **13**. The chemical shift was seen as a 2H multiplet in the range 4.56 to 4.63 ppm, which indicates that the hydroxyl group has been converted to a carbamate group.

Attempted synthesis of ((3a*R*,5*R*,6*S*,6a*R*)-6-hydroxy-2,2-dimethyltetrahydrofuro [2,3-d][1,3]dioxol-5-yl)methyl (((3a*S*,5*S*,6*R*,6a*S*)-6-hydroxy-2,2-dimethyltetrahydro furo[2,3-d][1,3]dioxol-5-yl)methyl) 1,3-phenylenedicarbamate (15) from 9

The attempted bis-Curtius rearrangement with 1,2-*O*-Isopropylidene-α-D-xylo furanose or monoacetate xylose (MAX) and **9** is shown in Equation 18. As with other carbamate syntheses, MAX and **9** were dissolved in toluene and allowed to reflux overnight. After reflux, the reaction mixture was concentrated under reduced pressure to yield a colorless syrup.

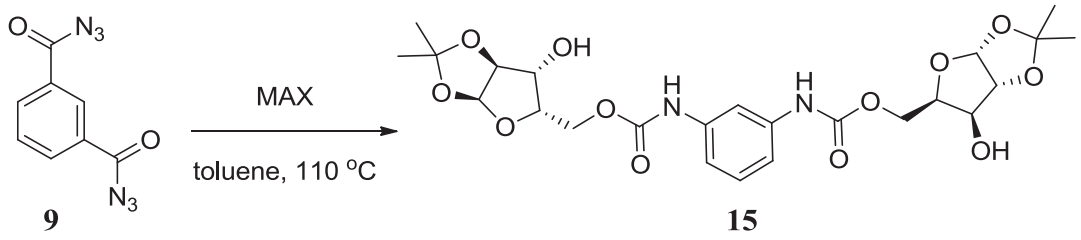

9 **15**

Equation 18

From the ^{1}H NMR, it was determined that benzyl proton region was a complex mixture, which suggests that product decomposition took place. The carbohydrate protons from MAX were seen without any change in their chemical shift, which also indicates there was no change to the chemical structure of the sugar.

Attempted synthesis of ((3a*R*,5*R*,6*S*,6a*R*)-6-hydroxy-2,2-dimethyltetrahydrofuro [2,3-d][1,3]dioxol-5-yl)methyl (((3a*S*,5*S*,6*R*,6a*S*)-6-hydroxy-2,2-dimethyltetrahydro furo[2,3-d][1,3]dioxol-5-yl)methyl) (16) 1,4-phenylenedicarbamate from 11

The attempted synthesis of **16** is seen in Equation 19. MAX and **11** were refluxed in toluene overnight, while monitoring the presence of **11** by IR.

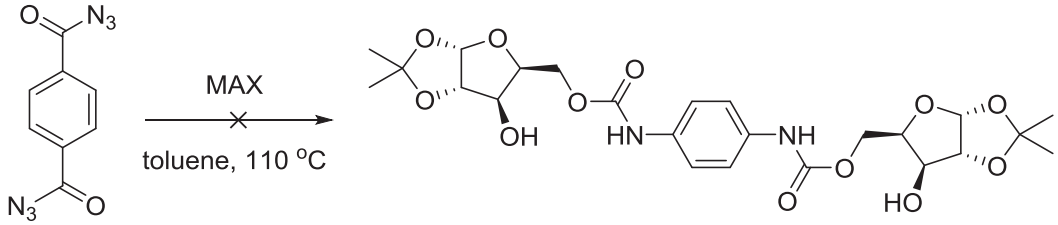

11 **16**

Equation 19

Analysis of ^{1}H NMR showed that no reaction took place, as the proton signals of MAX had no change. It was difficult to determine what was in solution, because TLC was not useful for this reaction. This was a result of diazide **11** degrading on the silica backing of the TLC plates. IR showed that there was no longer covalently bound azide starting material present in the solution, but ^{1}H NMR showed that the starting sugar signals had not been changed by the reaction process.

In conclusion, the synthesis of sugar-derived esters **2**, **4**, **6**, and **7** was successfully executed. Ideally, these esters could be used to synthesize diazo esters, but the conversion of ester to diazo ester was only attained in the synthesis of ester **2** to diazo ester **3**. In addition to these sugar-derived esters, some carbamate compounds were synthesized from diazides. The synthesis of **13** and **14** showed that two components can be linked through a similar process and this could be carried out with different compounds in the future.

Experimental

General Methods

All reactions were monitored using TLC and ultraviolet light detection with reaction materials that are UV-active. For some compounds, treating the TLC plates with a 5% sulfuric acid/ethanol solution was used to aid in determining reaction progress. Product isolation was done using flash column chromatography performed with 32-63 μm, 60-Å silica gel. Bruker Avance II/III 400 MHz Nuclear Magnetic Resonance (NMR) instruments with TOPSPIN software were used for ^{1}H and ^{13}C spectroscopy, using $CDCl_3$ as solvent. Proton and carbon chemical shifts are reported in parts per million (ppm). Splitting patterns of multiplets are labeled s (singlet), d (doublet), dd (doublet of doublets), ddd (doublet of doublet of doublets), t (triplet), q (quartet), and m (multiplet) with coupling constants measured in Hertz (Hz). A Thermo Electron Corporation IR 200 Infrared spectrometer was also utilized for additional analysis. The solid-state crystal structures of select compounds were determined by XRD using a Bruker-Nonius SMART APEX CCD diffractometer and a Bruker AXS Prospector CCD diffractometer with I-mu-S microsource X-ray tube and laterally graded multilayer (Goebel) mirror for creation of monochromatic Cu-K alpha X-radiation. XRD data was visualized using Shelxle software.

Sugar-Derived Ester Synthesis

Preparation of (3a*R*,5*R*,6*S*,6a*R*)-5-((*R*)-2,2-dimethyl-1,3-dioxolan-4-yl)-2,2-dimethyl tetrahydrofuro[2,3-d][1,3]dioxol-6-yl 2-phenylacetate (2) from DAG (1)

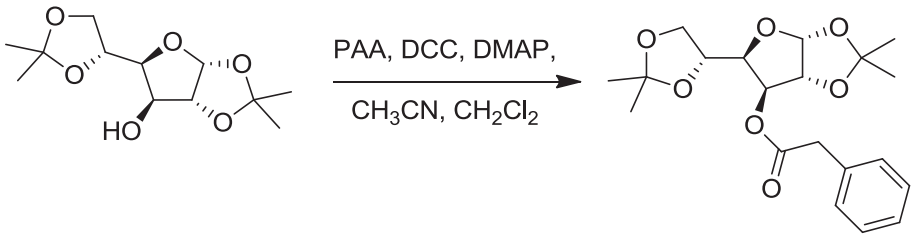

1 **2**

In a dry, clean 500 mL round bottom flask equipped with a magnetic stirring bar, DAG, **1**, (40 mmol, 10.40 g) and PAA (59 mmol, 7.98 g) was dissolved in 200 mL acetonitrile/methylene chloride and allowed to stir. Once a homogenous solution was achieved, 2.75 g DMAP was added to the mixture and allowed to dissolve. In a drop-wise manner, 55 mL of 1.0 M solution of DCC in CH_2Cl_2 was added to the reaction mixture and allowed to stir overnight. Reaction progress was monitored by TLC in 3:1 hexanes:ethyl acetate (H:EA). After 12 hours, the by-product was filtered off and crude **2** was isolated by concentration under reduced pressure. Crude ester **2** was recrystallized from hot ethanol, affording a colorless crystalline solid in 71% yield.

^{1}H NMR (400 MHz, $CDCl_3$): δ 1.26 (s, 3H, -CH_3), 1.28 (s, 3H, -CH_3), 1.39 (s, 3H, -CH_3), 1.51 (s, 3H, -CH_3), 3.67 (s, 2H, benzyl-CH_2), 3.94-4.02 (m, 2H, H-6, H-6'), 4.07-4.11 (m,

1H, H-5), 4.18 (dd, 1H, H-4, *J* = 3.0 Hz, 8.0 Hz), 4.43 (d, 1H, H-2, *J* = 3.5 Hz), 5.28 (d, 1H, H-3, *J* = 3.0 Hz), 5.82 (d, 1H, H-1, *J* = 3.5 Hz), 7.27-7.35 (m, 5H, phenyl).

^{13}C NMR (100 MHz, $CDCl_3$): δ 25.15, 26.18, 26.71, 26.78, 41.34, 67.20, 72.24, 76.35, 79.90, 83.21, 105.02, 109.30, 112.31, 127.31, 128.65, 129.19, 133.37, 170.12.

Melting Point: 63 ºC

Preparation of (3a*R*,5*R*,6*S*,6a*R*)-5-((*R*)-2,2-dimethyl-1,3-dioxolan-4-yl)-2,2-dimethyl tetrahydrofuro[2,3-d][1,3]dioxol-6-yl 2-diazo-2-phenylacetate (3) from 2

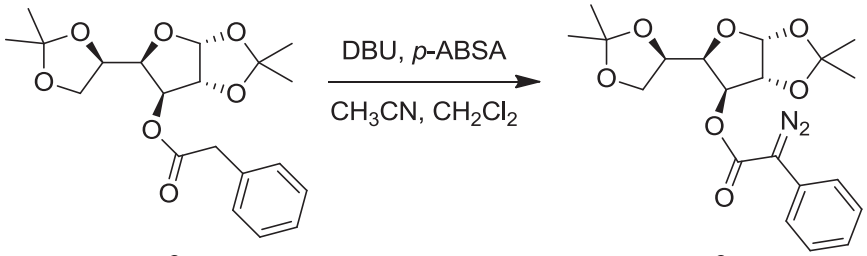

2 **3**

Diazo ester **3** was synthesized by dissolving ester **2** (1 mmol, 0.40 g) in 5 mL acetonitrile. The mixture was allowed to stir and DBU (1.3 mmol, 0.20 mL) was added to the reaction flask. Following introduction of base, *p*-ABSA (1 mmol, 0.24 g) was dissolved in a minimal volume of methylene chloride and added drop-wise to the solution. The diazo transfer was tracked using TLC in 3:1 (hexanes : ethyl acetate). The

solution of crude diazo compound was washed with dilute sulfuric acid (2 × 15 mL) and the resulting organic layer was rinsed with de-ionized water (2 × 15 mL). The solution was dried over anhydrous magnesium sulfate and concentrated under reduced pressure. Crude **3** was isolated by flash column chromatography in a 6:1 (hexanes : ethyl acetate) system, resulting in an orange syrup.

^{1}H NMR (400 MHz, $CDCl_3$): δ 1.26 (s, 6H, -CH_3), 1.32 (s, 3H, -CH_3), 1.35 (s, 3H, -CH_3), 4.03 (dd, 1H, H-6, *J* = 4.8 Hz, 8.6 Hz), 4.11 (dd, 1H, H-6', *J* = 6.1 Hz, 8.6 Hz), 4.17-4.22 (m, 1H, H-5), 4.27 (dd, 1H, H-4, *J* = 3.1 Hz, 8.1 Hz), 4.68 (d, 1H, H-2 *J* = 3.8 Hz), 5.39 (d, 1H, H-3, *J* = 3.1 Hz), 5.92 (d, 1H, H-1, *J* = 3.6 Hz), 7.20-7.49 (m, 5H, phenyl).

^{13}C NMR (100 MHz, $CDCl_3$): δ 25.19, 26.24, 26.75, 26.86, 67.42, 72.57, 79.94, 83.48, 105.09, 109.49, 112.38, 124.12, 124.88, 126.25, 129.06, 163.79.

IR absorption (selected peaks): 2093.70, 2306.25 cm^{-1} (diazo group).

Attempted decomposition of diazo ester 3

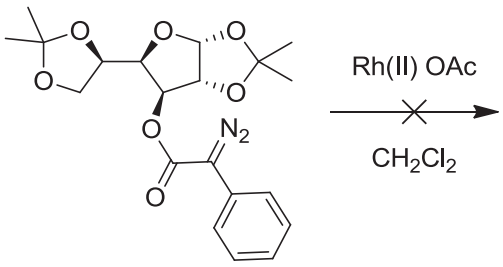

3

A decomposition of diazo ester **3** was attempted by suspending 15 mg of rhodium (II) acetate in 3 mL of dichloromethane in a clean and dry round bottom flask. 0.10 g of purified **3** was dissolved in minimal dichloromethane and added drop-wise to the flask. The reaction progress was monitored by TLC in 2:1 (hexanes : ethyl acetate). After 48 hours, the reaction mixture was filtered over celite and concentrated under reduced pressure. Analysis for TLC indicated that multiple compounds were present in the reaction mixture. From ^{1}H NMR, it was determined that decomposition was not successful and a complex mixture was present in solution.

Preparation of (3a*R*,5*R*,6*S*,6a*R*)-5-((*R*)-2,2-dimethyl-1,3-dioxolan-4-yl)-2,2-dimethyl tetrahydrofuro[2,3-d][1,3]dioxol-6-yl propionate (4) from 1

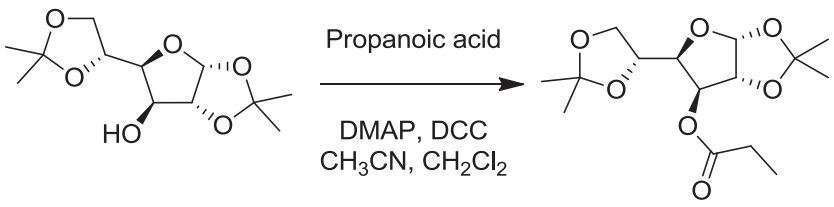

1 **4**

In a dry, clean 200 mL round bottom flask, **1** (19.23 mmol, 5.00 g) and 1.4 g DMAP were dissolved in 30 mL acetonitrile and allowed to stir. To the homogenous solution, propanoic acid (25 mmol, 1.87 mL) was added and allowed to stir. In a drop-wise manner, 25 mL of DCC (1 M in CH_2Cl_2) was added to the reaction mixture and allowed to stir overnight. Reaction progress was monitored by TLC in 3:1 (hexanes : ethyl acetate) and stained with 5% sulfuric acid. After 16 hours, the by-product was filtered off and ester **4** was obtained by concentrating under reduced pressure.

^{1}H NMR (400 MHz, $CDCl_3$): δ 1.16 (t, 3H, -CH_3, *J* = 7.7 Hz), 1.30 (s, 3H, -CH_3), 1.31 (s, 3H, -CH_3), 1.41 (s, 3H, -CH_3), 1.52 (s, 3H, -CH_3), 2.37 (dq, 2H, -CH_2, *J* = 3.5 Hz, 7.6 Hz), 4.01 (dd, 1H, H-6, *J* = 5.1 Hz, 8.6 Hz), 4.08 (dd, 1H, H-6', *J* = 5.8 Hz, 8.6 Hz), 4.22 (m, 2H, H-4, H-5), 4.49 (d, 1H, H-2, *J* = 3.5 Hz), 5.28 (d, 1H, H-3, *J* = 1.5 Hz), 5.88 (d, 1H, H-1, *J* = 3.5 Hz).

^{13}C NMR (100 MHz, $CDCl_3$): δ 9.02, 25.29, 26.23, 26.77, 26.83, 27.59, 67.30, 72.51, 75.95, 79.93, 83.46, 105.11, 109.32, 112.28, 172.97.

Preparation of (3a*R*,3b*S*,6*S*,6a*S*,7a*R*)-2,2-dimethyl-5-oxohexahydrofuro[2',3':4,5] furo[2,3-d][1,3]dioxol-6-yl 2-phenylacetate (6) from GLA (5)

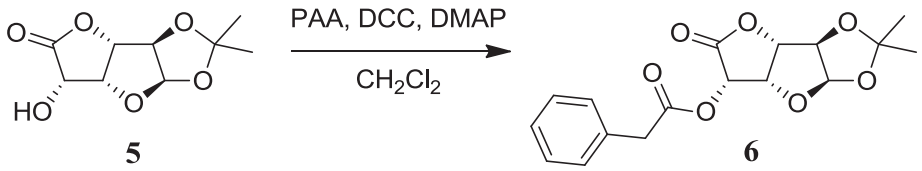

5 **6**

In a dry 250 mL round bottom flask, **5** (15 mmol, 3.24 g), phenyl acetic acid (15 mmol, 2.04 g), and 2.50 g DMAP were dissolved in 25 mL methylene chloride and allowed to stir. In a drop-wise manner, 15 mmol of DCC (1 M in CH_2Cl_2) was added to the reaction mixture and allowed to stir for three hours. Reaction progress was monitored by TLC 1:1 (hexanes : ethyl acetate) and staining with diluted sulfuric acid solution. The reaction mixture was washed with 5% sulfuric acid (2 × 20 mL), and the resulting organic layers were rinsed with de-ionized water (2 × 25 mL). The solution of crude product was dried over anhydrous magnesium sulfate and concentrated under reduced pressure. The resulting ester **6** was crystalized with hot ethanol, yielding colorless crystals.

^{1}H NMR (400 MHz, $CDCl_3$): δ 1.34 (s, 3H, -CH_3), 1.50 (s, 3H, -CH_3), 3.81 (d, 2H, -CH_2, J = 6.5 Hz), 4.83 (d, 1H, H-2, J = 3.8 Hz), 4.86 (d, 1H, H-3, J = 3.0 Hz), 5.05 (dd, 1H, H-4, J = 3.4 Hz, 4.4 Hz), 5.51 (d, 1H, H-5, J = 4.5 Hz), 6.01 (d, 1H, H-1, J = 3.8 Hz), 7.28-7.36 (m, 5H, benzene).

^{13}C NMR (100 MHz, $CDCl_3$): δ 26.53, 26.90, 40.20, 70.07, 76.99, 82.26, 82.60, 107.00, 113.54, 127.44, 128.88, 129.45, 132.76, 169.48, 170.52.

Melting Point: 214 ºC

Preparation of (3a*R*,5*R*,6*S*,6a*R*)-5-((*R*)-2,2-dimethyl-1,3-dioxolan-4-yl)-2,2-dimethyl tetrahydrofuro[2,3-d][1,3]dioxol-6-yl phenylmethanesulfonate (7) from GLA (5)

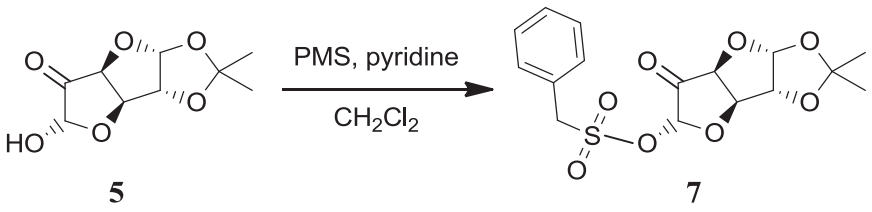

5 **7**

In a dry 100 mL round bottom flask, **5** (25 mmol, 5.40 g) and phenylmethanesulfonyl chloride (PMS) (25 mmol, 4.78 g) were dissolved in 30 mL methylene chloride and allowed to stir. Once a homogenous mixture was obtained, pyridine (27.2 mmol, 2.2 mL)

was added to the reaction flask and allowed to stir overnight. Reaction progress was monitored by TLC in 1:1 (hexanes : ethyl acetate). Following stirring, the reaction mixture was washed with 5% sulfuric acid (3 × 30 mL), and the resulting organic layers were rinsed with de-ionized water (2 × 20 mL). The solution of crude **7** was dried over anhydrous magnesium sulfate and concentrated under reduced pressure. This process resulted in 7.48 g of colorless crystals in 80.8% yield.

^{1}H NMR (400 MHz, $CDCl_3$): δ 1.35 (s, 3H, -CH_3), 1.51 (s, 3H, -CH_3), 4.64 (d, 2H, -CH_2, J = 7.0 Hz), 4.81 (s, 1H, H-2), 4.81 (s, 1H, H-3), 4.85-4.87 (m, 1H, H-4), 5.19 (d, 1H, H-5, J = 4.3 Hz), 6.03 (d, 1H, H-1, J = 3.5 Hz), 7.39-7.49 (m, 5H, aryl).

^{13}C NMR (100 MHz, $CDCl_3$): δ 26.54, 26.88, 58.61, 74.90, 82.20, 82.46, 107.11, 113.70, 126.90, 129.02, 129.37, 131.04, 168.29.

Melting Point: 167 ºC

Carbamate Synthesis

Preparation of isophthaloyl azide (9) from isophthaloyl dichloride (8)

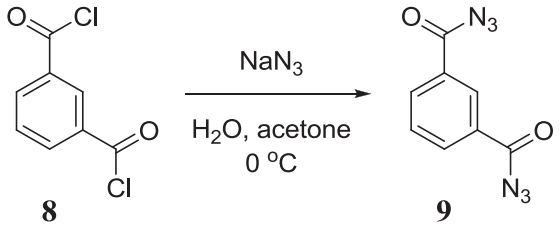

8 **9**

To a 200 mL round bottom flask, isophthaloyl dichloride (24.6 mmol, 5.00 g) was dissolved in 50 mL acetone and cooled to 0 °C. Sodium azide (76.9 mmol, 5.00 g) was suspended in 50 mL water and added to the round bottom flask by addition funnel over 45 minutes at 0 °C. Following the addition of azide, the reaction was allowed to stir for an additional hour. Diethyl ether (2 × 50 mL) was used to extract the reaction mixture. The organic layers were washed with de-ionized water (1 × 30 mL) and saturated sodium carbonate (1 × 30 mL). The organic extracts were rinsed with saturated NaCl (1 × 30 mL) and dried over anhydrous $MgSO_4$. The solution of diazide **9** was concentrated under reduced pressure and led to a colorless crystalline solid in 66% yield.

^{1}H NMR (400 MHz, $CDCl_3$): δ 7.73 (t, 1H, phenyl, J = 8.0 Hz), 8.42 (dd, 2H, phenyl, J = 1.9 Hz, 8.0 Hz), 8.84 (t, 1H, phenyl, J = 2.2 Hz).

^{13}C NMR (100 MHz, $CDCl_3$): δ 129.60, 135.31, 171.63.

IR absorption (selected peaks): 2141.27 cm^{-1} (covalent azide).

Preparation of terephthaloyl azide (11) from terephthaloyl dichloride (10)

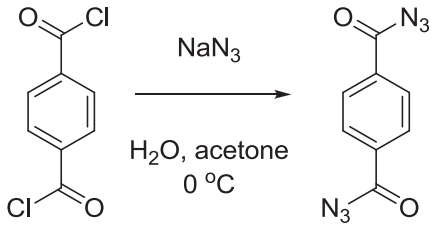

10 **11**

In a 200 mL round bottom flask, terephthaloyl dichloride (24.6 mmol, 5.00 g) was dissolved in 50 mL acetone at 0 °C. Sodium azide (76.9 mmol, 5.00 g) was suspended in 50 mL water and added to the round bottom flask by addition funnel over 45 minutes at 0 °C. Following the addition of azide, the reaction was allowed to stir for an additional hour. Diethyl ether (2 × 50 mL) was used to extract the reaction mixture. The organic layers were washed with de-ionized water (1 × 30 mL) and saturated sodium carbonate (1 × 30 mL). The organic extracts were rinsed with saturated NaCl (1 × 30 mL) and dried over anhydrous $MgSO_4$. The solution was concentrated under reduced pressure and led to **11** as a brown powder.

^{1}H NMR (400 MHz, $CDCl_3$): δ 8.11 (s, phenyl).

^{13}C NMR (100 MHz, $CDCl_3$): δ 129.61, 135.31, 171.63.

IR absorption (selected peaks): 2137.60 cm^{-1} (covalent azide).

Attempted preparation of bis(5-(2,2-dimethyl-1,3-dioxolan-4-yl)-2,2-dimethyltetra hydrofuro[2,3-d][1,3]dioxol-6-yl) 1,3-phenylenedicarbamate (12) from 9

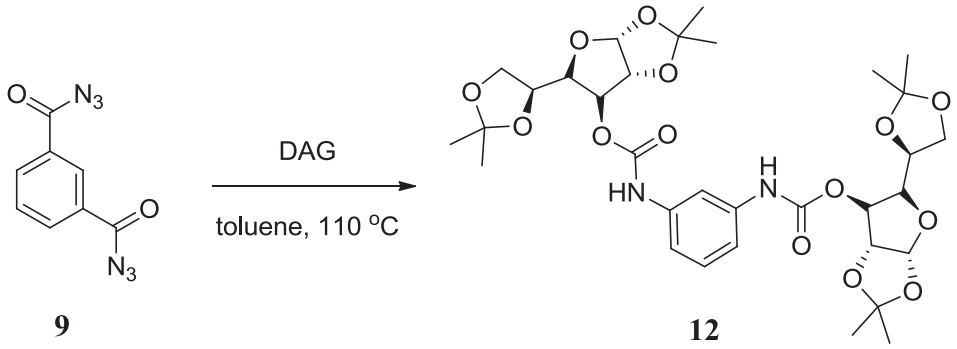

9 **12**

In a 25 mL round bottom flask, **1** (2.0 mmol, 0.52 g) and diazide **9** (1.5 mmol, 0.32 g) were dissolved in 5 mL toluene. The reaction mixture was allowed to reflux at 110 ºC for 8 hours. Reaction progress was monitored by TLC (1:1 hexanes : ethyl acetate). Diazide **9** seemed to break-down on silica gel, so TLC was not the ideal means of monitoring reaction progress, so IR was utilized to determine if any azide stretching

peaks were present in solution. After reflux, the reaction mixture was cooled to room temperature and isolated by concentrating under reduced pressure. The crude solution afforded a brown syrup. ^{1}H NMR showed that **1** and diazide **9** did not appear to react with each other and the synthesis of **12** was not successful.

Preparation of (8*S*,9*S*,10*R*,13*R*,14*S*,17*R*)-10,13-dimethyl-17-((*R*)-6-methylheptan-2-yl)-2,3,4,7,8,9,10,11,12,13,14,15,16,17-tetradecahydro-1H-cyclopenta[a]phenanthren-3-yl ((8*R*,9*R*,10*S*,13*S*,14*R*,17*S*)-10,13-dimethyl-17-((*S*)-6-methylheptan-2-yl)-2,3,4,7,8,9,10,11,12,13,14,15,16,17-tetradecahydro-1H-cyclopenta[a]phenanthren-3-yl) 1,3-phenylenedicarbamate (13) from 9

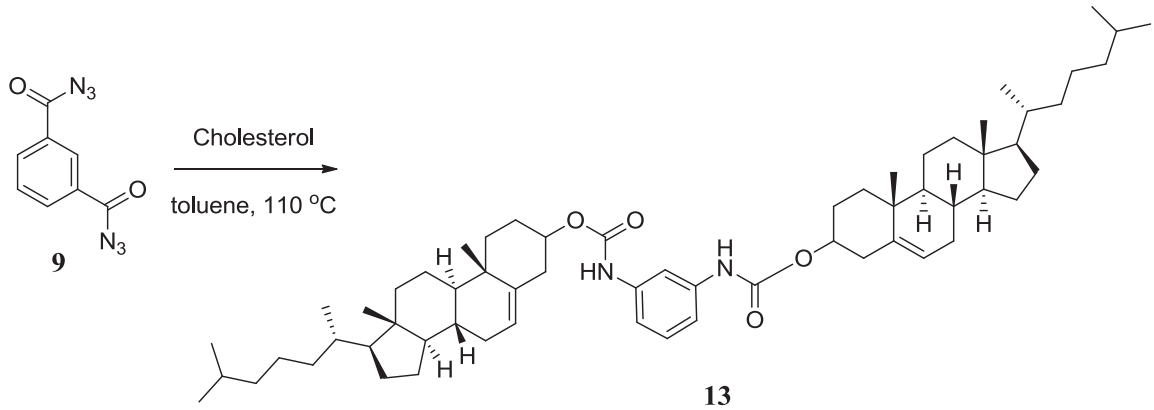

9 **13**

Cholesterol (2.0 mmol, 0.27 g) and diazide **9** (2.0 mmol, 0.43 g) were dissolved in 5 mL toluene. The reaction mixture was allowed to reflux at 110 ºC for 18 hours. IR was used to monitor reaction progress. Once the presence of azide disappeared, the reaction

was cooled to room temperature and concentrated under reduced pressure. Crude **13** yielded a colorless powder. Efforts of crystallization were unsuccessful.

^{1}H NMR (400 MHz, $CDCl_3$): δ 0.68 (s, 6H, -CH_3), 0.86 (d, 6H, -CH_2), 0.88 (d, 6H, -CH_2), 0.92 (d, 6H, -CH), 1.02 (s, 6H, -CH_3), 1.08-1.66 (m, 40H, alkyl), 1.79-2.03 (m, 11H, alkyl), 2.36 (s, 5H, alkyl), 2.40-2.44 (m, 2H, alkyl), 4.55-4.63 (m, 2H), 5.38-5.41 (m, 2H, alkene), 7.06 (t, 2H, aryl, J = 10.4 Hz), 7.21 (t, 1H, aryl, J = 4.05 Hz), 7.24 (t, 1H, aryl, J = 2.75 Hz), 7.55 (bs, 2H, -NH).

^{13}C NMR (100 MHz, $CDCl_3$): δ 11.89, 18.75, 19.35, 21.09, 22.57, 22.82, 23.87, 24.32, 28.04, 28.25, 31.92, 35.82, 36.23, 36.62, 38.45, 39.95, 39.79, 42.36, 50.07, 56.21, 56.74, 75.06, 113.27, 122.77, 129.60, 138.84, 139.65, 152.95.

Preparation of (8*S*,9*S*,10*R*,13*R*,14*S*,17*R*)-10,13-dimethyl-17-((*R*)-6-methylheptan-2-yl)-2,3,4,7,8,9,10,11,12,13,14,15,16,17-tetradecahydro-1H-cyclopenta[a]phenanthren-3-yl ((8*R*,9*R*,10*S*,13*S*,14*R*,17*S*)-10,13-dimethyl-17-((*S*)-6-methylheptan-2-yl)-2,3,4,7,8,9,10,11,12,13,14,15,16,17-tetradecahydro-1H-cyclopenta[a]phenanthren-3-yl) 1,4-phenylenedicarbamate (14) from (11)

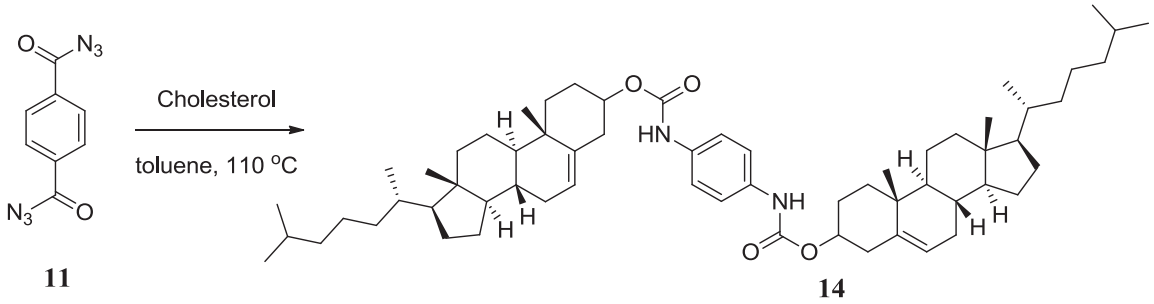

11 **14**

In a 25 mL round bottom flask, cholesterol (2.0 mmol, 0.27 g) and **9** (1.5 mmol, 0.32 g) were dissolved in 5 mL toluene. The reaction mixture was allowed to reflux at 110 ºC for 18 hours. IR was used to monitor reaction progress. After reflux, the reaction was cooled to room temperature and concentrated under reduced pressure. Crude **13** was collected as a colorless solid. Attempts at crystallization were unsuccessful.

^{1}H NMR (400 MHz, $CDCl_3$): δ 0.68 (s, 6H, -CH_3), 0.87 (dd, 12H, -CH_3, J = 2.4 Hz, 6.7 Hz), 0.92 (d, 6H, -CH_3, J = 6.6 Hz), 1.03 (s, 7H, alkyl), 1.05-1.66 (m, 40H, alkyl), 1.79-2.03 (m, 11H, alkyl), 2.31-2.44 (m, 4H, alkyl), 4.56-4.63 (m, 2H), 5.40 (m, 2H, alkene), 6.58 (d, 2H, alkyl, J = 5.8 Hz), 7.07 (t, 2H, phenyl, J = 9.45 Hz), 7.19-7.22 (m, 1H, phenyl), 7.55 (bs, 2H, -NH).

Attempted preparation of ((3a*R*,5*R*,6*S*,6a*R*)-6-hydroxy-2,2-dimethyltetrahydrofuro [2,3-d][1,3]dioxol-5-yl) methyl (((3a*S*,5*S*,6*R*,6a*S*)-6-hydroxy-2,2-dimethyltetrahydro furo[2,3-d][1,3]dioxol-5-yl)methyl)1,3-phenylenedicarbamate (15) from 9

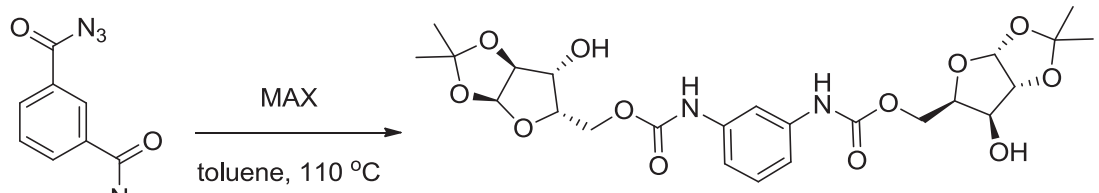

9 **15**

Monoacetone xylose (MAX) (1.0 mmol, 0.19 g) and diazide **9** (1.0 mmol, 0.22 g) were dissolved in 5 mL toluene in a 25 mL round bottom flask and allowed to stir. Once a homogenous mixture was obtained, the reaction was set to reflux at 110 ºC for 18 hours. Reaction progress was monitored by IR and once azide was determined to no longer be present in solution, the crude product was isolated by concentrating under reduced pressure to yield a colorless syrup. After isolation, ^{1}H NMR determined that the desired reaction did not take place. Diazide **9** did not react with either hydroxyl group on the xylose platform. NMR showed evidence that both starting materials were still present in solution.

Attempted preparation of ((3a*R*,5*R*,6*S*,6a*R*)-6-hydroxy-2,2-dimethyltetrahydrofuro [2,3-d][1,3]dioxol-5-yl) methyl (((3a*S*,5*S*,6*R*,6a*S*)-6-hydroxy-2,2-dimethyltetrahydro furo[2,3-d] [1,3]dioxol-5-yl)methyl)-1,4-phenylenedicarbamate (16) from 11

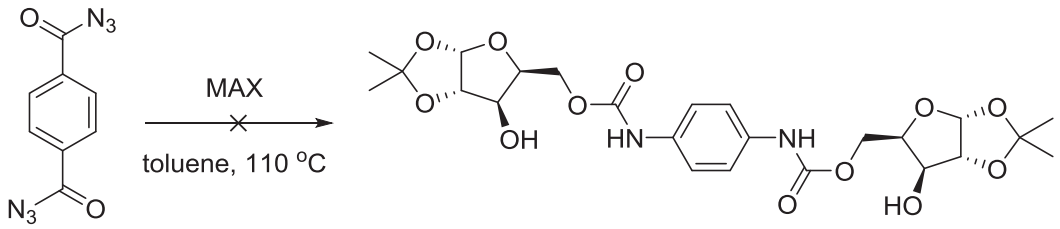

11 **16**

In a 25 mL round bottom flask, monoacetone xylose (MAX) (1.0 mmol, 0.22 g) and 7 (1.0 mmol, 0.19 g) were dissolved in 5 mL toluene and allowed to stir. The reaction mixture was monitored by IR and allowed to reflux at 110 ºC for 18 hours. Once there was no presence of azide by IR, the reaction was cooled to room temperature and concentrated under reduced pressure. Following isolation, ^{1}H NMR showed that no reaction took place and the synthesis of **16** did not take place as anticipated.

References

[1] - Corson, T.W.; Aberle, N.; Crews, C.M.; Design and applications of bifunctional small molecules: why two heads are better than one. *ACS Chem. Bio.* **2008**, *3,* 677-692.

[2] - Bartzatt, R.; Cirillo, S.L.G.; Donigan, L.; Bifunctional constructs of asprin and ibuprofen (non-steroidal anti-inflammatory drugs; NSAIDs) that express antibacterial and alkylation activities. *Biotechnol. Appl. Biochem.* **2001**, *37,* 273-282.

[3] - Youdin, M.B.H.; Fridkin, M.; Zheng, H.; Novel bifunctional drugs targeting monoamine oxidase inhibition and iron chelation as an approach to neuroprotection in Parkinson's disease and other neurodegenerative diseases. *J. Neural Trans.* **2004**, *111,* 1455-1471.

[4] - Wessjohann, L.A.; Voigt, B.; Rivera, D.G.; Diversity oriented one-pot synthesis of complex macrocycles: very large steroid-peptoid hybrids from multiple multicomponent reactions including bifunctional building blocks. *Angew. Chem. Int. Ed.* **2005**, *44,* 4785-4790.

[5] - Wendlandt, A.E.; Stahl, S.S.; Bioinspired aerobic oxidation of secondary amines of nitrogen heterocycles with a bifunctional quinone catalyst. *J. Am. Chem. Soc.* **2014**, *136,* 506-512.

[6] - May, J.F.; Levengood, M.R.; Splain, R.A.; Brown, C.D.; Kiessling, L.L.; A processive carbohydrate polymerase that mediates bifunctional catalysis using a single active site. *Biochemistry.* **2012**, *51,* 1148-1159.

[7] - Hudak, J.E.; Barfield, R.M.; de Hart, G.W.; Grob, P.; Nogales, E.; Bertozzi, C.R.; Rabuka, D.; Synthesis of heterobifunctional protein fusions using copper-free click chemistry and the aldehyde tag. *Angew. Chem. Int. Ed.* **2012**, *51,* 4161-4165.

[8] - Huttunen, K.M.; Raunio, H.; Rautio, J.; Prodrugs - from serendipity to rational design. *Pharm. Rev.* **2011**, *63,* 750-771.

[9] - Davies, B.E.; Pharmacokinetics of oseltamivir: an oral antiviral for the treatment and prophylaxis of influenza in diverse populations. *J. Antimicrob. Chemother.* **2010**, *65,* ii5-ii10.

[10] – Adesoye, O. G.; Mills, I. N.; Temelkoff, D. P.; Jackson, J. A.; Norris, P.; Synthesis of D-glucopyranosyl azide: spectroscopic evidence for stereochemical inversion in the S_N2 reaction. *J. Chem. Ed.* **2012**, *89,* 943-945.

[11] - Bräse, S.; Gil, C.; Knepper, K.; Zimmermann, V.; Organic azides: an exploding diversity of a unique class of compounds. *Angew. Chem. Int. Ed.* **2005**, *44,* 5188-5240.

[12] - Kaiser, C.; Weinstock, J.; Amines from mixed carboxylic-carbonic anhydrides: 1-phenylcyclopentylamine. *Org. Synth.* **1971**, *51,* 48.

[13] – Ninomiya, K.; Shioiri, T.; Yamada, S.; Phosphorus in organic synthesis---VII: diphenyl phosphoazidate (DPPA). A new convenient reagent for a modified Curtius reaction. *Tetrahedron.* **1974**, *30,* 2151-2157.

[14] – Doyle, M. P.; McKervey, M. A.; Ye, T. *Modern catalytic methods for organic synthesis for organic synthesis with diazo compounds: from cyclopropanes to ylides*, John Wiley & Sons Inc.: New York, 1998.

[15] - Regitz, M.; Synthese von diacyl-diazomethanen durch diazogruppenübertrangung. *Chem. Ber.* **1966**, *99,* 3128-3147.

[16] – Taber, D. F.; Hennessy, M. J.; Louey, J. P. Rh-mediated cyclopentane construction can compete with *β*-hydride elimination: synthesis of (±)-Tochuinyl acetate. *J. Org. Chem.* **1995**, *60,* 1093-1094.

[17] – Sacui, I. A., "Synthesis and decomposition of novel diazosugars," Youngstown State University MS Thesis, 2006.

[18] – Malich, A. M., "Decomposition of novel diazosugars: effects on regioselectivity," Youngstown State University MS Thesis, 2008.

[19] – Adero, P. O., "Heterocycle synthesis via rhodium (II)-catalyzed azido carbenoid cyclization," Youngstown State University MS Thesis, 2012.

[20] – Mehrotra, M. M.; Heath, J. A.; Smyth, M. S.; Pandey, A.; Rose, J. W.; Seroogy, J. M.; Volkots, D. L.; Nannizzi-Alaimo, L.; Park, G. L.; Lambing, J. L.; Hollenbach, S. J.; Scarborough, R. M.; Discovery of novel 2,8-diazaspiro[4.5]decanes as orally active glycoprotein IIb-IIIa antagonists. *J. Med. Chem.* **2004**, *47,* 2037-2061.

[21] – Davis, M. C.; Nitration of ethyl carbamates of phenylenediamines and aniline. *Synth. Comm.* **2007**, *37,* 2079-2089.

Appendix A

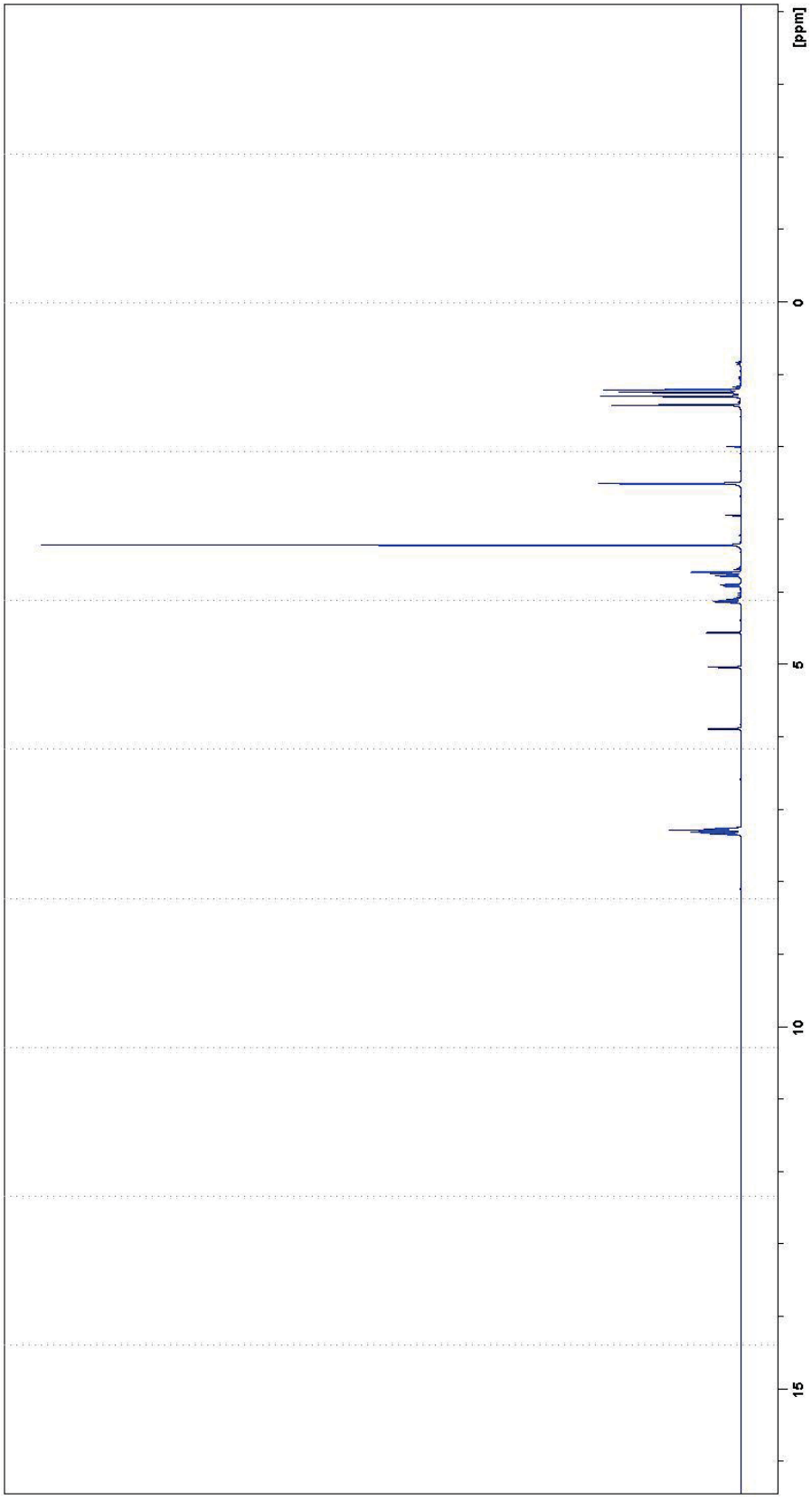

Figure 12: ^{1}H NMR of (3a*R*,5*R*,6*S*,6a*R*)-5-((*R*)-2,2-dimethyl-1,3-dioxolan-4-yl)-2,2-dimethyltetrahydrofuro[2,3-d][1,3]dioxol-6-yl 2-phenylacetate **2**

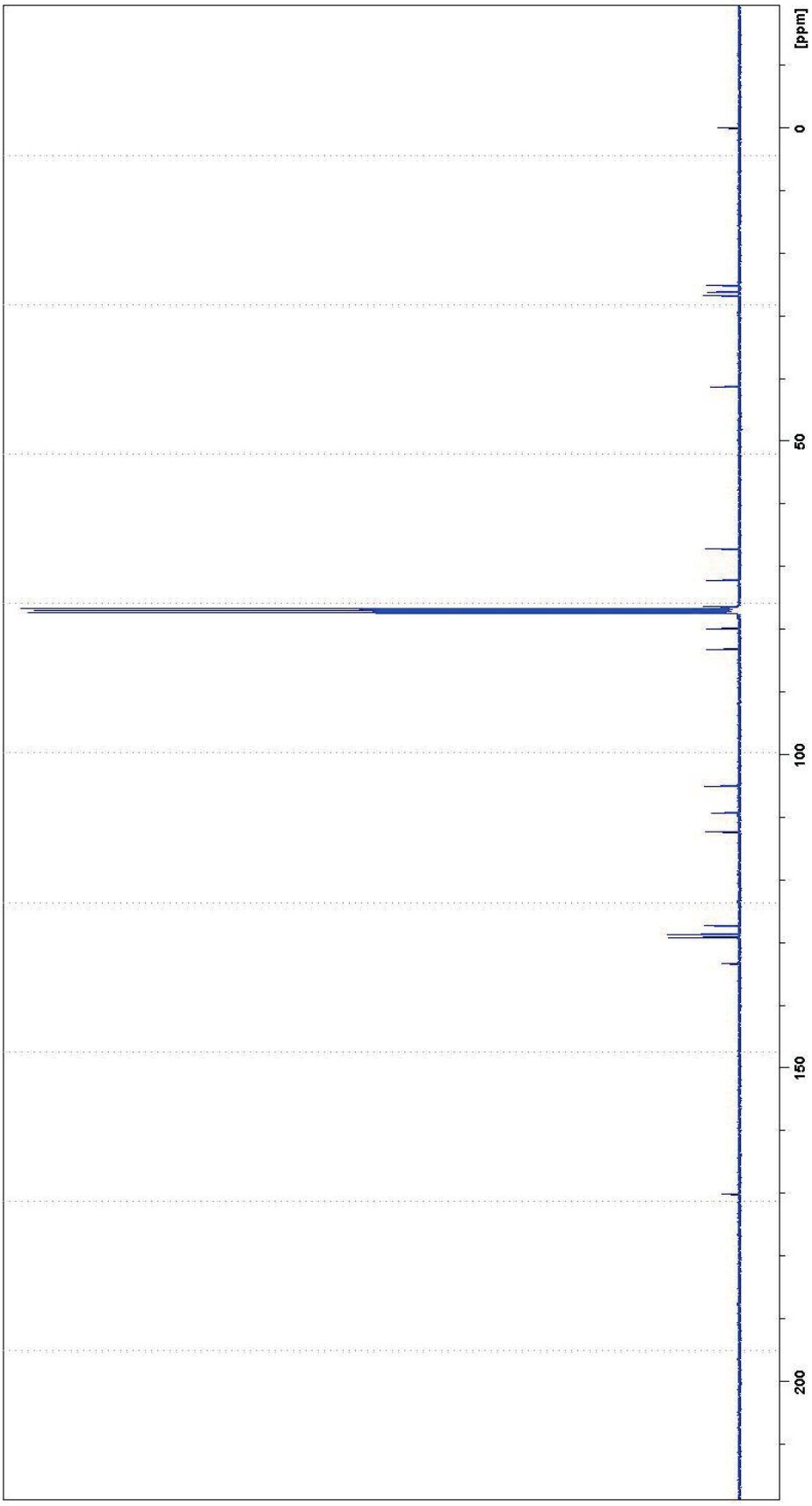

Figure 13: ^{13}C NMR of (3a*R*,5*R*,6*S*,6a*R*)-5-((*R*)-2,2-dimethyl-1,3-dioxolan-4-yl)-2,2-dimethyltetrahydrofuro[2,3-d][1,3]dioxol-6-yl 2-phenylacetate **2**

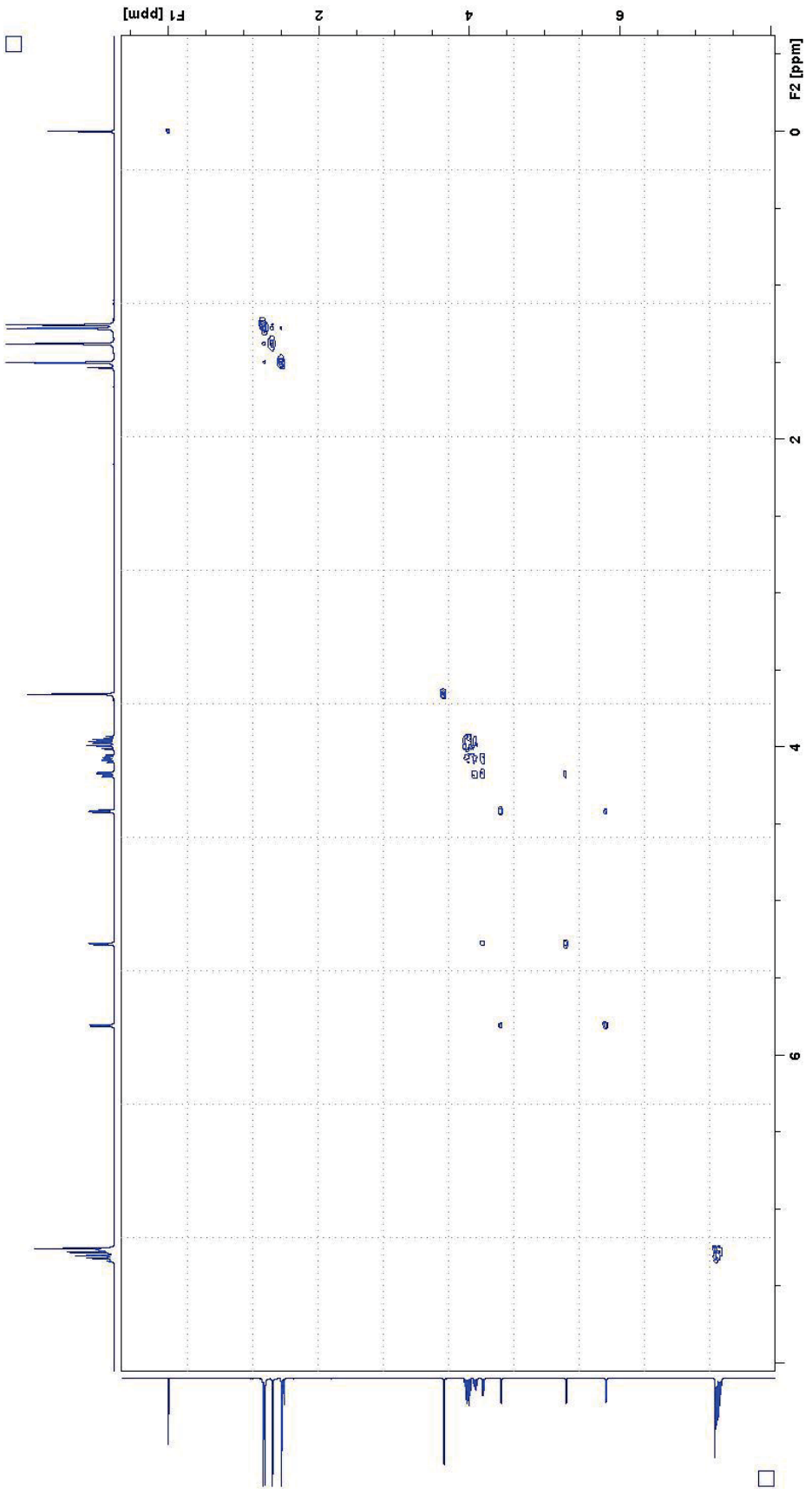

Figure 14: COSY of (3a*R*,5*R*,6*S*,6a*R*)-5-((*R*)-2,2-dimethyl-1,3-dioxolan-4-yl)-2,2-dimethyltetrahydrofuro[2,3-d][1,3]dioxol-6-yl 2-phenylacetate **2**

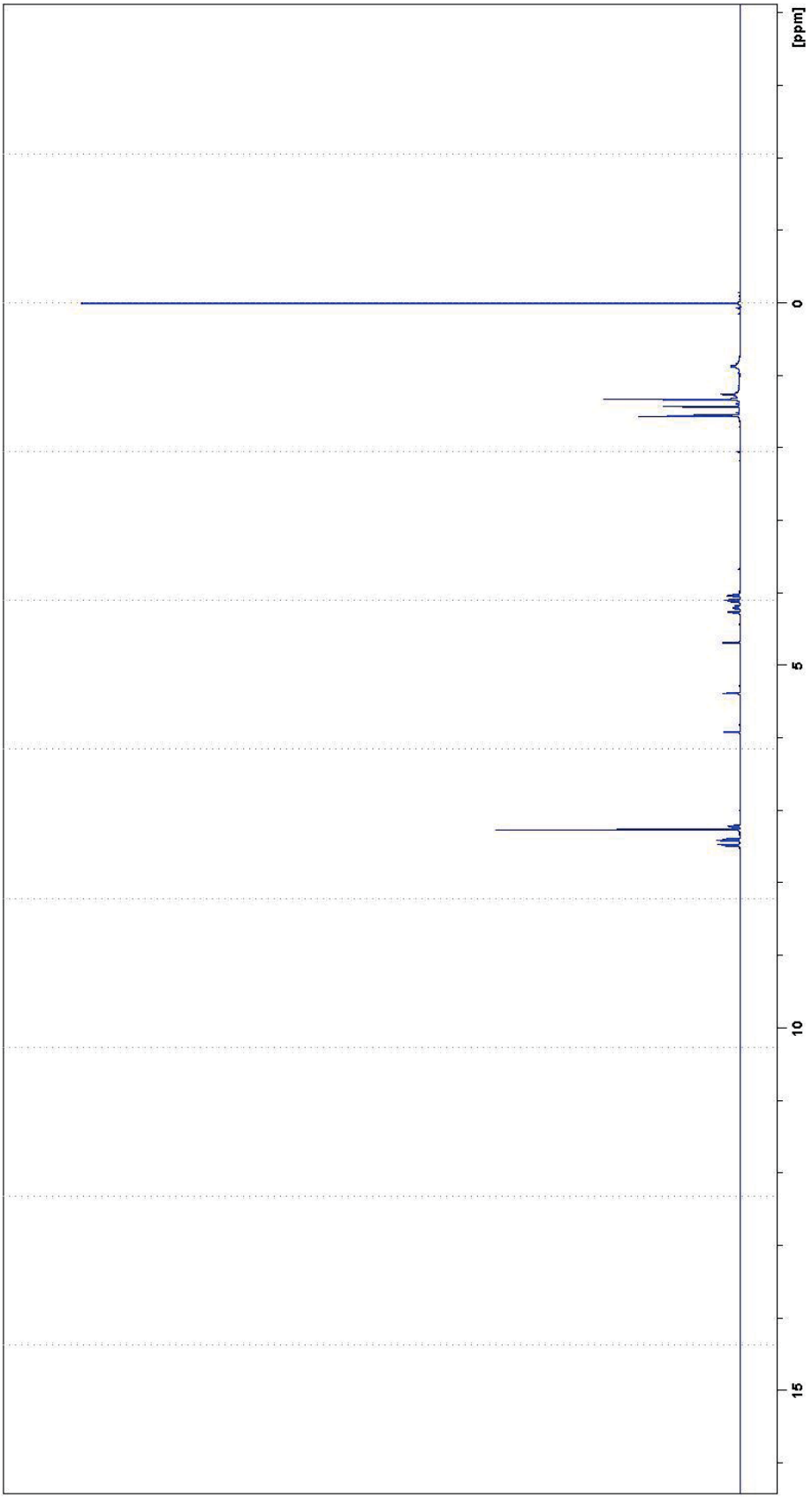

Figure 15: ^{1}H NMR of (3a*R*,5*R*,6*S*,6a*R*)-5-((*R*)-2,2-dimethyl-1,3-dioxolan-4-yl)-2,2-dimethyltetrahydrofuro[2,3-d][1,3]dioxol-6-yl 2-diazo-2-phenylacetate **3**

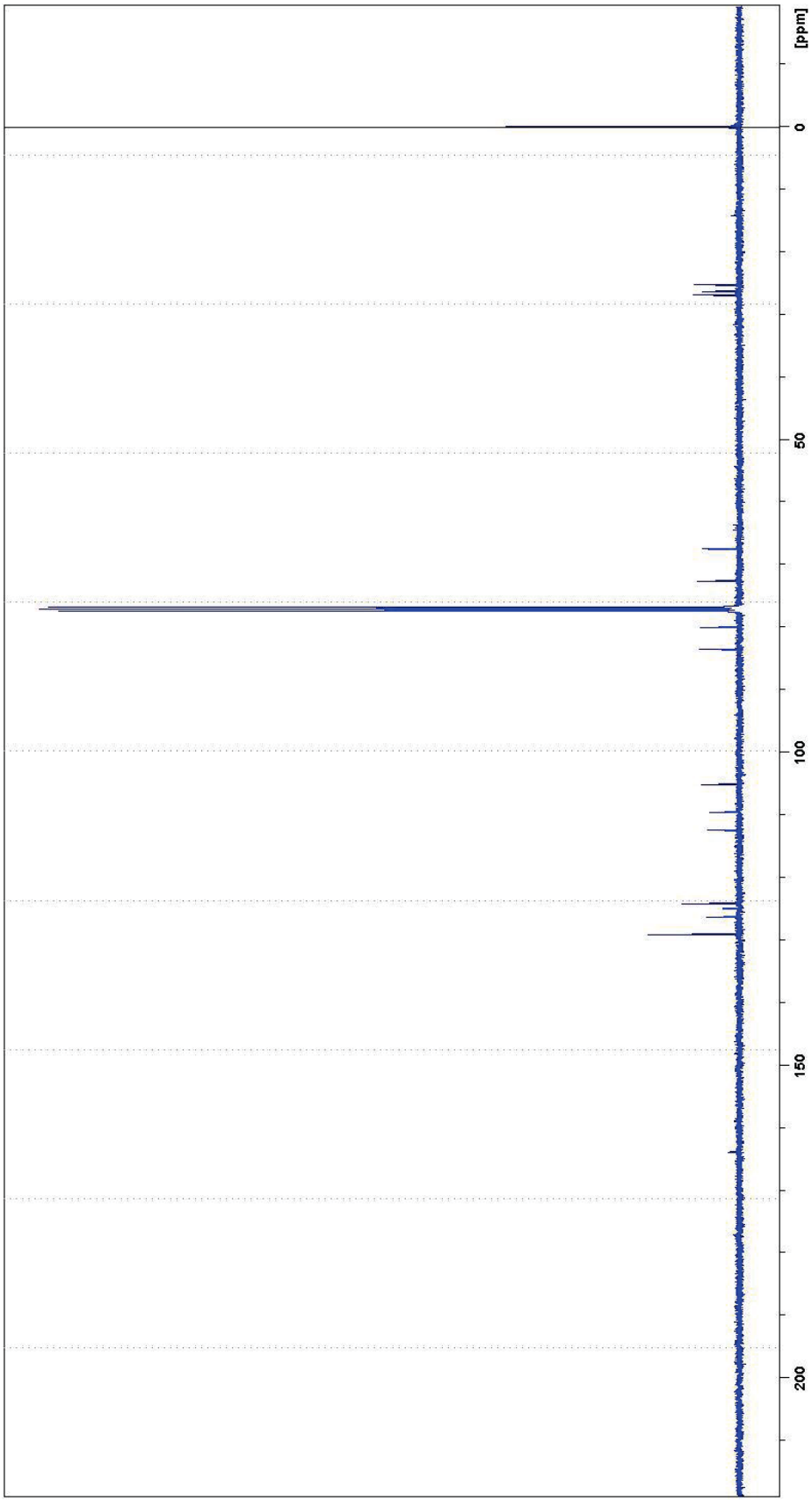

Figure 16: ^{13}C NMR of (3a*R*,5*R*,6*S*,6a*R*)-5-((*R*)-2,2-dimethyl-1,3-dioxolan-4-yl)-2,2-dimethyltetrahydrofuro[2,3-d][1,3]dioxol-6-yl 2-diazo-2-phenylacetate **3**

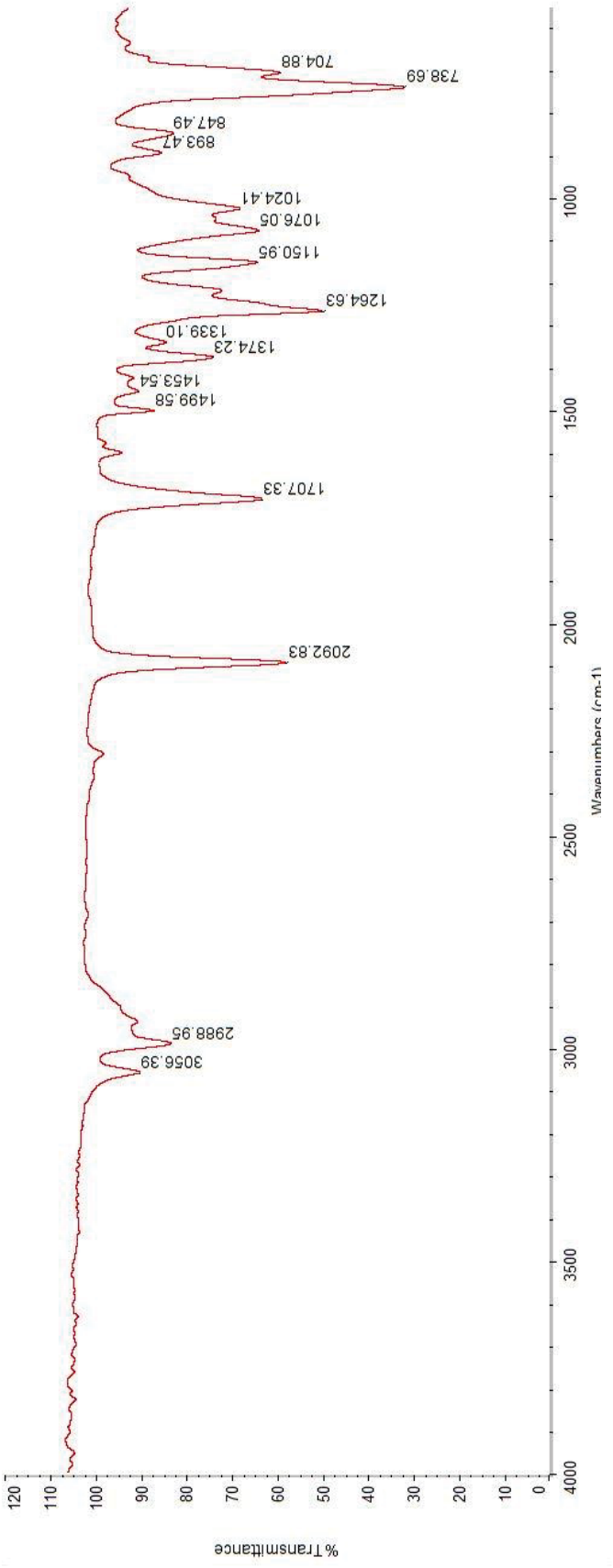

Figure 17: IR of (3a*R*,5*R*,6*S*,6a*R*)-5-((*R*)-2,2-dimethyl-1,3-dioxolan-4-yl)-2,2-dimethyltetrahydrofuro[2,3-d][1,3]dioxol-6-yl 2-diazo-2-phenylacetate **3**

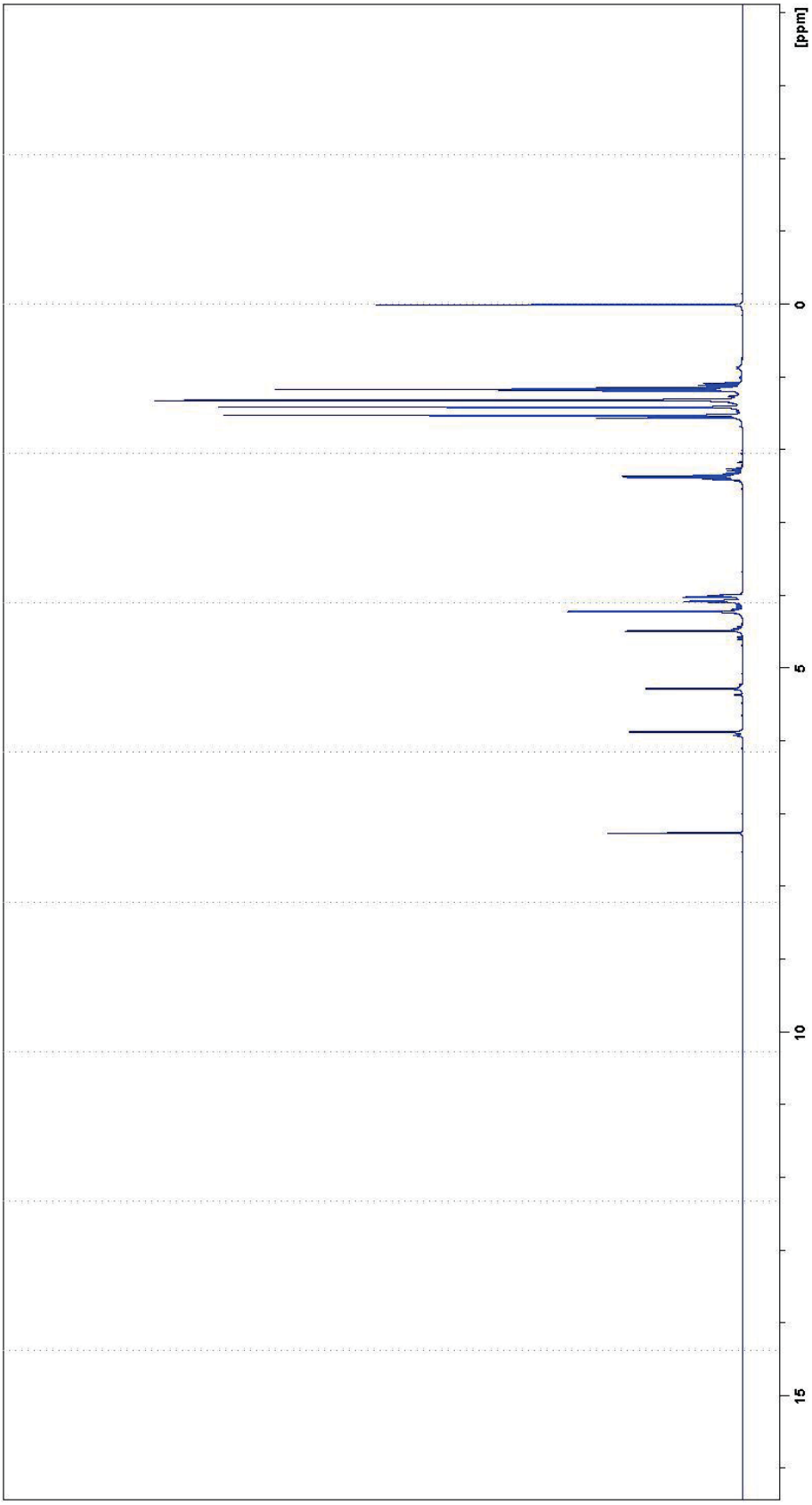

Figure 18: ^{1}H NMR of (3a*R*,5*R*,6*S*,6a*R*)-5-((*R*)-2,2-dimethyl-1,3-dioxolan-4-yl)-2,2-dimethyltetrahydrofuro[2,3-d][1,3]dioxol-6-yl propionate **4**

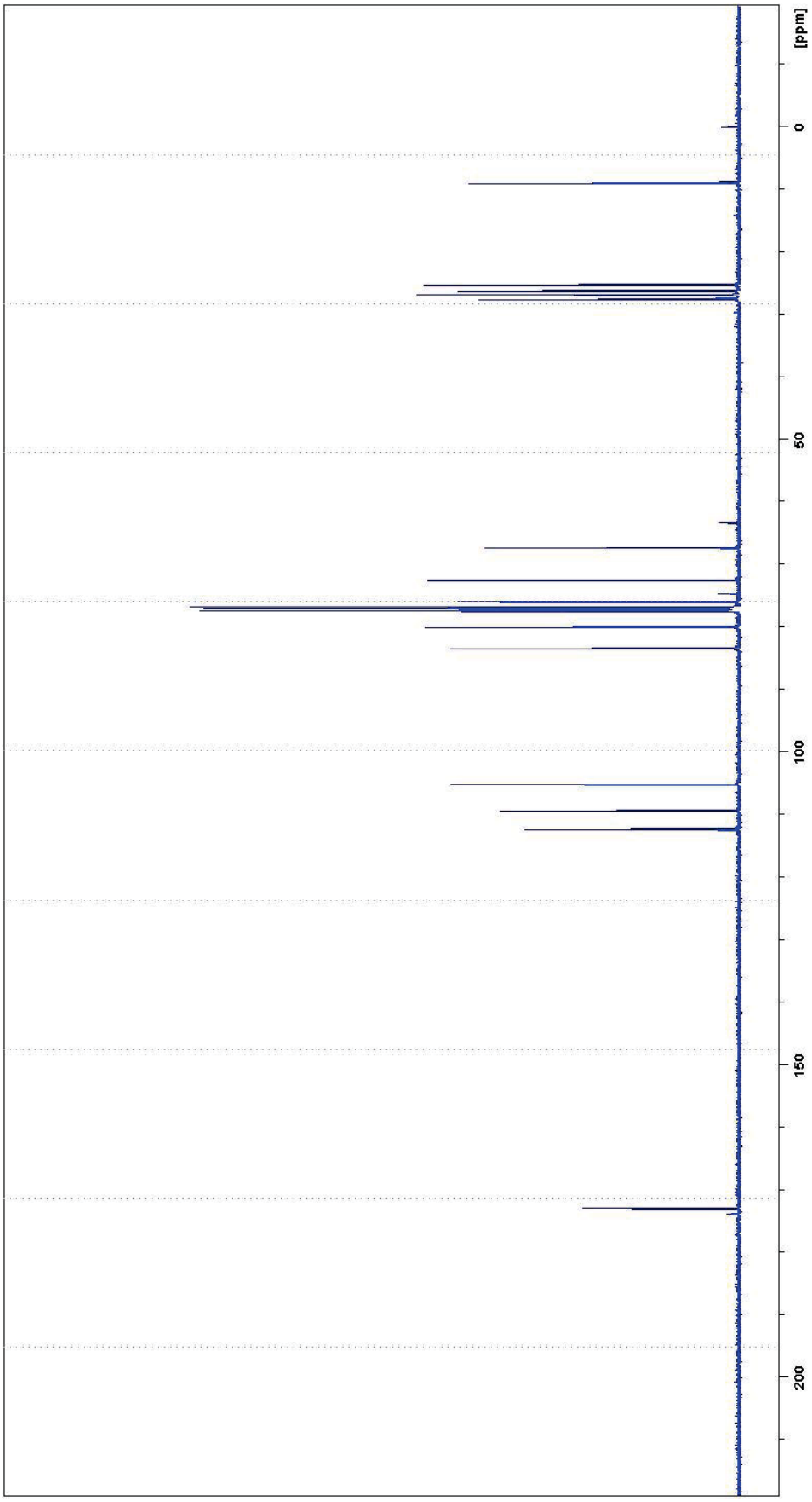

Figure 19: ^{13}C NMR of (3a*R*,5*R*,6*S*,6a*R*)-5-((*R*)-2,2-dimethyl-1,3-dioxolan-4-yl)-2,2-dimethyltetrahydrofuro[2,3-d][1,3]dioxol-6-yl propionate **4**

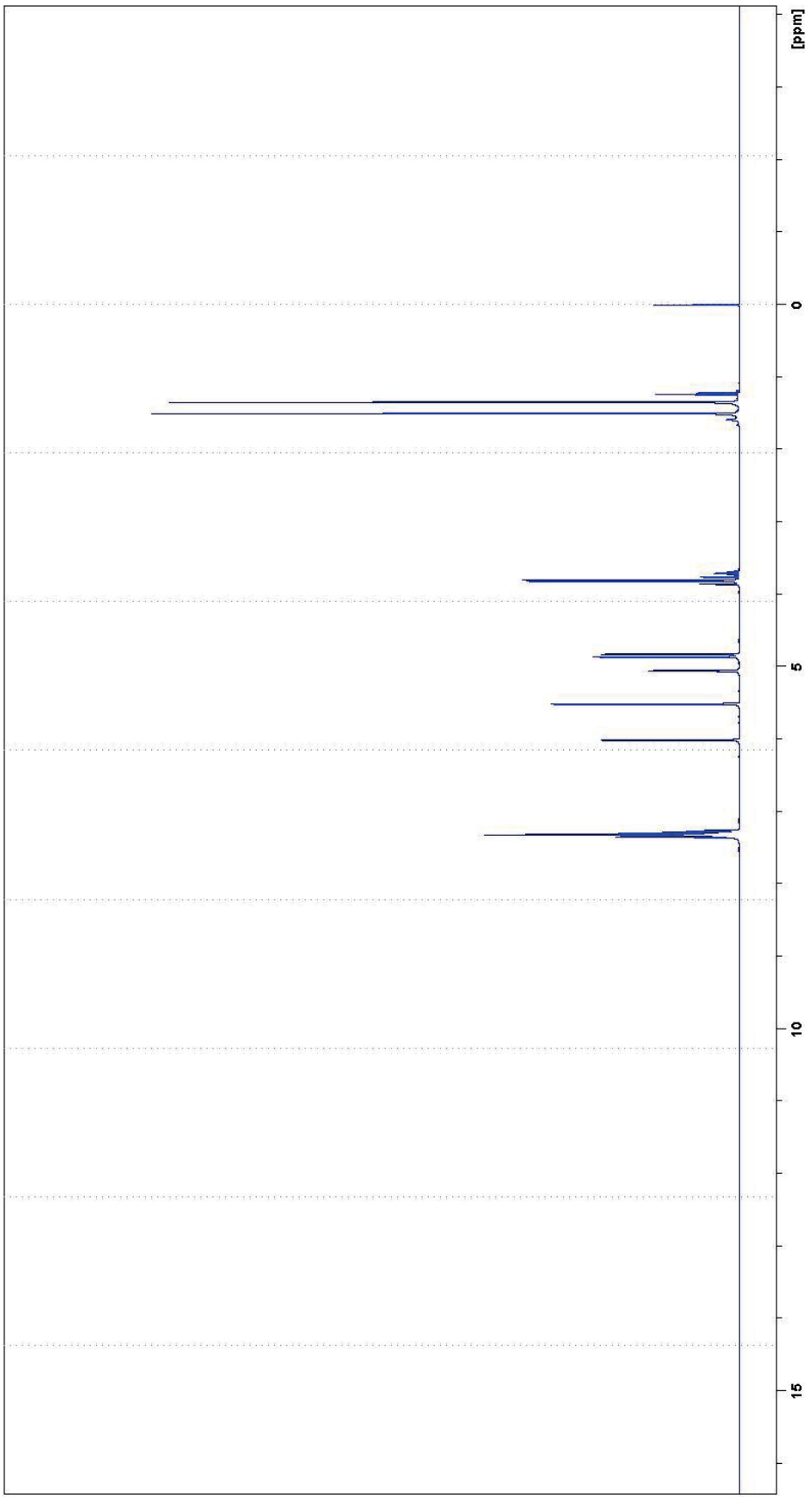

Figure 20: ^{1}H NMR of (3a*R*,3b*S*,6*S*,6a*S*,7a*R*)-2,2-dimethyl-5-oxohexahydrofuro[2',3':4,5]furo[2,3-d][1,3]dioxol-6-yl 2-phenylacetate **6**

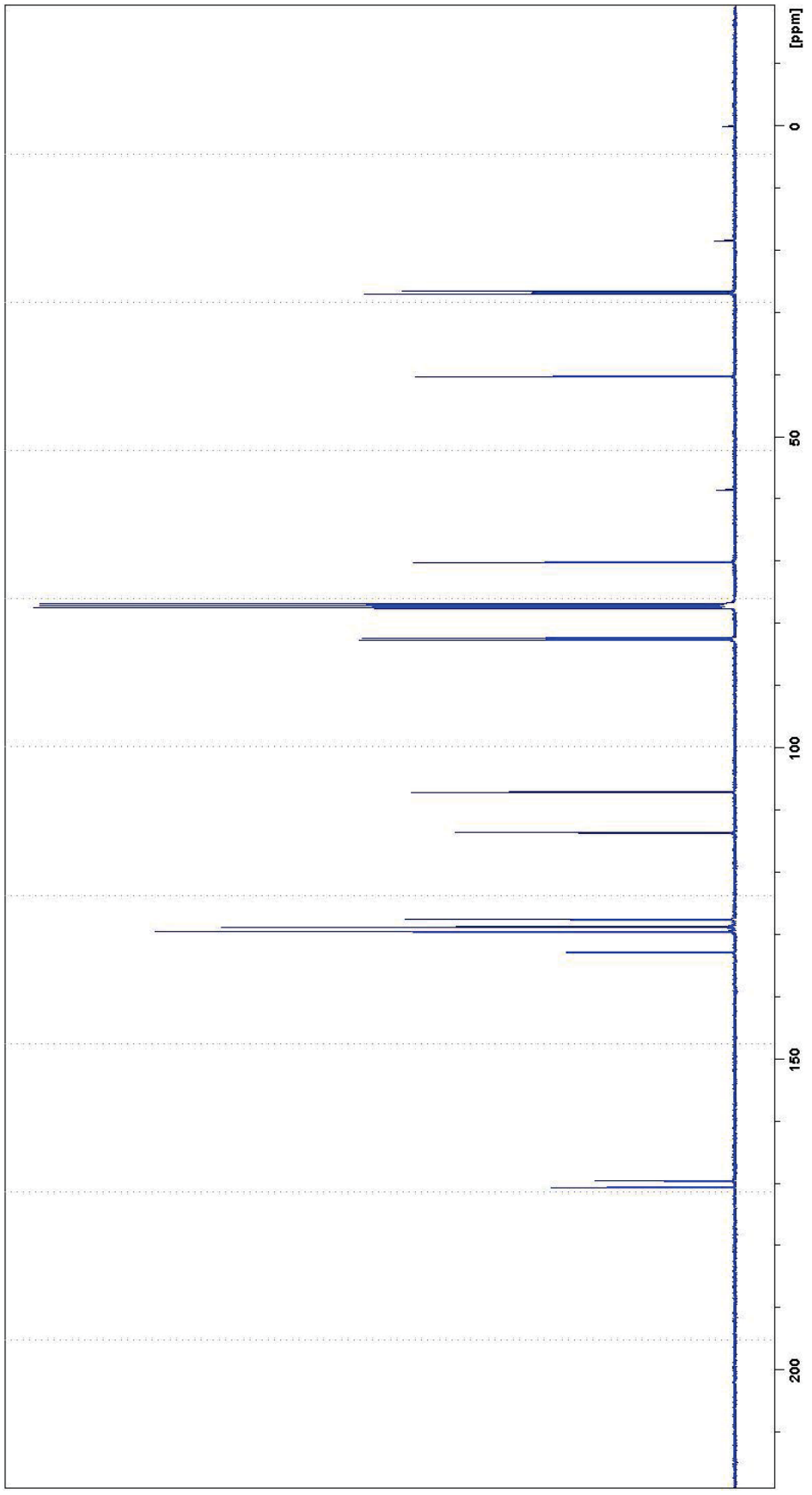

Figure 21: ^{13}C NMR of (3a*R*,3b*S*,6*S*,6a*S*,7a*R*)-2,2-dimethyl-5-oxohexahydrofuro[2',3':4,5]furo[2,3-d][1,3]dioxol-6-yl 2-phenylacetate **6**

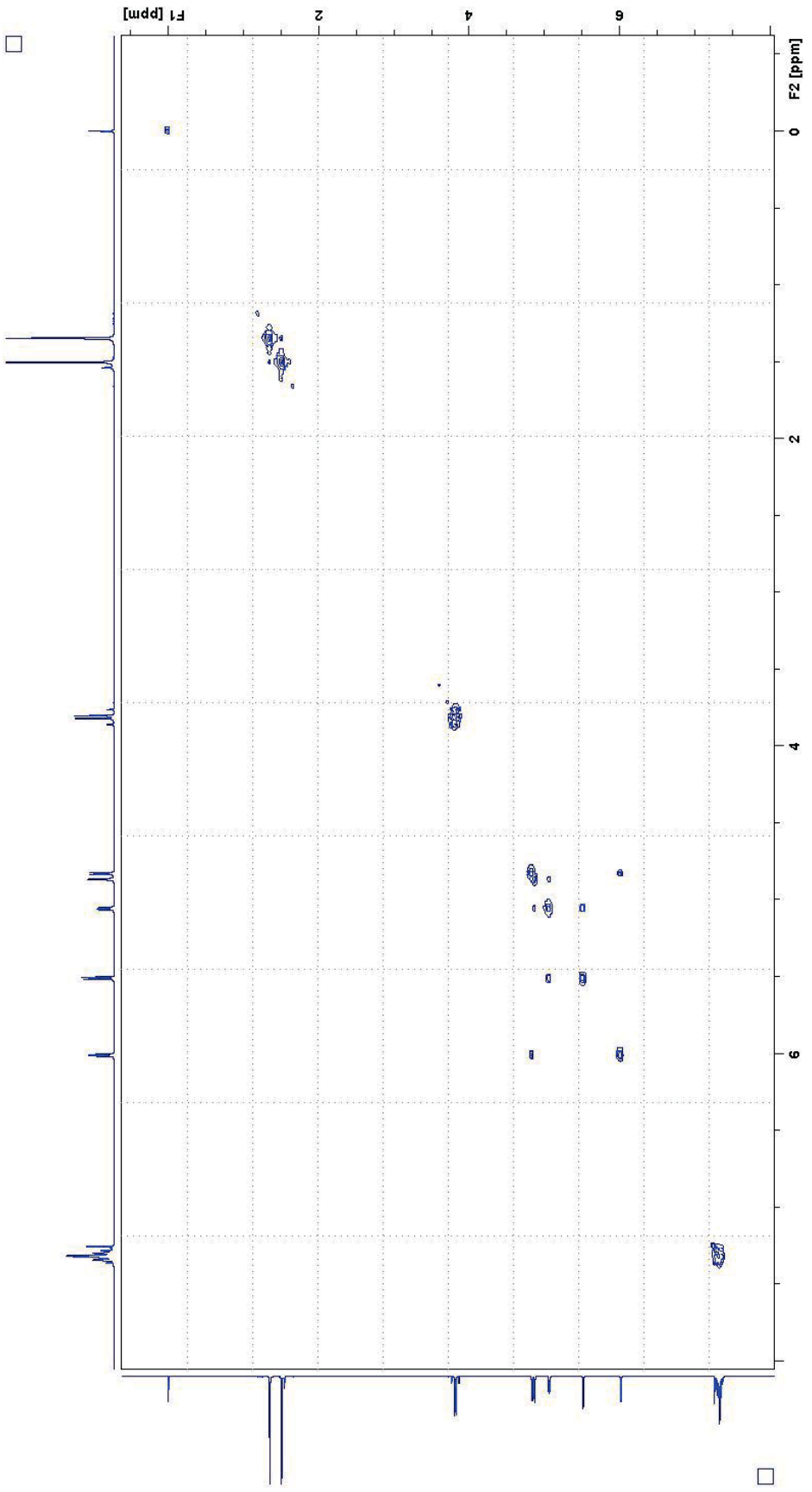

Figure 22: COSY of (3a*R*,3b*S*,6*S*,6a*S*,7a*R*)-2,2-dimethyl-5-oxohexahydrofuro[2',3':4,5]furo[2,3-d][1,3]dioxol-6-yl 2-phenylacetate **6**

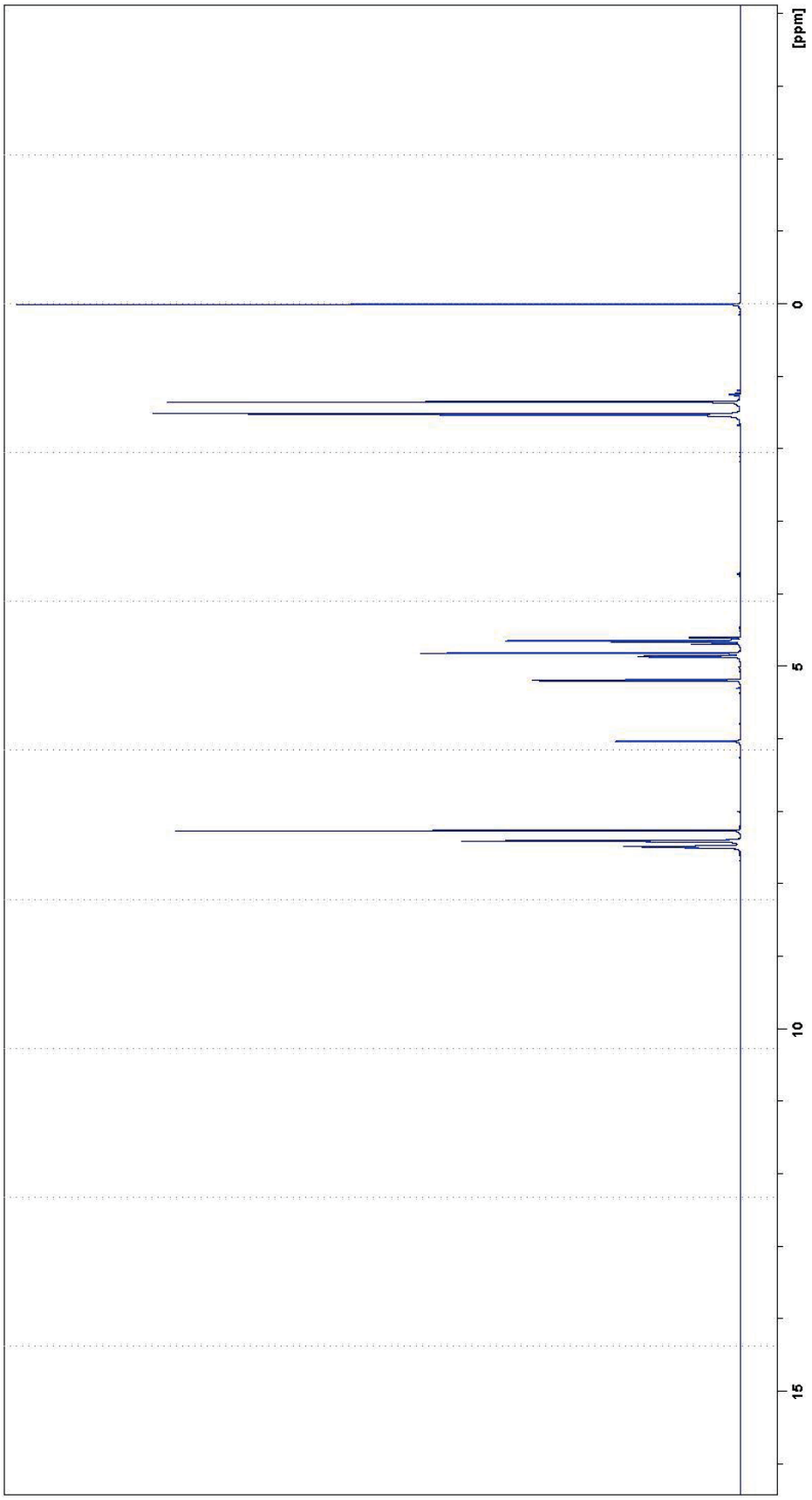

Figure 23: ^{1}H NMR of (3a*R*,5*R*,6*S*,6a*R*)-5-((*R*)-2,2-dimethyl-1,3-dioxolan-4-yl)-2,2-dimethyltetrahydrofuro[2,3-d][1,3]dioxol-6-yl phenylmethanesulfonate **7**

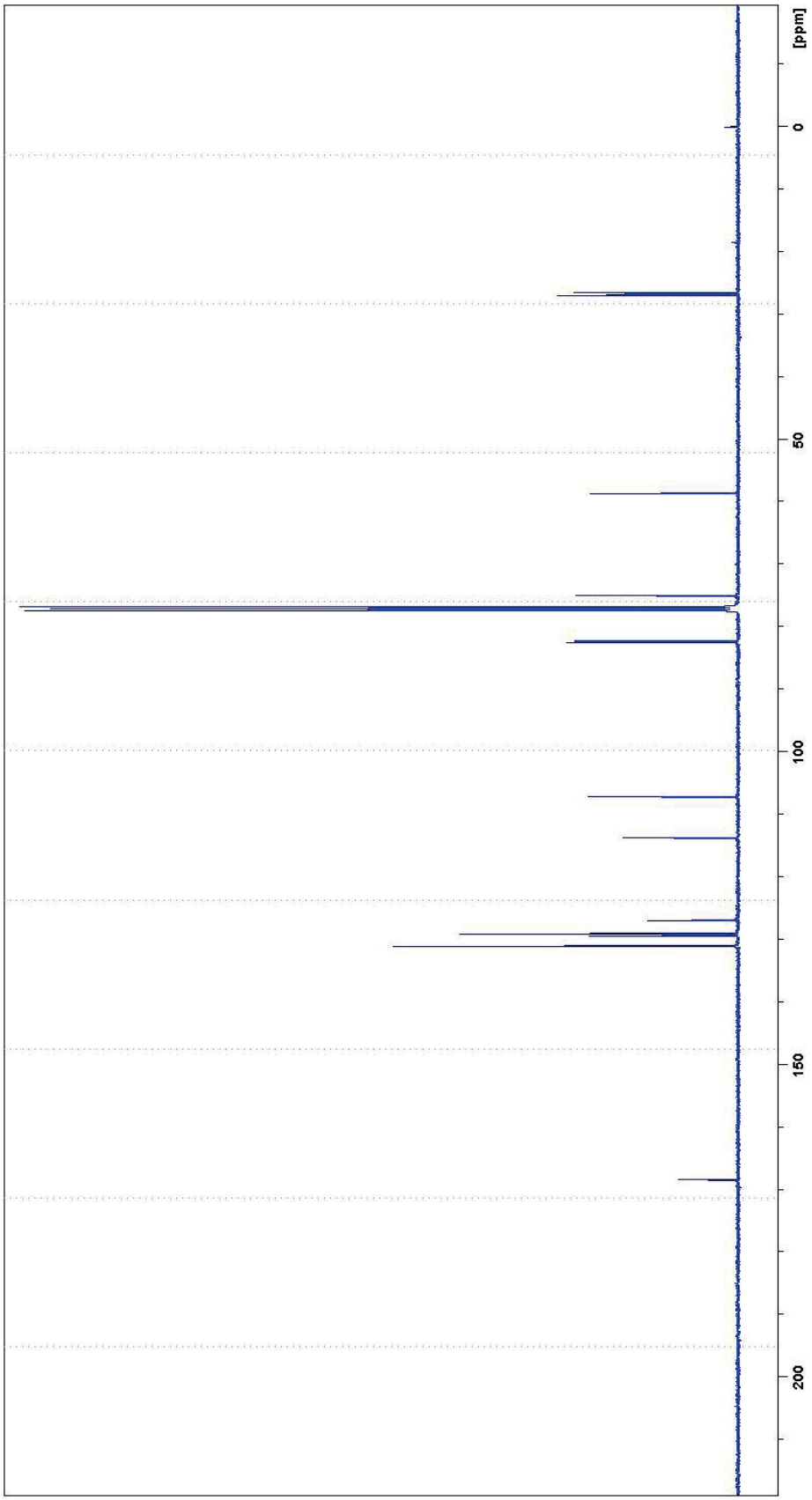

Figure 24: ^{13}C NMR of (3a*R*,5*R*,6*S*,6a*R*)-5-((*R*)-2,2-dimethyl-1,3-dioxolan-4-yl)-2,2-dimethyltetrahydrofuro[2,3-d][1,3]dioxol-6-yl phenylmethanesulfonate **7**

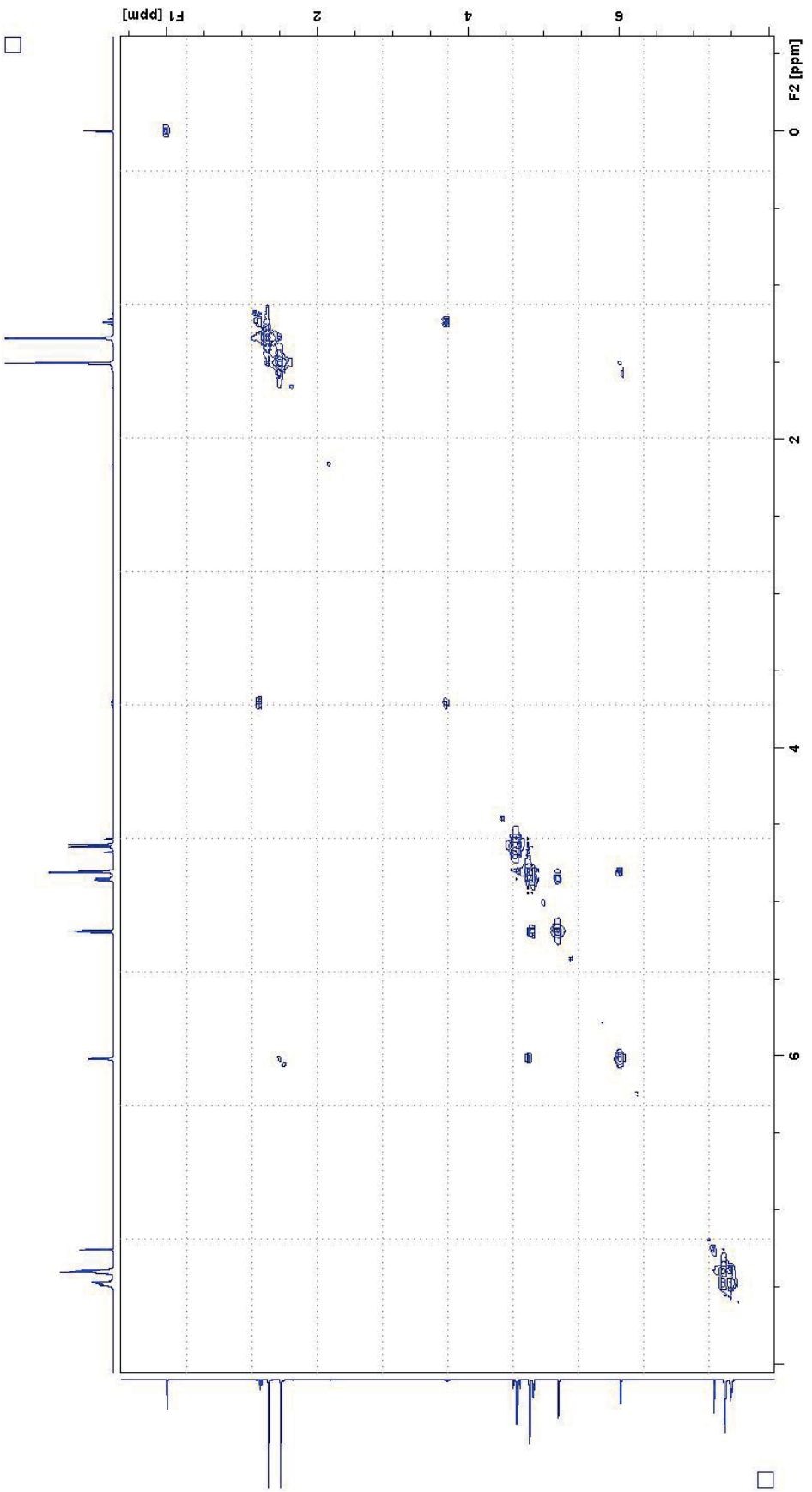

Figure 25: COSY of (3a*R*,5*R*,6*S*,6a*R*)-5-((*R*)-2,2-dimethyl-1,3-dioxolan-4-yl)-2,2-dimethyltetrahydrofuro[2,3-d][1,3]dioxol-6-yl phenylmethanesulfonate **7**

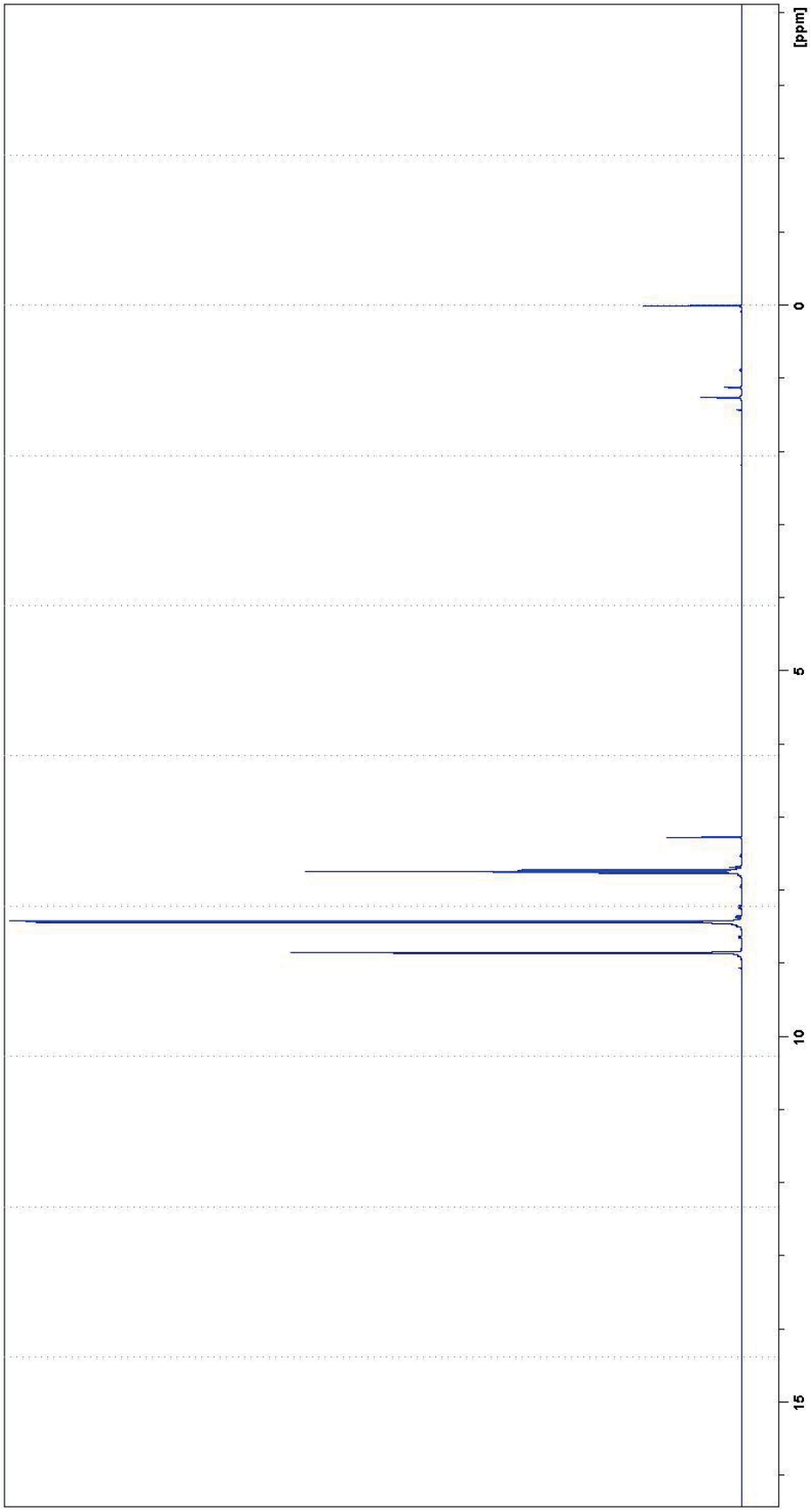

Figure 26: ^{1}H NMR of isophthaloyl diazide **9**

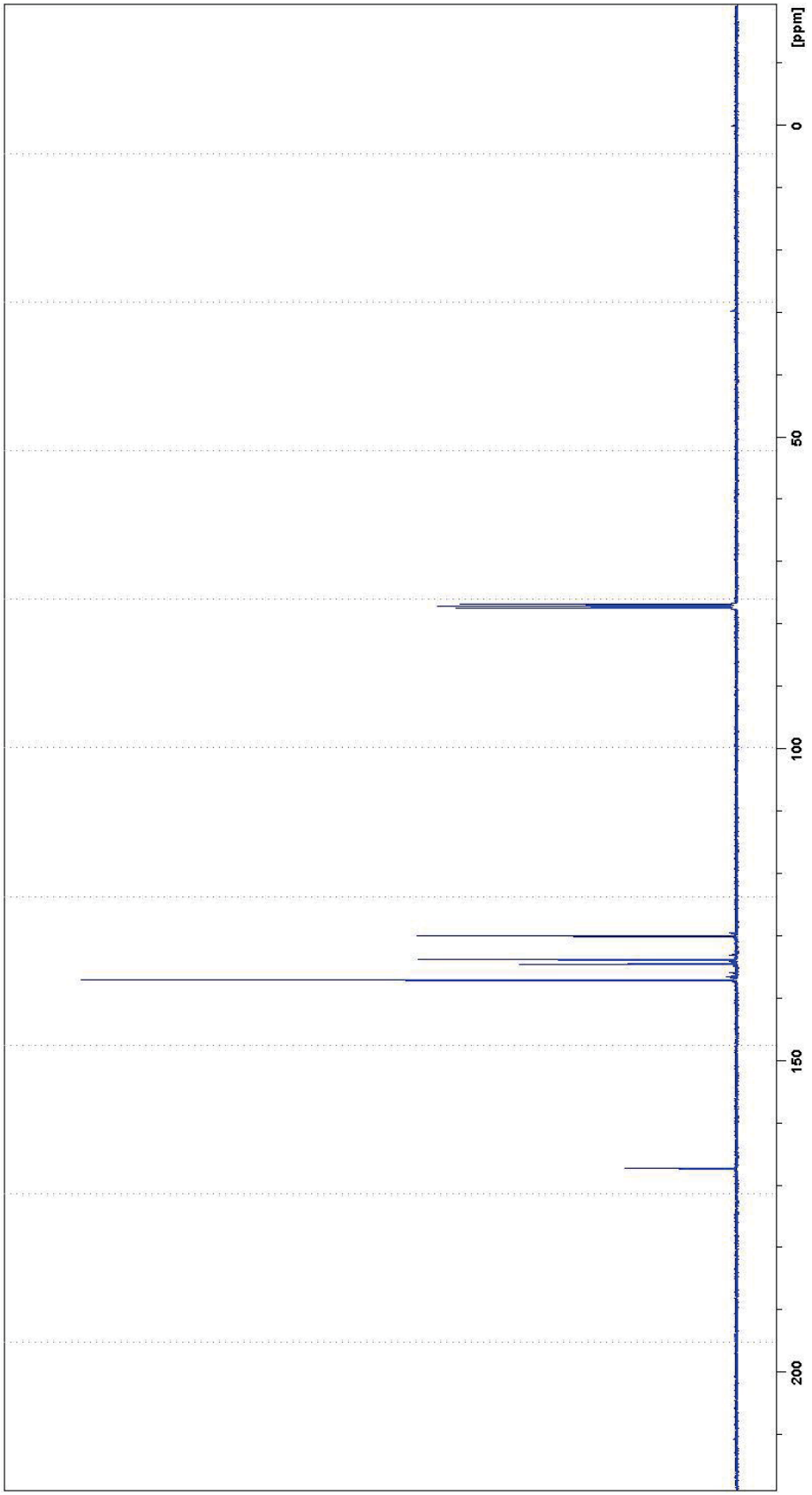

Figure 27: ^{13}C NMR of isophthaloyl diazide **9**

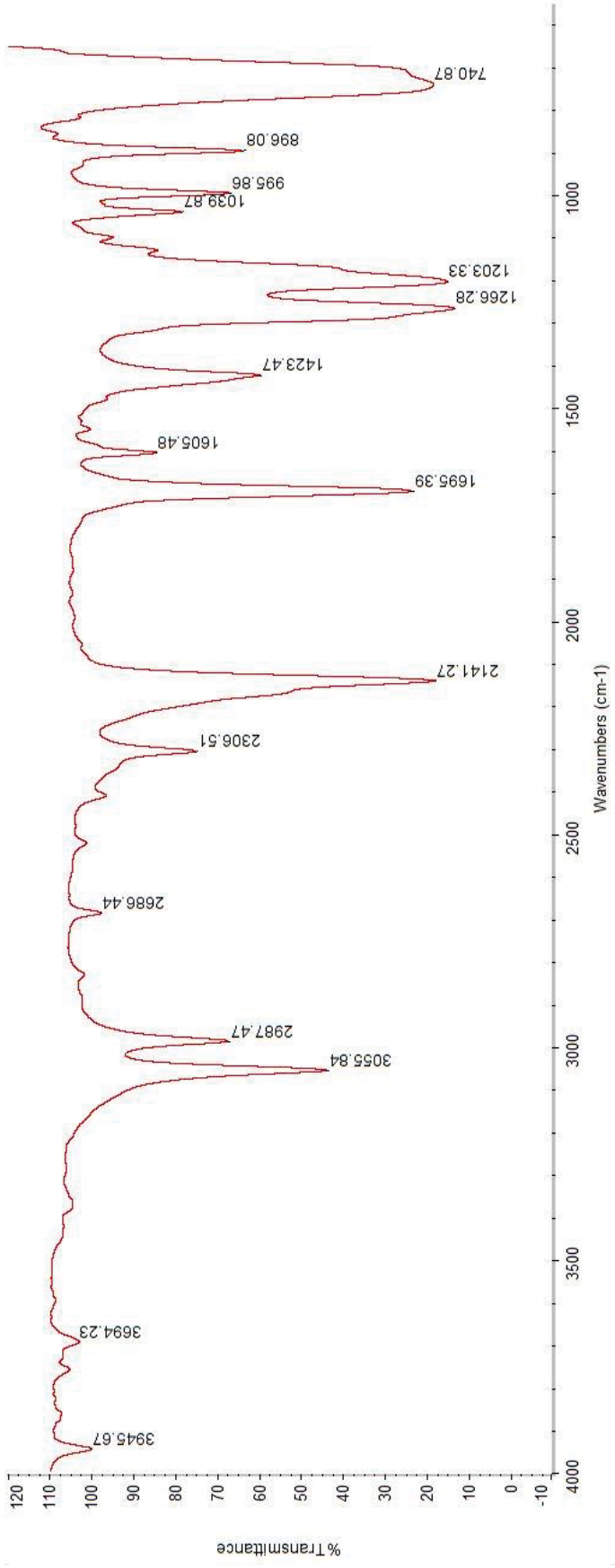

Figure 28: IR of isophthaloyl diazide **9**

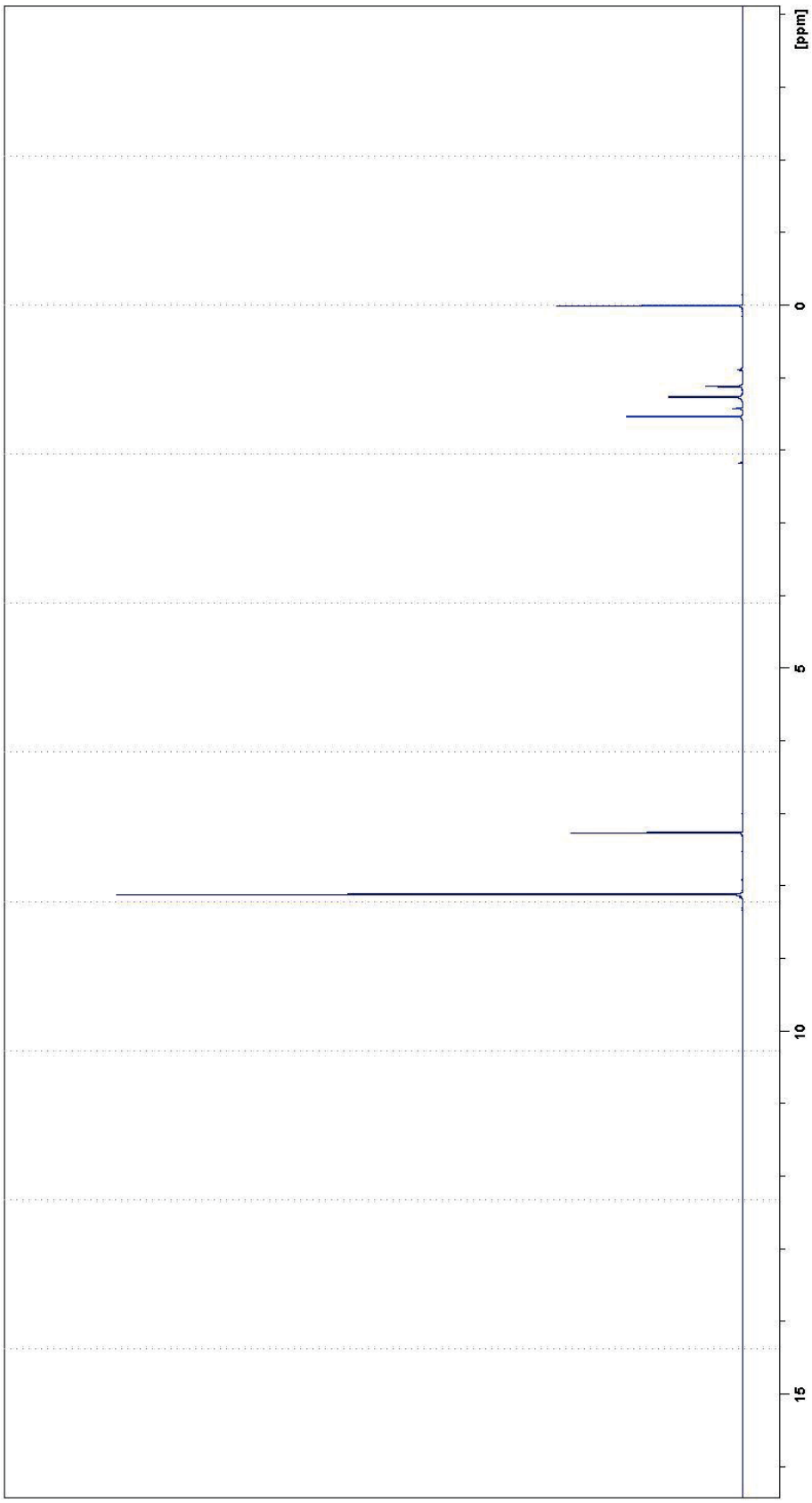

Figure 29: ^{1}H NMR of terephthaloyl diazide **11**

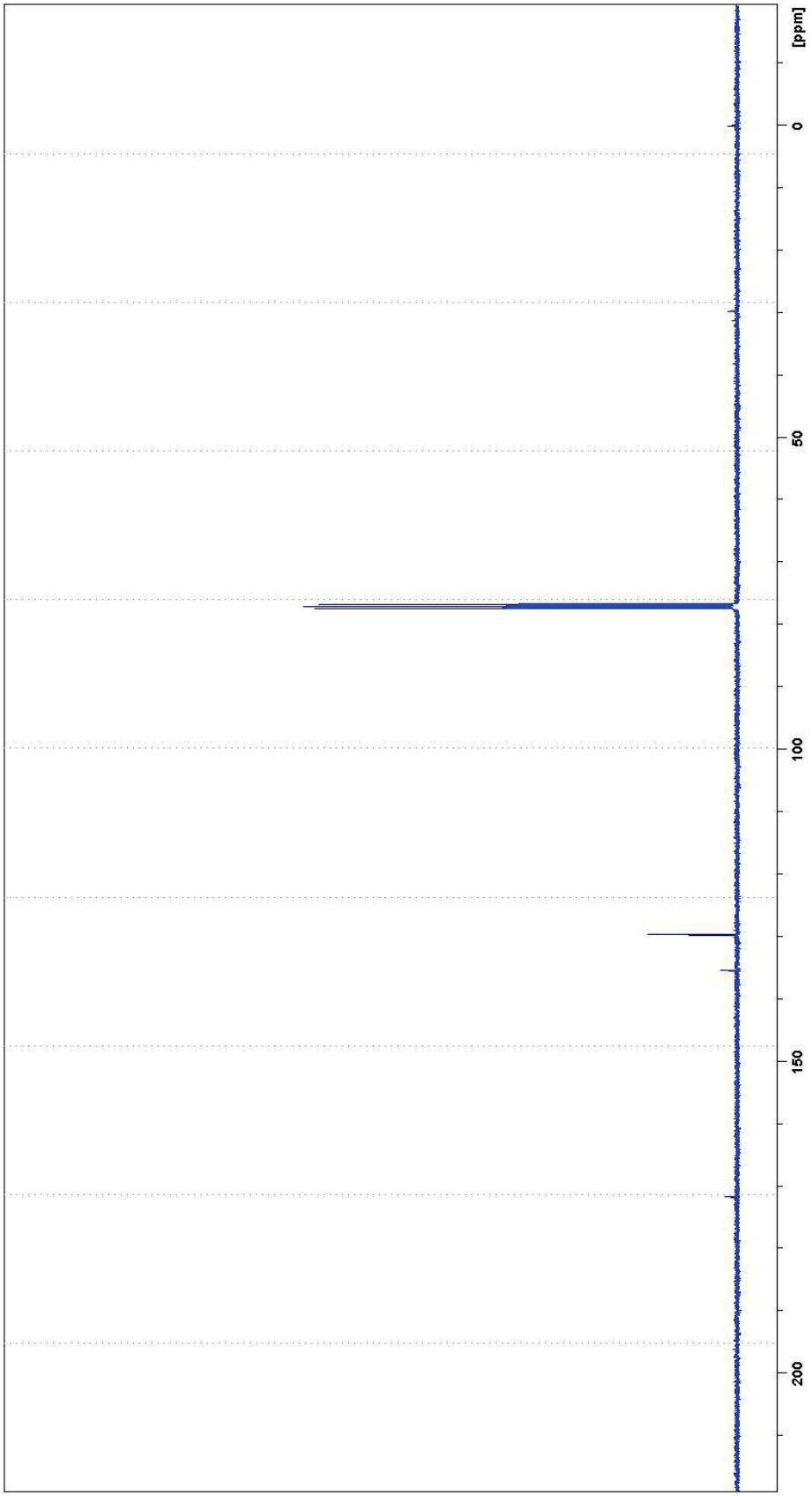

Figure 30: ^{13}C NMR of terephthaloyl diazide **11**

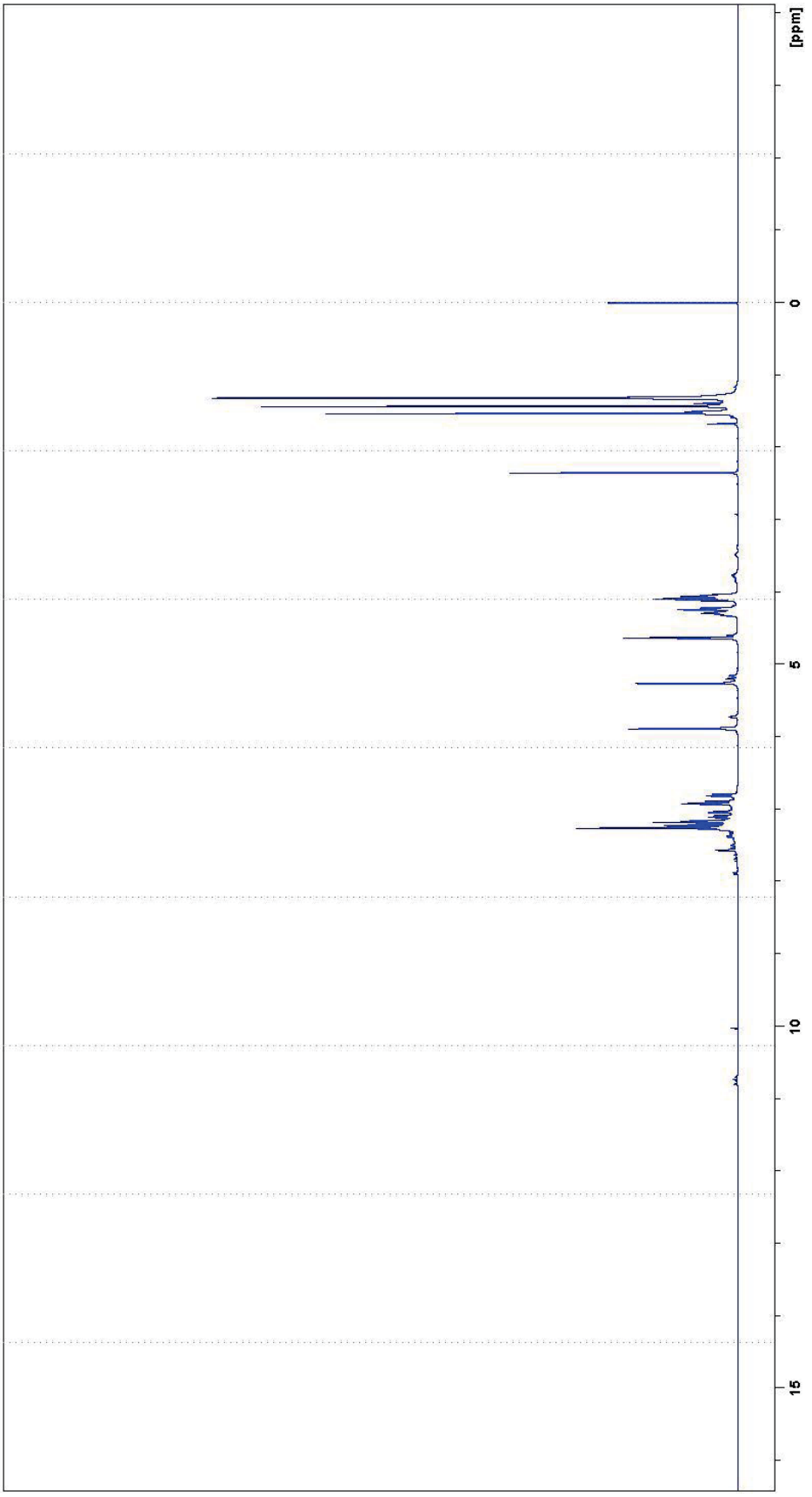

Figure 31: ^{1}H NMR of bis(5-(2,2-dimethyl-1,3-dioxolan-4-yl)-2,2-dimethyltetrahydrofuro[2,3-d][1,3]dioxol-6-yl) 1,3-phenylenedicarbamate **12**

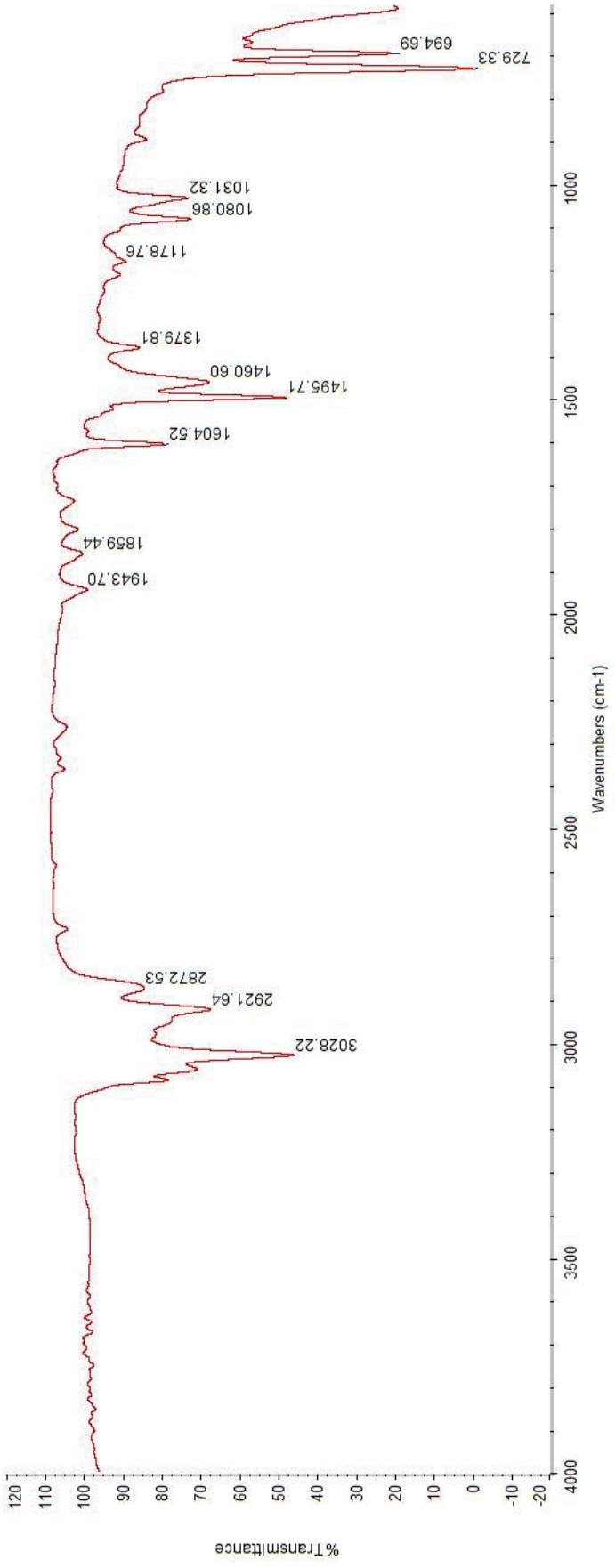

Figure 32: IR of bis(5-(2,2-dimethyl-1,3-dioxolan-4-yl)-2,2-dimethyltetrahydrofuro[2,3-d][1,3]dioxol-6-yl) 1,3-phenylenedicarbamate **12**

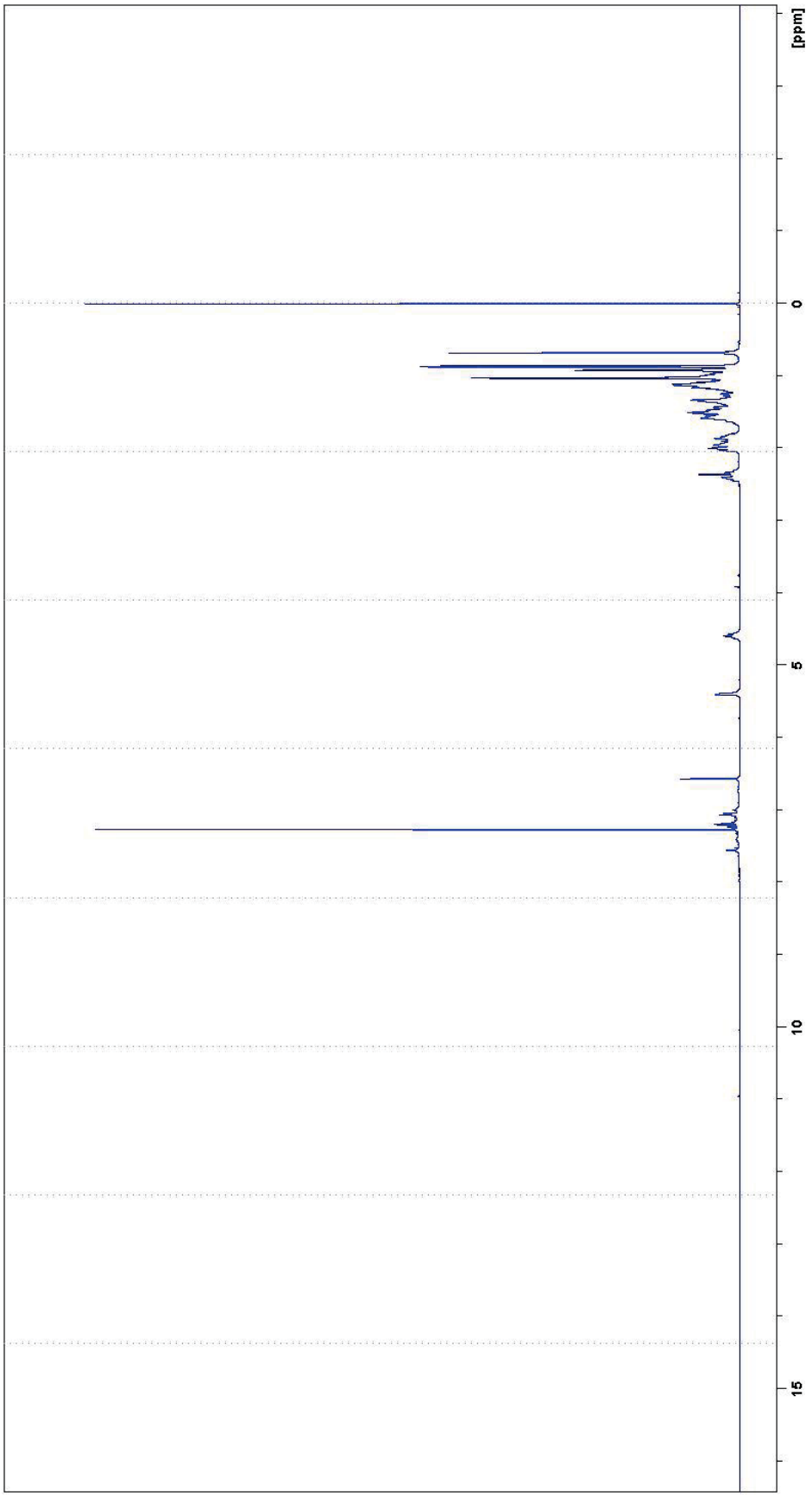

Figure 33: ^{1}H NMR of (8*S*,9*S*,10*R*,13*R*,14*S*,17*R*)-10,13-dimethyl-17-((*R*)-6-methylheptan-2-yl)-2,3,4,7,8,9,10,11,12,13,14,15,16,17-tetradecahydro-1H-cyclopenta[a]phenanthren-3-yl ((8*R*,9*R*,10*S*,13*S*,14*R*,17*S*)-10,13-dimethyl-17-((*S*)-6-methylheptan-2-yl)-2,3,4,7,8,9,10,11,12,13,14,15,16,17-tetradecahydro-1H-cyclopenta[a]phenanthren-3-yl) 1,3-phenylenedicarbamate **13**

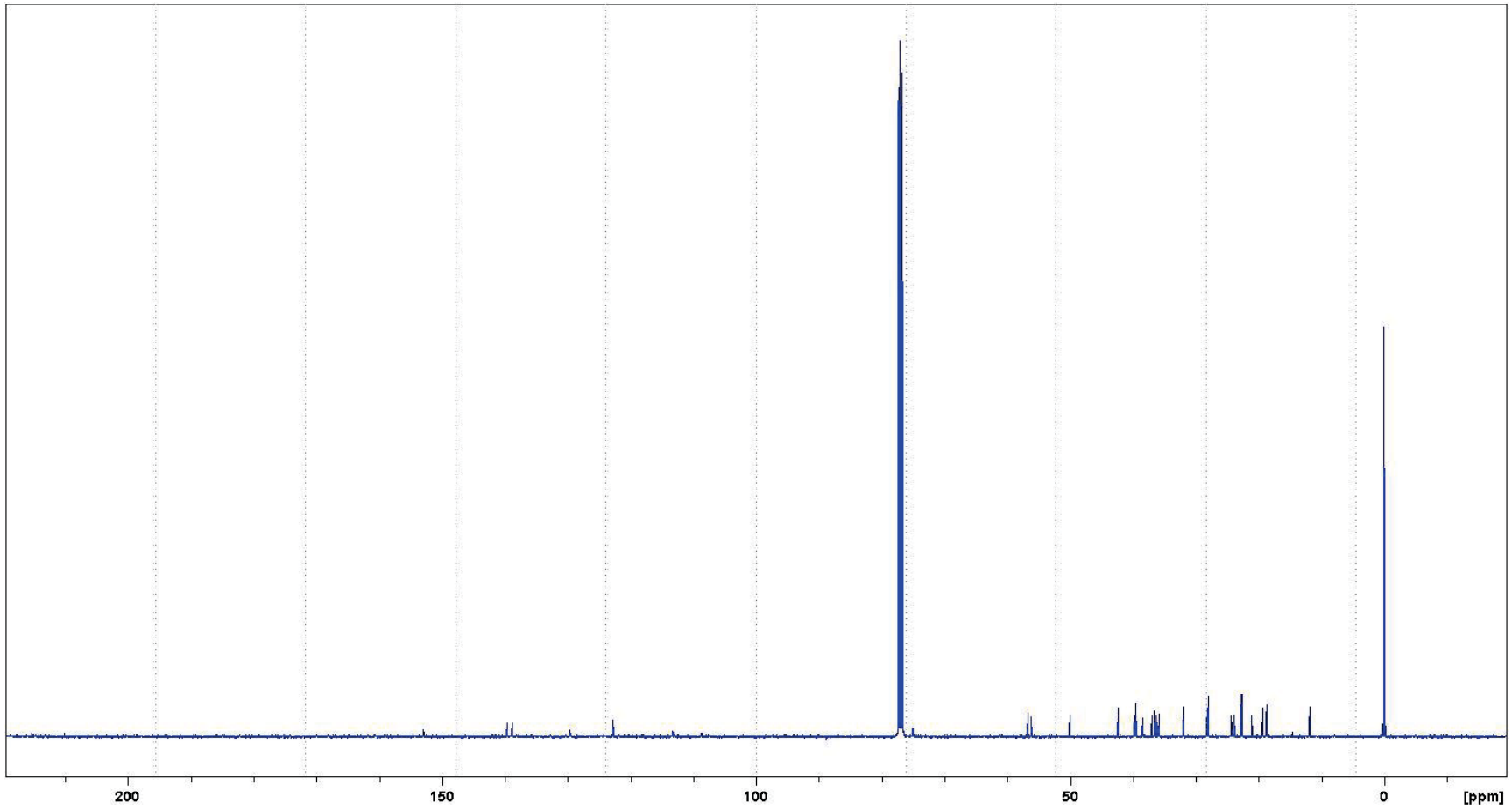

Figure 34: ^{13}C NMR of (8*S*,9*S*,10*R*,13*R*,14*S*,17*R*)-10,13-dimethyl-17-((*R*)-6-methylheptan-2-yl)-2,3,4,7,8,9,10,11,12,13,14,15,16,17-tetradecahydro-1H-cyclopenta[a]phenanthren-3-yl ((8*R*,9*R*,10*S*,13*S*,14*R*,17*S*)-10,13-dimethyl-17-((*S*)-6-methylheptan-2-yl)-2,3,4,7,8,9,10,11,12,13,14,15,16,17-tetradecahydro-1H-cyclopenta[a]phenanthren-3-yl) 1,3-phenylenedicarbamate **13**

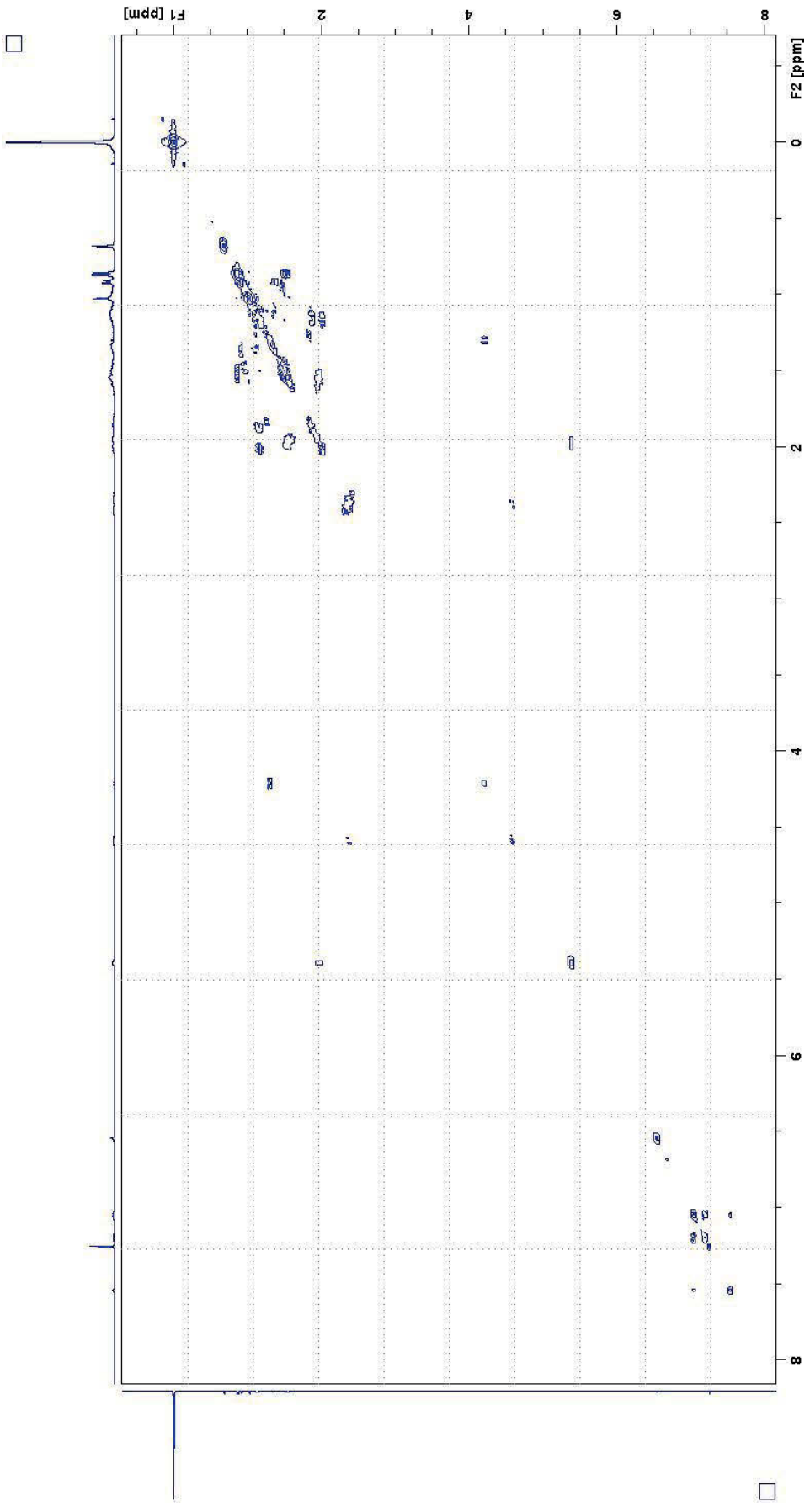

Figure 35: COSY of (8*S*,9*S*,10*R*,13*R*,14*S*,17*R*)-10,13-dimethyl-17-((*R*)-6-methylheptan-2-yl)-2,3,4,7,8,9,10,11,12,13,14,15,16,17-tetradecahydro-1H-cyclopenta[a]phenanthren-3-yl ((8*R*,9*R*,10*S*,13*S*,14*R*,17*S*)-10,13-dimethyl-17-((*S*)-6-methylheptan-2-yl)-2,3,4,7,8,9,10,11,12,13,14,15,16,17-tetradecahydro-1H-cyclopenta[a]phenanthren-3-yl) 1,3-phenylenedicarbamate **13**

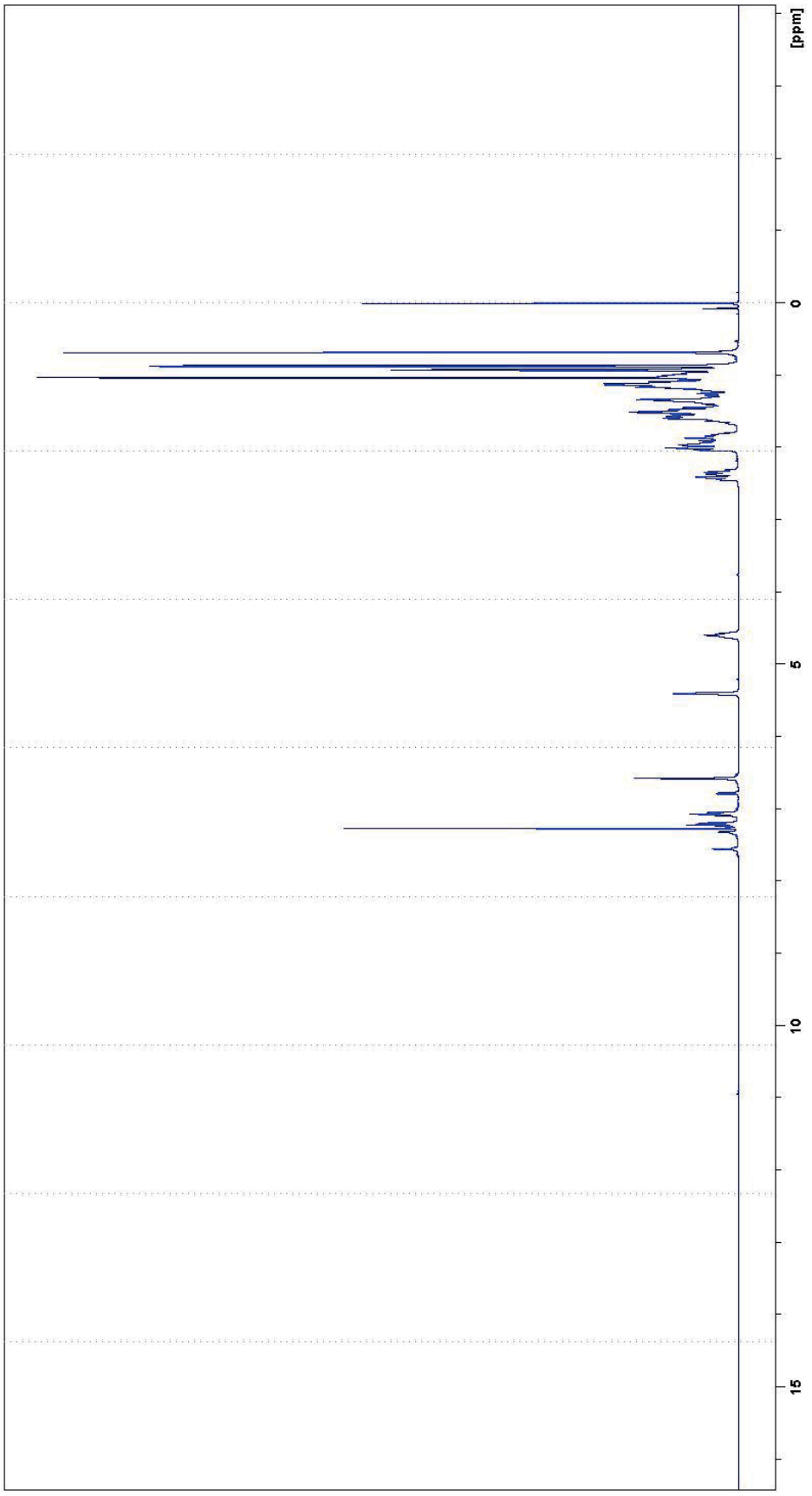

Figure 36: ^{1}H NMR of (8*S*,9*S*,10*R*,13*R*,14*S*,17*R*)-10,13-dimethyl-17-((*R*)-6-methylheptan-2-yl)-2,3,4,7,8,9,10,11,12,13,14,15,16,17-tetradecahydro-1H-cyclopenta[a]phenanthren-3-yl ((8*R*,9*R*,10*S*,13*S*,14*R*,17*S*)-10,13-dimethyl-17-((*S*)-6-methylheptan-2-yl)-2,3,4,7,8,9,10,11,12,13,14,15,16,17-tetradecahydro-1H-cyclopenta[a]phenanthren-3-yl) 1,4-phenylenedicarbamate **14**

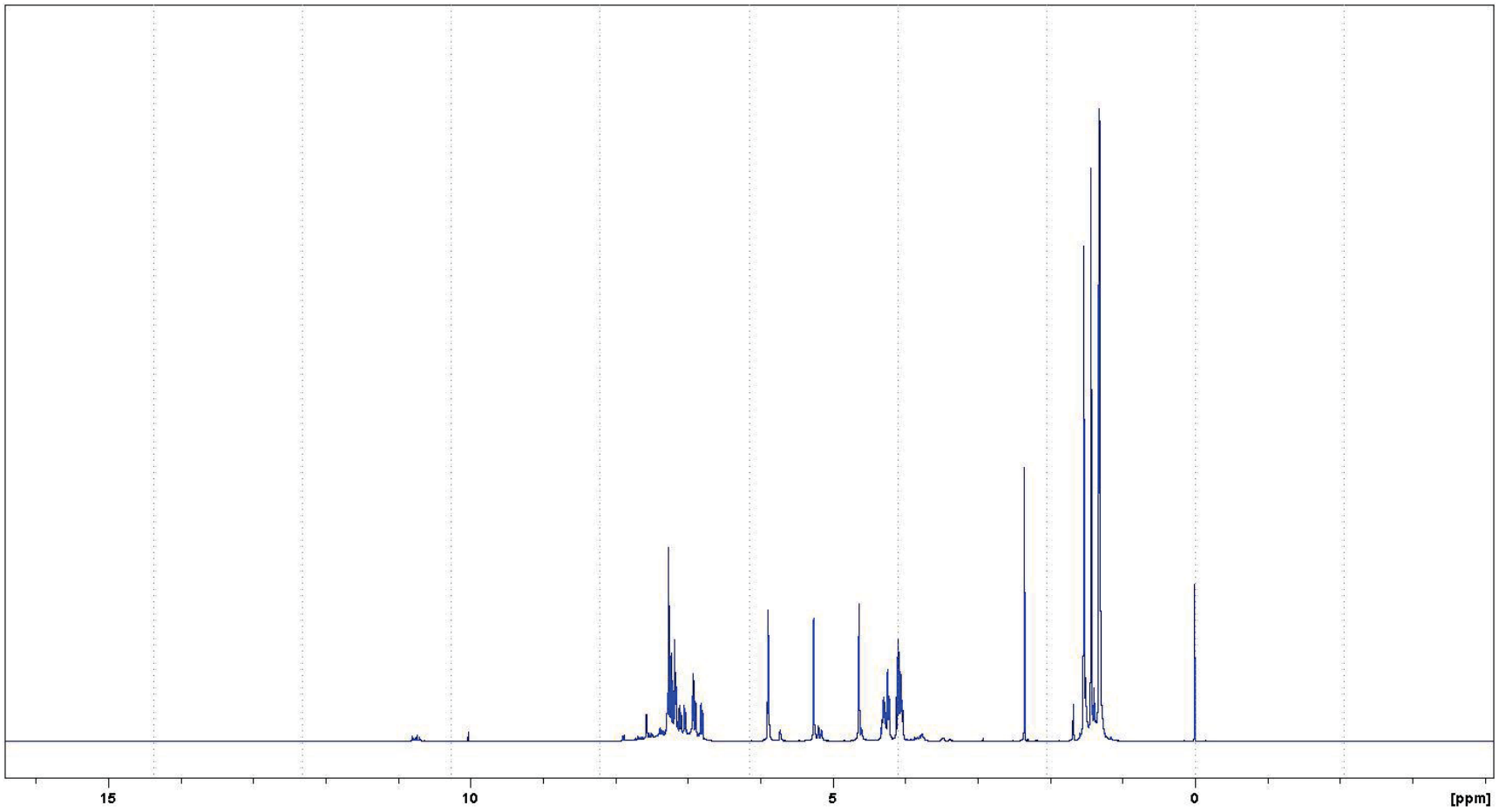

Figure 37: ^{1}H NMR of ((3a*R*,5*R*,6*S*,6a*R*)-6-hydroxy-2,2-dimethyltetrahydrofuro[2,3-d][1,3]dioxol-5-yl)methyl (((3a*S*,5*S*,6*R*,6a*S*)-6-hydroxy-2,2-dimethyltetrahydrofuro[2,3-d][1,3]dioxol-5-yl)methyl) 1,3-phenylenedicarbamate **15**

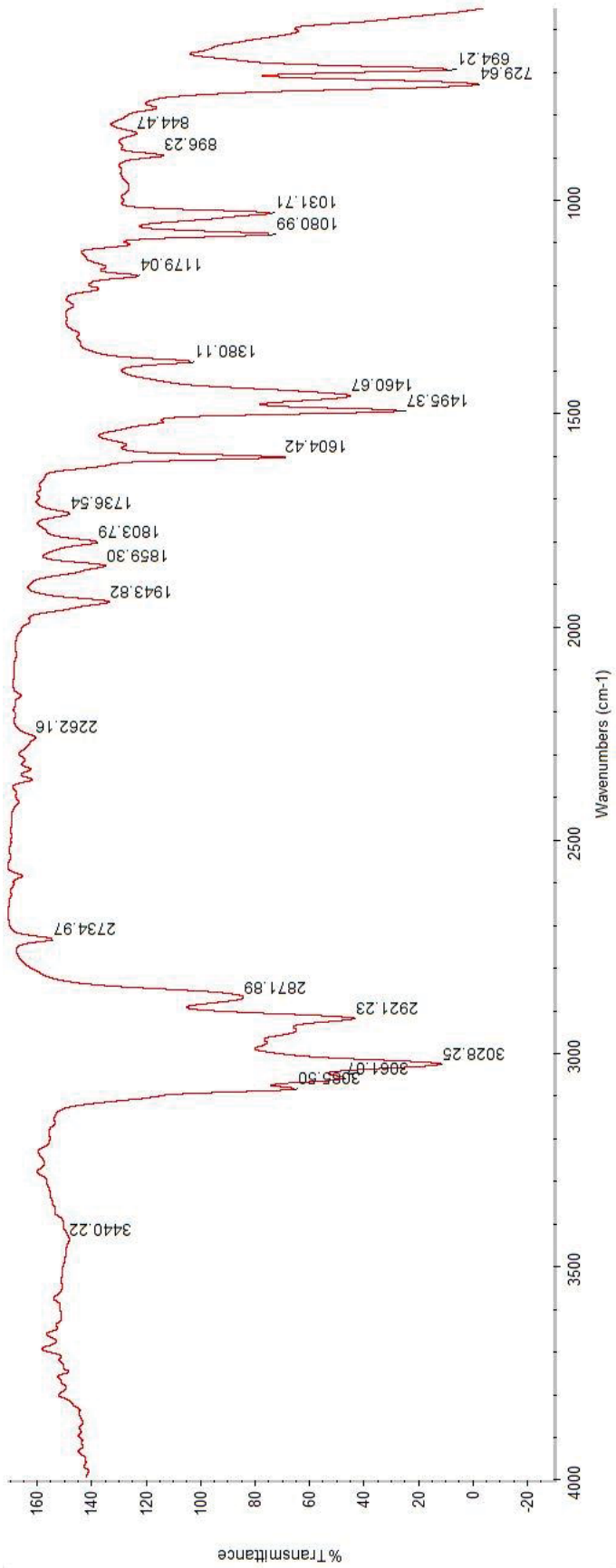

Figure 38: IR of ((3a*R*,5*R*,6*S*,6a*R*)-6-hydroxy-2,2-dimethyltetrahydrofuro[2,3-d][1,3]dioxol-5-yl)methyl (((3a*S*,5*S*,6*R*,6a*S*)-6-hydroxy-2,2-dimethyltetrahydrofuro[2,3-d][1,3]dioxol-5-yl)methyl) 1,3-phenylenedicarbamate **15**

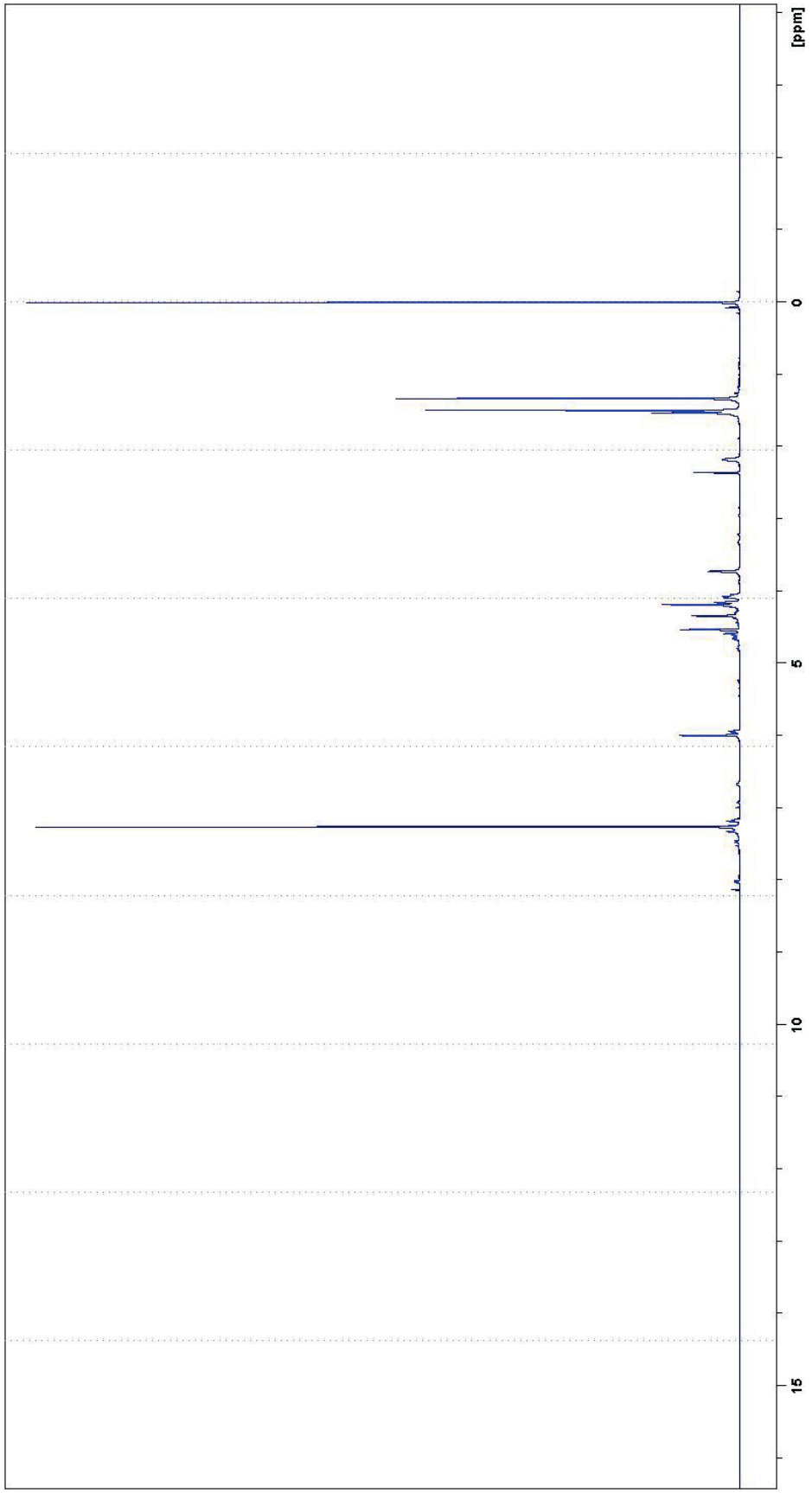

Figure 39: ^{1}H NMR of ((3a*R*,5*R*,6*S*,6a*R*)-6-hydroxy-2,2-dimethyltetrahydrofuro[2,3-d][1,3]dioxol-5-yl)methyl (((3a*S*,5*S*,6*R*,6a*S*)-6-hydroxy-2,2-dimethyltetrahydrofuro[2,3-d][1,3]dioxol-5-yl)methyl) 1,4-phenylenedicarbamate **16**

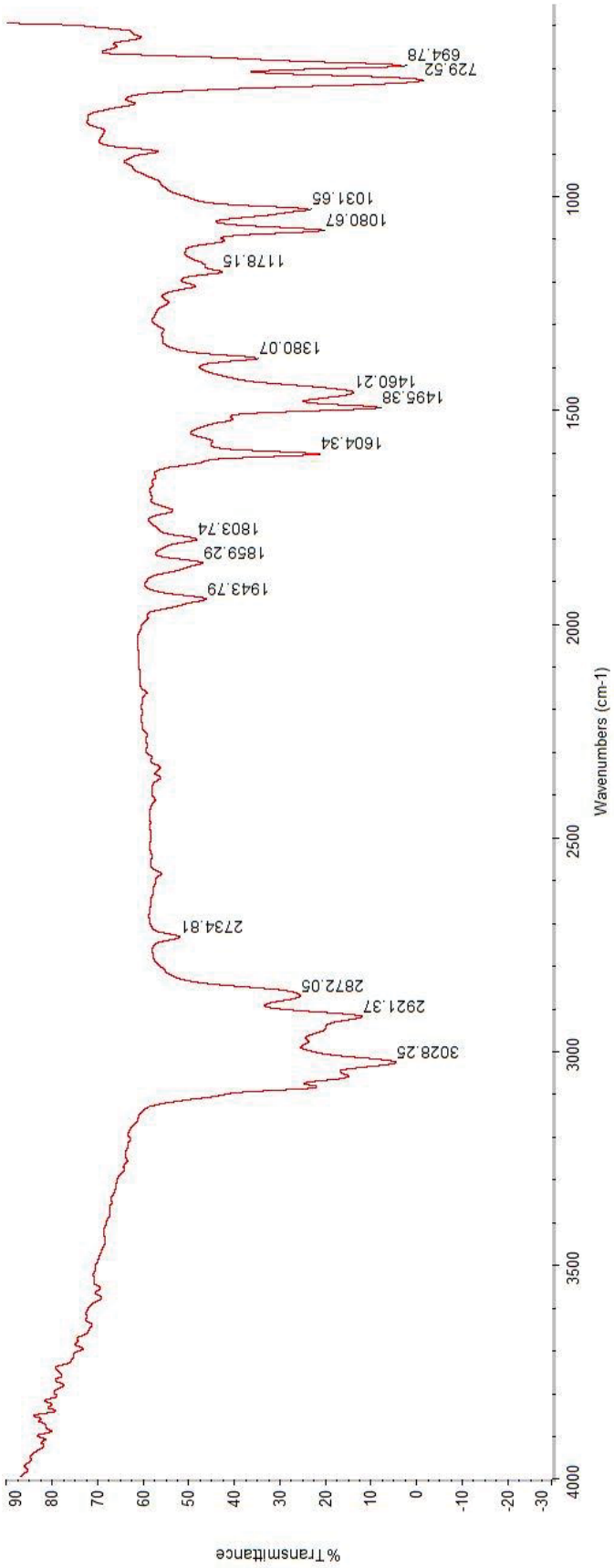

Figure 40: IR of ((3a*R*,5*R*,6*S*,6a*R*)-6-hydroxy-2,2-dimethyltetrahydrofuro[2,3-d][1,3]dioxol-5-yl)methyl (((3a*S*,5*S*,6*R*,6a*S*)-6-hydroxy-2,2-dimethyltetrahydrofuro[2,3-d][1,3]dioxol-5-yl)methyl) 1,4-phenylenedicarbamate **16**

Appendix B

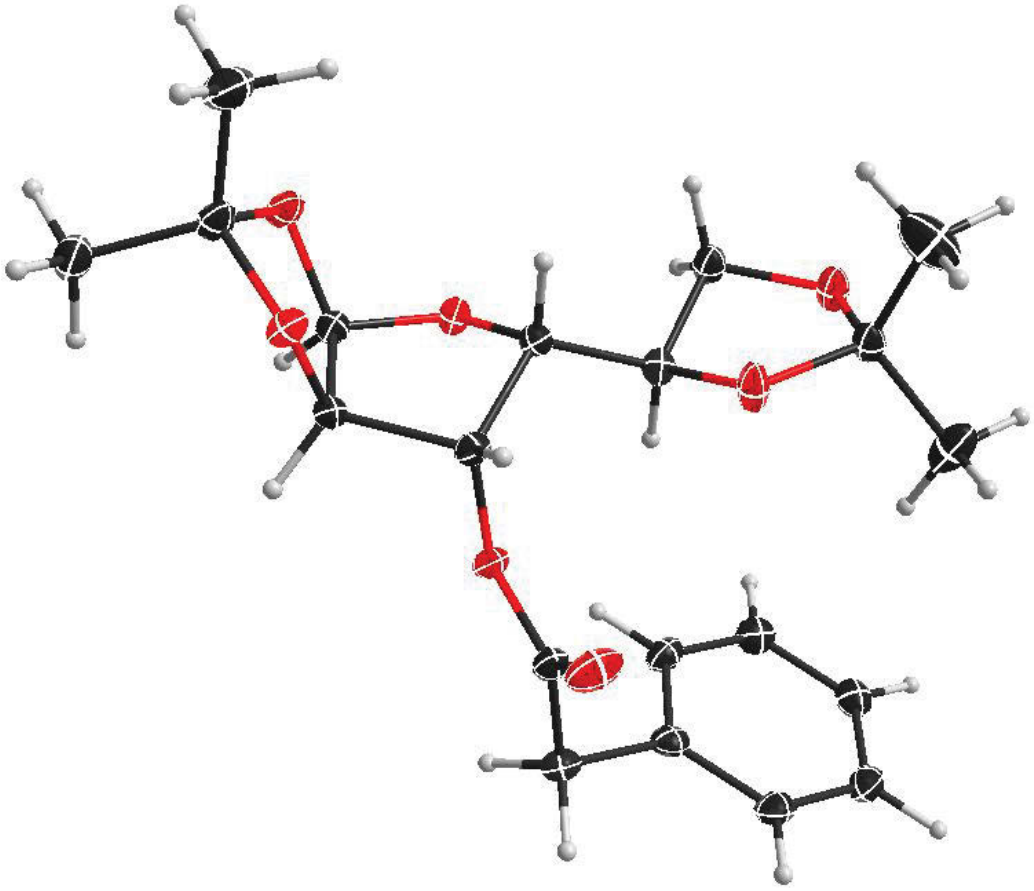

Figure 41: X-ray crystal structure of ester **2**

Table 1: Experimental Details

	Prosp14AN010_0m
Crystal data	
Chemical Formula	C40H52O14
M_r	756.81
Crystal system, space group	Orthorhombic, P212121
Temperature (K)	100
a, *b*, *c* (Å)	9.8991, 10.0445, 19.6723
V(Å^{-3})	1956.05
Z	2
Radiation type	Cu *K*alpha
mew (mm^{-1})	0.81
Crystal size (mm)	0.31 × 0.22 × 0.10
Data collection	
Diffractometer	Bruker *AXS* Prospector CCD diffractometer
Absorption correction	Multi-scan Apex2 v2014.1-0 (Bruker, 2014)
T_{min}, T_{max}	0.509, 0.753
No. of measured, independent and observed [$I > 2\sigma(I)$] reflections	22375, 3423, 3406
R_{int}	0.039
Refinement	
$R[F^2 > 2\sigma(F^2)]$, $wR(F^2)$, S	0.024, 0.062, 1.04
No. of reflections	3423
No. of parameters	249
No. of restraints	0
H-atom treatment	H-atom parameters constrained
$\Delta\rho_{max}$, $\Delta\rho_{min}$, (e Å^{-3})	0.16, -0.14

Computer programs: Apex2 v2014.1-0 (Bruker, 2014), shelXle (Hübschle *et al*, 2011)

Table 2: Bond Lenghts (Å)

C1—O1	1.4057 (19)	C9—H9C	0.98
C1—O2	1.4240 (19)	C10—O7	1.197 (2)
C1—C2	1.547 (2)	C10—O4	1.3598 (19)
C1—H1	1	C10—C11	1.513 (2)
C2—O3	1.4224 (19)	C11—C12	1.521 (2)
C2—C3	1.530 (2)	C11—H11A	0.99
C2—H2	1	C11—H11B	0.99
C3—O4	1.4421 (19)	C12—C17	1.389 (2)
C3—C4	1.528 (2)	C12—C13	1.394 (2)
C3—H3	1	C13—C14	1.389 (2)
C4—O1	1.436 (2)	C13—H13	0.95
C4—C5	1.510 (2)	C14—C15	1.385 (2)
C4—H4	1	C14—H14	0.95
C5—O5	1.427 (2)	C15—C16	1.387 (3)
C5—C6	1.518 (2)	C15—H15	0.95
C5—H5	1	C16—C17	1.389 (2)
C6—O6	1.420 (2)	C16—H16	0.95
C6—H6A	0.99	C17—H17	0.95
C6—H6B	0.99	C18—O6	1.430 (2)
C7—O2	1.4331 (19)	C18—O5	1.4391 (19)
C7—O3	1.4360 (19)	C18—C20	1.503 (2)
C7—C8	1.506 (2)	C18—C19	1.503 (3)
C7—C9	1.514 (2)	C19—H19A	0.98
C8—H8A	0.98	C19—H19B	0.98
C8—H8B	0.98	C19—H19C	0.98
C8—H8C	0.98	C20—H20A	0.98
C9—H9A	0.98	C20—H20B	0.98
C9—H9B	0.98	C20—H20C	0.98

Table 3: Bond Angles (º)

O1—C1—O2	110.11 (13)	H9B—C9—H9C	109.5
O1—C1—C2	107.48 (12)	O7—C10—O4	124.13 (15)
O2—C1—C2	104.37 (12)	O7—C10—C11	125.67 (15)
O1—C1—H1	111.5	O4—C10—C11	110.19 (13)
O2—C1—H1	111.5	C10—C11—C12	110.09 (13)
C2—C1—H1	111.5	C10—C11—H11A	109.6
O3—C2—C3	108.62 (12)	C12—C11—H11A	109.6
O3—C2—C1	104.64 (12)	C10—C11—H11B	109.6
C3—C2—C1	103.87 (12)	C12—C11—H11B	109.6
O3—C2—H2	113	H11A—C11—H11B	108.2
C3—C2—H2	113	C17—C12—C13	119.14 (15)
C1—C2—H2	113	C17—C12—C11	120.25 (15)
O4—C3—C4	109.86 (12)	C13—C12—C11	120.59 (15)
O4—C3—C2	107.33 (12)	C14—C13—C12	120.52 (16)
C4—C3—C2	101.99 (12)	C14—C13—H13	119.7
O4—C3—H3	112.4	C12—C13—H13	119.7
C4—C3—H3	112.4	C15—C14—C13	120.09 (16)
C2—C3—H3	112.4	C15—C14—H14	120
O1—C4—C5	107.35 (12)	C13—C14—H14	120
O1—C4—C3	104.30 (12)	C14—C15—C16	119.57 (16)
C5—C4—C3	116.96 (13)	C14—C15—H15	120.2
O1—C4—H4	109.3	C16—C15—H15	120.2
C5—C4—H4	109.3	C15—C16—C17	120.52 (16)
C3—C4—H4	109.3	C15—C16—H16	119.7
O5—C5—C4	108.25 (13)	C17—C16—H16	119.7
O5—C5—C6	102.52 (13)	C16—C17—C12	120.16 (16)
C4—C5—C6	114.88 (14)	C16—C17—H17	119.9
O5—C5—H5	110.3	C12—C17—H17	119.9
C4—C5—H5	110.3	O6—C18—O5	106.23 (12)
C6—C5—H5	110.3	O6—C18—C20	107.83 (14)
O6—C6—C5	102.18 (13)	O5—C18—C20	110.30 (14)
O6—C6—H6A	111.3	O6—C18—C19	110.24 (14)
C5—C6—H6A	111.3	O5—C18—C19	108.02 (14)
O6—C6—H6B	111.3	C20—C18—C19	113.96 (17)
C5—C6—H6B	111.3	C18—C19—H19A	109.5
H6A—C6—H6B	109.2	C18—C19—H19B	109.5
O2—C7—O3	104.10 (12)	H19A—C19—H19B	109.5

O2—C7—C8	109.50 (14)	C18—C19—H19C	109.5
O3—C7—C8	108.69 (14)	H19A—C19—H19C	109.5
O2—C7—C9	109.71 (14)	H19B—C19—H19C	109.5
O3—C7—C9	110.88 (13)	C18—C20—H20A	109.5
C8—C7—C9	113.53 (14)	C18—C20—H20B	109.5
C7—C8—H8A	109.5	H20A—C20—H20B	109.5
C7—C8—H8B	109.5	C18—C20—H20C	109.5
H8A—C8—H8B	109.5	H20A—C20—H20C	109.5
C7—C8—H8C	109.5	H20B—C20—H20C	109.5
H8A—C8—H8C	109.5	C1—O1—C4	107.80 (11)
H8B—C8—H8C	109.5	C1—O2—C7	108.46 (12)
C7—C9—H9A	109.5	C2—O3—C7	107.23 (12)
C7—C9—H9B	109.5	C10—O4—C3	117.33 (12)
H9A—C9—H9B	109.5	C5—O5—C18	108.15 (12)
C7—C9—H9C	109.5	C6—O6—C18	107.21 (12)
H9A—C9—H9C	109.5		

Table 4: Torsion Angles (º)

O1—C1—C2—O3	112.26 (13)	C11—C12—C17—C16	−178.78 (16)
O2—C1—C2—O3	−4.67 (15)	O2—C1—O1—C4	90.77 (14)
O1—C1—C2—C3	−1.59 (16)	C2—C1—O1—C4	−22.33 (16)
O2—C1—C2—C3	−118.52 (13)	C5—C4—O1—C1	162.22 (13)
O3—C2—C3—O4	156.33 (11)	C3—C4—O1—C1	37.49 (15)
C1—C2—C3—O4	−92.70 (13)	O1—C1—O2—C7	−131.26 (13)
O3—C2—C3—C4	−88.20 (14)	C2—C1—O2—C7	−16.17 (16)
C1—C2—C3—C4	22.77 (15)	O3—C7—O2—C1	30.97 (16)
O4—C3—C4—O1	76.98 (14)	C8—C7—O2—C1	147.04 (14)
C2—C3—C4—O1	−36.64 (14)	C9—C7—O2—C1	−87.74 (15)
O4—C3—C4—C5	−41.37 (19)	C3—C2—O3—C7	134.17 (13)
C2—C3—C4—C5	−154.98 (13)	C1—C2—O3—C7	23.72 (15)
O1—C4—C5—O5	177.17 (12)	O2—C7—O3—C2	−33.96 (15)
C3—C4—C5—O5	−66.14 (18)	C8—C7—O3—C2	−150.60 (13)
O1—C4—C5—C6	63.30 (17)	C9—C7—O3—C2	83.94 (15)
C3—C4—C5—C6	179.99 (14)	O7—C10—O4—C3	−0.3 (2)
O5—C5—C6—O6	36.10 (16)	C11—C10—O4—C3	−179.03 (12)
C4—C5—C6—O6	153.27 (14)	C4—C3—O4—C10	121.54 (14)

O7—C10—C11—C12	−93.26 (19)	C2—C3—O4—C10	−128.33 (13)
O4—C10—C11—C12	85.46 (16)	C4—C5—O5—C18	−147.05 (13)
C10—C11—C12—C17	101.40 (17)	C6—C5—O5—C18	−25.25 (16)
C10—C11—C12—C13	−77.12 (19)	O6—C18—O5—C5	5.05 (17)
C17—C12—C13—C14	−0.1 (2)	C20—C18—O5—C5	−111.54 (16)
C11—C12—C13—C14	178.43 (15)	C19—C18—O5—C5	123.31 (16)
C12—C13—C14—C15	0.5 (3)	C5—C6—O6—C18	−34.09 (16)
C13—C14—C15—C16	−0.6 (2)	O5—C18—O6—C6	19.20 (17)
C14—C15—C16—C17	0.2 (3)	C20—C18—O6—C6	137.43 (15)
C15—C16—C17—C12	0.2 (2)	C19—C18—O6—C6	−97.60 (16)
C13—C12—C17—C16	−0.2 (2)		

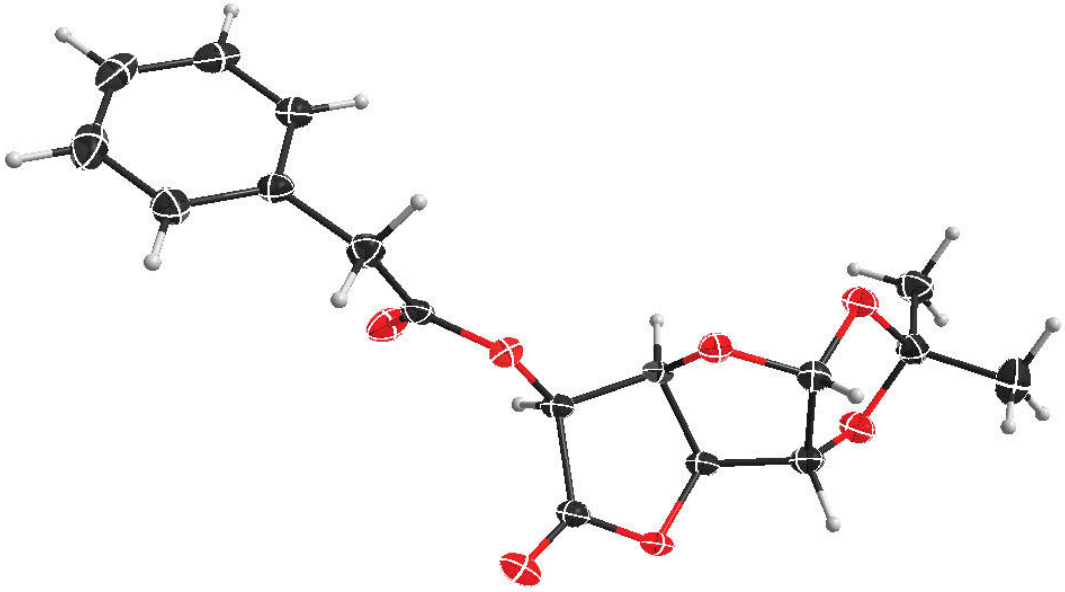

Figure 42: X-ray crystal structure of ester **6**

Table 1: Experimental Details

	13RN075_0m
Crystal data	
Chemical Formula	$C_{17}H_{18}O_7$
M_r	334.31
Crystal system, space group	Monoclinic, $P2_1$
Temperature (K)	150
a, b, c (Å)	11.160, 5.768, 12.214
V(Å^{-3})	783
Z	2
Radiation type	Mo $K\alpha$
μ (mm^{-1})	0.11
Crystal size (mm)	0.55 × 0.15 × 0.08
Data collection	
Diffractometer	Bruker *AXS SMART* APEX CCD diffractometer
Absorption correction	Multi-scan
	Apex2 v2013.4-1 (Bruker, 2012)
T_{min}, T_{max}	0.584, 0.746
No. of measured, independent and observed [$I > 2\sigma(I)$] reflections	15677, 4675, 3809
R_{int}	0.059
Refinement	
$R[F^2 > 2\sigma(F^2)]$, $wR(F^2)$, S	0.042, 0.103, 1.00
No. of reflections	4675
No. of parameters	219
No. of restraints	1
H-atom treatment	H-atom parameters constrained
$\Delta\rho_{max}$, $\Delta\rho_{min}$, (e Å^{-3})	0.28, -0.26

Computer programs: Apex2 v2013.4-1 (Bruker 2012), shelXle (Hübschle *et al*, 2011)

Table 2: Bond Lengths (Å)

O1—C1	1.402 (3)	C7—C9	1.519 (3)
O1—C4	1.432 (2)	C8—H8A	0.98
O2—C1	1.422 (3)	C8—H8B	0.98
O2—C7	1.424 (3)	C8—H8C	0.98
O3—C2	1.428 (3)	C9—H9A	0.98
O3—C7	1.428 (3)	C9—H9B	0.98
O4—C6	1.353 (3)	C9—H9C	0.98
O4—C3	1.454 (3)	C10—C11	1.505 (3)
O5—C10	1.354 (3)	C11—C12	1.508 (3)
O5—C5	1.425 (3)	C11—H11A	0.99
O6—C6	1.189 (3)	C11—H11B	0.99
O7—C10	1.197 (3)	C12—C17	1.389 (3)
C1—C2	1.541 (3)	C12—C13	1.396 (3)
C1—H1	1	C13—C14	1.385 (3)
C2—C3	1.511 (3)	C13—H13	0.95
C2—H2	1	C14—C15	1.384 (4)
C3—C4	1.536 (3)	C14—H14	0.95
C3—H3	1	C15—C16	1.380 (5)
C4—C5	1.510 (3)	C15—H15	0.95
C4—H4	1	C16—C17	1.390 (4)
C5—C6	1.519 (3)	C16—H16	0.95
C5—H5	1	C17—H17	0.95
C7—C8	1.508 (3)		

Table 3: Bond Angles (º)

C1—O1—C4	107.92 (16)	O3—C7—C9	109.6 (2)
C1—O2—C7	107.63 (17)	C8—C7—C9	113.5 (2)
C2—O3—C7	107.12 (16)	C7—C8—H8A	109.5
C6—O4—C3	110.93 (16)	C7—C8—H8B	109.5
C10—O5—C5	116.35 (16)	H8A—C8—H8B	109.5
O1—C1—O2	110.73 (17)	C7—C8—H8C	109.5
O1—C1—C2	107.71 (17)	H8A—C8—H8C	109.5
O2—C1—C2	103.20 (17)	H8B—C8—H8C	109.5
O1—C1—H1	111.6	C7—C9—H9A	109.5
O2—C1—H1	111.6	C7—C9—H9B	109.5
C2—C1—H1	111.6	H9A—C9—H9B	109.5

O3—C2—C3	109.41 (17)	C7—C9—H9C	109.5
O3—C2—C1	105.69 (18)	H9A—C9—H9C	109.5
C3—C2—C1	103.98 (17)	H9B—C9—H9C	109.5
O3—C2—H2	112.4	O7—C10—O5	123.7 (2)
C3—C2—H2	112.4	O7—C10—C11	126.3 (2)
C1—C2—H2	112.4	O5—C10—C11	109.91 (17)
O4—C3—C2	108.73 (17)	C10—C11—C12	114.23 (18)
O4—C3—C4	105.03 (16)	C10—C11—H11A	108.7
C2—C3—C4	104.55 (17)	C12—C11—H11A	108.7
O4—C3—H3	112.6	C10—C11—H11B	108.7
C2—C3—H3	112.6	C12—C11—H11B	108.7
C4—C3—H3	112.6	H11A—C11—H11B	107.6
O1—C4—C5	110.08 (17)	C17—C12—C13	119.1 (2)
O1—C4—C3	104.34 (16)	C17—C12—C11	120.5 (2)
C5—C4—C3	101.79 (17)	C13—C12—C11	120.4 (2)
O1—C4—H4	113.2	C14—C13—C12	120.4 (2)
C5—C4—H4	113.2	C14—C13—H13	119.8
C3—C4—H4	113.2	C12—C13—H13	119.8
O5—C5—C4	115.80 (17)	C15—C14—C13	119.9 (3)
O5—C5—C6	110.13 (17)	C15—C14—H14	120
C4—C5—C6	103.14 (17)	C13—C14—H14	120
O5—C5—H5	109.2	C16—C15—C14	120.2 (2)
C4—C5—H5	109.2	C16—C15—H15	119.9
C6—C5—H5	109.2	C14—C15—H15	119.9
O6—C6—O4	122.8 (2)	C15—C16—C17	120.1 (2)
O6—C6—C5	128.5 (2)	C15—C16—H16	119.9
O4—C6—C5	108.65 (18)	C17—C16—H16	119.9
O2—C7—O3	104.67 (17)	C12—C17—C16	120.3 (2)
O2—C7—C8	109.1 (2)	C12—C17—H17	119.9
O3—C7—C8	108.75 (19)	C16—C17—H17	119.9
O2—C7—C9	110.79 (19)		

Table 4: Torsion Angles (º)

C4—O1—C1—O2	84.61 (19)	C3—C4—C5—C6	31.2 (2)
C4—O1—C1—C2	−27.6 (2)	C3—O4—C6—O6	−175.2 (2)
C7—O2—C1—O1	−140.35 (17)	C3—O4—C6—C5	5.7 (2)
C7—O2—C1—C2	−25.3 (2)	O5—C5—C6—O6	32.6 (3)
C7—O3—C2—C3	126.18 (19)	C4—C5—C6—O6	156.8 (2)

C7—O3—C2—C1	14.8 (2)	O5—C5—C6—O4	−148.29 (17)
O1—C1—C2—O3	123.48 (18)	C4—C5—C6—O4	−24.1 (2)
O2—C1—C2—O3	6.3 (2)	C1—O2—C7—O3	35.4 (2)
O1—C1—C2—C3	8.3 (2)	C1—O2—C7—C8	151.64 (19)
O2—C1—C2—C3	−108.88 (18)	C1—O2—C7—C9	−82.7 (2)
C6—O4—C3—C2	126.37 (19)	C2—O3—C7—O2	−30.5 (2)
C6—O4—C3—C4	14.9 (2)	C2—O3—C7—C8	−147.07 (19)
O3—C2—C3—O4	148.05 (17)	C2—O3—C7—C9	88.3 (2)
C1—C2—C3—O4	−99.42 (19)	C5—O5—C10—O7	2.8 (3)
O3—C2—C3—C4	−100.19 (19)	C5—O5—C10—C11	−179.47 (17)
C1—C2—C3—C4	12.3 (2)	O7—C10—C11—C12	−12.3 (3)
C1—O1—C4—C5	143.70 (17)	O5—C10—C11—C12	170.06 (18)
C1—O1—C4—C3	35.16 (19)	C10—C11—C12—C17	115.7 (2)
O4—C3—C4—O1	85.78 (18)	C10—C11—C12—C13	−65.3 (3)
C2—C3—C4—O1	−28.6 (2)	C17—C12—C13—C14	0.6 (3)
O4—C3—C4—C5	−28.8 (2)	C11—C12—C13—C14	−178.5 (2)
C2—C3—C4—C5	−143.16 (17)	C12—C13—C14—C15	−0.7 (4)
C10—O5—C5—C4	123.3 (2)	C13—C14—C15—C16	0.0 (4)
C10—O5—C5—C6	−120.21 (19)	C14—C15—C16—C17	0.6 (4)
O1—C4—C5—O5	41.4 (2)	C13—C12—C17—C16	0.1 (3)
C3—C4—C5—O5	151.59 (17)	C11—C12—C17—C16	179.1 (2)
O1—C4—C5—C6	−79.0 (2)	C15—C16—C17—C12	−0.7 (4)

Figure 43: X-ray crystal structure of ester **7**

Table 1: Experimental Details

	13mz145_0m
Crystal data	
Chemical Formula	$C_{16}H_{18}O_8S$
M_r	370.36
Crystal system, space group	Orthorhombic, $P2_12_12_1$
Temperature (K)	150
a, b, c (Å)	10.0018, 10.7583, 15.9353
V(Å^{-3})	1714.7
Z	4
Radiation type	Mo $K\alpha$
μ (mm^{-1})	0.23
Crystal size (mm)	0.44 × 0.36 × 0.20
Data collection	
Diffractometer	Bruker *AXS SMART* APEX CCD diffractometer
Absorption correction	Multi-scan Apex2 v2013.4-1 (Bruker, 2012)
T_{min}, T_{max}	0.646, 0.746
No. of measured, independent and observed [$I > 2\sigma(I)$] reflections	27953, 5374, 5169
R_{int}	0.026
Refinement	
$R[F^2 > 2\sigma(F^2)]$, $wR(F^2)$, S	0.034, 0.090, 1.04
No. of reflections	5374
No. of parameters	252
No. of restraints	0
H-atom treatment	H-atom parameters constrained
$\Delta\rho_{max}$, $\Delta\rho_{min}$, (e Å^{-3})	0.45, -0.20

Table 2: Bond Lengths (Å)

S1—O8	1.4309 (13)	C8—H8A	0.98
S1—O7	1.4316 (15)	C8—H8B	0.98
S1—O5	1.5997 (11)	C8—H8C	0.98
S1—C10	1.7802 (19)	C9—H9A	0.98
O1—C1	1.4021 (18)	C9—H9B	0.98
O1—C4	1.4315 (18)	C9—H9C	0.98
O2—C1	1.4215 (19)	C7B—C8B	1.482 (17)
O2—C7	1.439 (3)	C7B—C9B	1.516 (18)
O2—C7B	1.480 (14)	C8B—H8D	0.98
O3—C2	1.4144 (19)	C8B—H8E	0.98
O3—C7	1.434 (4)	C8B—H8F	0.98
O3—C7B	1.445 (14)	C9B—H9B1	0.98
O4—C6	1.344 (2)	C9B—H9B2	0.98
O4—C3	1.4557 (18)	C9B—H9B3	0.98
O5—C5	1.4321 (17)	C10—C11	1.502 (2)
O6—C6	1.1963 (19)	C10—H10A	0.99
C1—C2	1.543 (2)	C10—H10B	0.99
C1—H1	1	C11—C12	1.380 (2)
C2—C3	1.524 (2)	C11—C16	1.387 (2)
C2—H2	1	C12—C13	1.397 (3)
C3—C4	1.5348 (19)	C12—H12	0.95
C3—H3	1	C13—C14	1.379 (5)
C4—C5	1.515 (2)	C13—H13	0.95
C4—H4	1	C14—C15	1.373 (5)
C5—C6	1.524 (2)	C14—H14	0.95

C5—H5	1	C15—C16	1.385 (3)
C7—C8	1.502 (5)	C15—H15	0.95
C7—C9	1.509 (5)	C16—H16	0.95

Table 3: Bond Angles (º)

O8—S1—O7	120.63 (9)	C7—C8—H8B	109.5
O8—S1—O5	104.51 (8)	H8A—C8—H8B	109.5
O7—S1—O5	109.06 (7)	C7—C8—H8C	109.5
O8—S1—C10	109.07 (10)	H8A—C8—H8C	109.5
O7—S1—C10	109.87 (9)	H8B—C8—H8C	109.5
O5—S1—C10	101.99 (8)	C7—C9—H9A	109.5
C1—O1—C4	108.24 (11)	C7—C9—H9B	109.5
C1—O2—C7	107.1 (2)	H9A—C9—H9B	109.5
C1—O2—C7B	113.5 (6)	C7—C9—H9C	109.5
C2—O3—C7	108.27 (19)	H9A—C9—H9C	109.5
C2—O3—C7B	113.8 (6)	H9B—C9—H9C	109.5
C6—O4—C3	110.96 (11)	O3—C7B—O2	102.1 (9)
C5—O5—S1	119.89 (10)	O3—C7B—C8B	107.9 (15)
O1—C1—O2	110.11 (13)	O2—C7B—C8B	112.1 (14)
O1—C1—C2	107.37 (11)	O3—C7B—C9B	109.2 (11)
O2—C1—C2	103.66 (12)	O2—C7B—C9B	104.6 (11)
O1—C1—H1	111.8	C8B—C7B—C9B	119.5 (18)
O2—C1—H1	111.8	C7B—C8B—H8D	109.5
C2—C1—H1	111.8	C7B—C8B—H8E	109.5
O3—C2—C3	109.62 (13)	H8D—C8B—H8E	109.5
O3—C2—C1	105.79 (12)	C7B—C8B—H8F	109.5
C3—C2—C1	103.95 (11)	H8D—C8B—H8F	109.5

O3—C2—H2	112.3	H8E—C8B—H8F	109.5
C3—C2—H2	112.3	C7B—C9B—H9B1	109.5
C1—C2—H2	112.3	C7B—C9B—H9B2	109.5
O4—C3—C2	109.47 (12)	H9B1—C9B—H9B2	109.5
O4—C3—C4	105.62 (11)	C7B—C9B—H9B3	109.5
C2—C3—C4	104.60 (11)	H9B1—C9B—H9B3	109.5
O4—C3—H3	112.2	H9B2—C9B—H9B3	109.5
C2—C3—H3	112.2	C11—C10—S1	112.28 (11)
C4—C3—H3	112.2	C11—C10—H10A	109.1
O1—C4—C5	108.89 (11)	S1—C10—H10A	109.1
O1—C4—C3	104.63 (11)	C11—C10—H10B	109.1
C5—C4—C3	102.87 (11)	S1—C10—H10B	109.1
O1—C4—H4	113.2	H10A—C10—H10B	107.9
C5—C4—H4	113.2	C12—C11—C16	119.44 (17)
C3—C4—H4	113.2	C12—C11—C10	121.15 (17)
O5—C5—C4	111.97 (12)	C16—C11—C10	119.41 (16)
O5—C5—C6	110.68 (12)	C11—C12—C13	119.2 (2)
C4—C5—C6	103.06 (12)	C11—C12—H12	120.4
O5—C5—H5	110.3	C13—C12—H12	120.4
C4—C5—H5	110.3	C14—C13—C12	120.9 (2)
C6—C5—H5	110.3	C14—C13—H13	119.6
O6—C6—O4	123.45 (15)	C12—C13—H13	119.6
O6—C6—C5	126.78 (15)	C15—C14—C13	119.9 (2)
O4—C6—C5	109.78 (12)	C15—C14—H14	120.1
O3—C7—O2	104.8 (2)	C13—C14—H14	120.1
O3—C7—C8	108.6 (3)	C14—C15—C16	119.6 (2)
O2—C7—C8	108.1 (3)	C14—C15—H15	120.2

O3—C7—C9	109.6 (3)	C16—C15—H15	120.2
O2—C7—C9	111.1 (3)	C15—C16—C11	121.1 (2)
C8—C7—C9	114.3 (3)	C15—C16—H16	119.5
C7—C8—H8A	109.5	C11—C16—H16	119.5

Table 4: Torsion Angles (º)

O8—S1—O5—C5	146.54 (12)	O5—C5—C6—O4	−140.88 (12)
O7—S1—O5—C5	16.29 (13)	C4—C5—C6—O4	−21.01 (15)
C10—S1—O5—C5	−99.88 (12)	C2—O3—C7—O2	−26.7 (4)
C4—O1—C1—O2	83.16 (14)	C7B—O3—C7—O2	86 (3)
C4—O1—C1—C2	−29.06 (15)	C2—O3—C7—C8	−142.0 (2)
C7—O2—C1—O1	−141.0 (3)	C7B—O3—C7—C8	−29 (2)
C7B—O2—C1—O1	−125.8 (8)	C2—O3—C7—C9	92.5 (3)
C7—O2—C1—C2	−26.4 (3)	C7B—O3—C7—C9	−155 (3)
C7B—O2—C1—C2	−11.2 (8)	C1—O2—C7—O3	33.5 (4)
C7—O3—C2—C3	121.9 (3)	C7B—O2—C7—O3	−83 (3)
C7B—O3—C2—C3	105.9 (8)	C1—O2—C7—C8	149.2 (3)
C7—O3—C2—C1	10.4 (3)	C7B—O2—C7—C8	33 (2)
C7B—O3—C2—C1	−5.6 (8)	C1—O2—C7—C9	−84.7 (3)
O1—C1—C2—O3	126.40 (13)	C7B—O2—C7—C9	159 (3)
O2—C1—C2—O3	9.86 (16)	C2—O3—C7B—O2	−0.9 (13)
O1—C1—C2—C3	10.95 (16)	C7—O3—C7B—O2	−74 (2)
O2—C1—C2—C3	−105.59 (13)	C2—O3—C7B—C8B	−119.2 (18)
C6—O4—C3—C2	124.68 (13)	C7—O3—C7B—C8B	168 (3)
C6—O4—C3—C4	12.56 (15)	C2—O3—C7B—C9B	109.5 (14)
O3—C2—C3—O4	144.01 (12)	C7—O3—C7B—C9B	37 (2)
C1—C2—C3—O4	−103.27 (13)	C1—O2—C7B—O3	8.0 (13)
O3—C2—C3—C4	−103.20 (13)	C7—O2—C7B—O3	77 (2)
C1—C2—C3—C4	9.51 (15)	C1—O2—C7B—C8B	123 (2)
C1—O1—C4—C5	144.37 (12)	C7—O2—C7B—C8B	−168 (4)
C1—O1—C4—C3	34.94 (14)	C1—O2—C7B—C9B	−105.9 (13)

O4—C3—C4—O1	89.02 (13)	C7—O2—C7B—C9B	−37 (2)
C2—C3—C4—O1	−26.48 (14)	O8—S1—C10—C11	168.85 (13)
O4—C3—C4—C5	−24.74 (14)	O7—S1—C10—C11	−56.87 (15)
C2—C3—C4—C5	−140.24 (12)	O5—S1—C10—C11	58.70 (14)
S1—O5—C5—C4	149.53 (10)	S1—C10—C11—C12	84.29 (18)
S1—O5—C5—C6	−96.10 (13)	S1—C10—C11—C16	−94.72 (17)
O1—C4—C5—O5	35.23 (15)	C16—C11—C12—C13	1.1 (3)
C3—C4—C5—O5	145.84 (12)	C10—C11—C12—C13	−177.9 (2)
O1—C4—C5—C6	−83.75 (13)	C11—C12—C13—C14	−0.1 (4)
C3—C4—C5—C6	26.86 (14)	C12—C13—C14—C15	−0.9 (4)
C3—O4—C6—O6	−174.63 (15)	C13—C14—C15—C16	0.9 (4)
C3—O4—C6—C5	5.30 (16)	C14—C15—C16—C11	0.1 (3)
O5—C5—C6—O6	39.1 (2)	C12—C11—C16—C15	−1.2 (3)
C4—C5—C6—O6	158.92 (16)	C10—C11—C16—C15	177.86 (16)

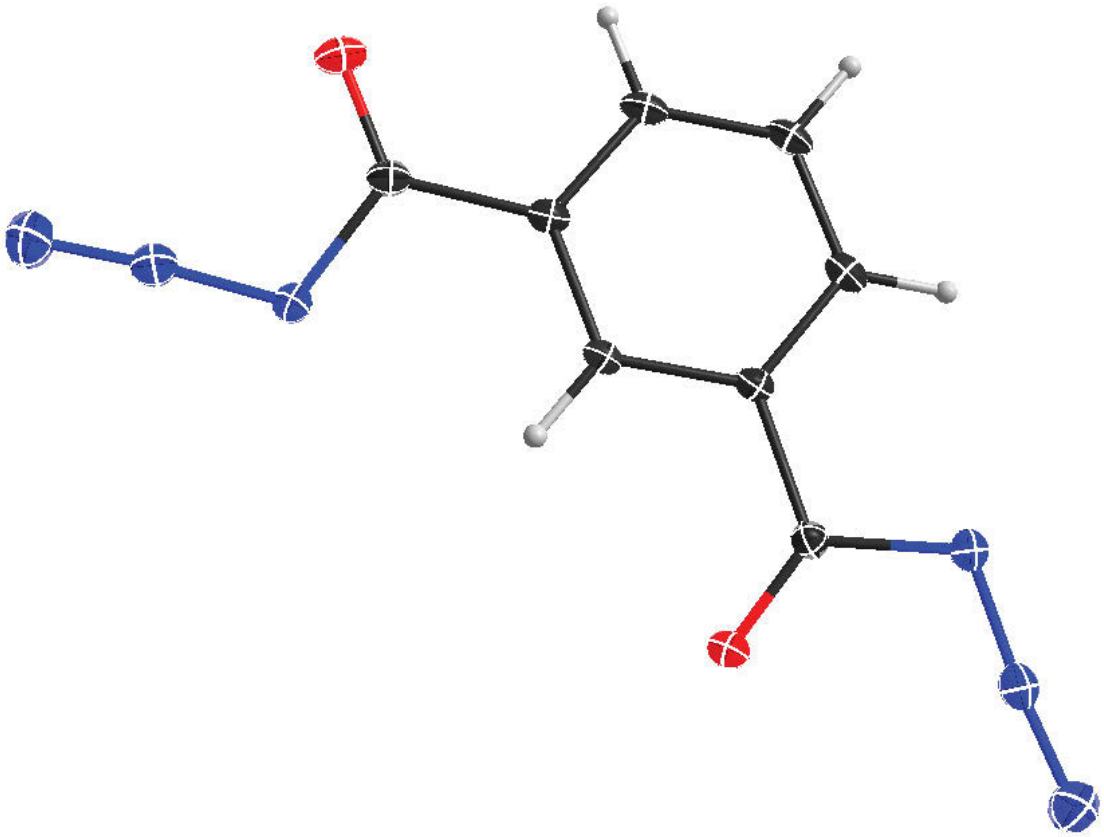

Figure 44: X-ray crystal structure of diazide **9**

Table 1: Experimental Details

	14mz043_0m
Crystal data	
Chemical Formula	$C_8H_4N_6O_2$
M_r	216.17
Crystal system, space group	Monoclinic, $P2_1/c$
Temperature (K)	100
a, b, c (Å)	3.6645, 19.361, 12.906
V(Å^{-3})	914.2
Z	4
Radiation type	Mo *K*alpha
mew (mm^{-1})	0.12
Crystal size (mm)	0.44 × 0.29 × 0.11
Data collection	
Diffractometer	Bruker *AXS SMART* APEX CCD diffractometer
Absorption correction	Multi-scan Apex2 v2013.4-1 (Bruker, 2012)
T_{min}, T_{max}	0.623, 0.746
No. of measured, independent and observed [$I > 2\sigma(I)$] reflections	8341, 2835, 2504
R_{int}	0.029
Refinement	
$R[F^2 > 2\sigma(F^2)]$, $wR(F^2)$, S	0.038, 0.110, 1.04
No. of reflections	2835
No. of parameters	145
No. of restraints	0
H-atom treatment	H-atom parameters constrained
$\Delta\rho_{max}$, $\Delta\rho_{min}$, (e Å^{-3})	0.47, -0.18

Table 2: Bond Lengths (Å)

C1—C6	1.3886 (11)	C5—H5	0.95
C1—C2	1.3935 (12)	C6—C8	1.4777 (12)
C1—H1	0.95	C7—O1	1.2088 (10)
C2—C3	1.3946 (11)	C7—N1	1.4159 (11)
C2—C7	1.4792 (12)	C8—O2	1.2093 (11)
C3—C4	1.3902 (12)	C8—N4	1.4267 (11)
C3—H3	0.95	N1—N2	1.2595 (11)
C4—C5	1.3826 (13)	N2—N3	1.1124 (12)
C4—H4	0.95	N4—N5	1.2631 (11)
C5—C6	1.4002 (11)	N5—N6	1.1131 (12)

Table 3: Bond Angles (º)

C6—C1—C2	119.51 (7)	C6—C5—H5	120
C6—C1—H1	120.2	C1—C6—C5	120.19 (8)
C2—C1—H1	120.2	C1—C6—C8	122.32 (7)
C1—C2—C3	120.27 (8)	C5—C6—C8	117.49 (7)
C1—C2—C7	117.50 (7)	O1—C7—N1	123.51 (8)
C3—C2—C7	122.22 (8)	O1—C7—C2	124.20 (8)
C4—C3—C2	119.90 (8)	N1—C7—C2	112.30 (7)
C4—C3—H3	120.1	O2—C8—N4	122.49 (8)
C2—C3—H3	120.1	O2—C8—C6	124.27 (8)
C5—C4—C3	120.12 (8)	N4—C8—C6	113.25 (7)
C5—C4—H4	119.9	N2—N1—C7	111.69 (7)
C3—C4—H4	119.9	N3—N2—N1	175.19 (9)
C4—C5—C6	120.01 (8)	N5—N4—C8	110.22 (7)
C4—C5—H5	120	N6—N5—N4	176.05 (10)

Table 4: Torsion Angles (º)

C6—C1—C2—C3	−0.33 (12)	C3—C2—C7—O1	−171.61 (8)
C6—C1—C2—C7	−179.53 (7)	C1—C2—C7—N1	−172.68 (7)
C1—C2—C3—C4	0.07 (13)	C3—C2—C7—N1	8.14 (11)
C7—C2—C3—C4	179.23 (7)	C1—C6—C8—O2	173.67 (8)
C2—C3—C4—C5	0.11 (13)	C5—C6—C8—O2	−6.07 (13)
C3—C4—C5—C6	−0.02 (12)	C1—C6—C8—N4	−6.02 (12)
C2—C1—C6—C5	0.42 (12)	C5—C6—C8—N4	174.25 (7)

C2—C1—C6—C8	−179.31 (7)	O1—C7—N1—N2	−1.06 (13)
C4—C5—C6—C1	−0.25 (12)	C2—C7—N1—N2	179.19 (8)
C4—C5—C6—C8	179.49 (7)	O2—C8—N4—N5	4.41 (13)
C1—C2—C7—O1	7.58 (13)	C6—C8—N4—N5	−175.90 (7)